九州大学学術情報リポジトリ
Kyushu University Institutional Repository

The Study on the Temperature-Responsive Phase Behavior of Multimeric Short-Chain Elastin-like Peptides via Branched Scaffolds

田中, 尚輝

https://hdl.handle.net/2324/7443250

出版情報：Kyushu University, 2025, 博士（理学）, 課程博士
バージョン：
権利関係：

KYUSHU UNIVERSITY

The Study on the Temperature-Responsive Phase Behavior of Multimeric Short-Chain Elastin-like Peptides via Branched Scaffolds

田　中　尚　輝

The Study on the Temperature-Responsive Phase Behavior of Multimeric Short-Chain Elastin-like Peptides via Branched Scaffolds

Naoki Tanaka

Laboratory of Biomolecular Chemistry
Department of Chemistry
Graduate School of Science
Kyushu University

March 2026

Contents

The Study on the Temperature-Responsive Phase Behavior of Multimeric Short-Chain Elastin-like Peptides via Branched Scaffolds

Chapter 1

An Introduction to Elastin-like Peptides and Their Phase Behavior 1

1. Overview of Elastin-like Peptides (ELPs) 2

2. Factors Controlling the Phase Behavior of ELPs 4

3. Mechanism of Temperature-responsive Behavior 7

4. Applications of ELPs 10

5. Conclusion and Motivation of This Thesis 14

6. References 15

Chapter 2

Development of covalent two- to four-armed short-chain ELPs via EDTA-mediated multimerization and investigation of their temperature-responsive behavior 33

1. Introduction 34

2. Materials and Methods 35

3. Results and Discussion 37

4. Conclusion 41

5. References 42

Chapter 3

Investigation of temperature-responsive behavior of branched molecules containing repeat units of elastin-like peptide FPGVG as side components 53

1. Introduction 54

2. Materials and Methods 55

3. Results and Discussion 58

4. Conclusion 63

5. References 64

Chapter 4

Investigation of LCST-type phase behavior in mixtures of short-chain elastin-like peptides with minimal structural differences 83

1. Introduction 84

2. Materials and Methods 85
3. Results and Discussion 89
4. Conclusion 97
5. References 97

Chapter 5
General Conclusion and Future Perspectives 122
References 124

Acknowledgements 136

Chapter 1

An Introduction to Elastin-like Peptides and Their Phase Behavior

Abstract

Stimuli-responsive materials are a class of functional materials that undergo reversible changes in their physical or chemical properties in response to external or internal stimuli, and they have gained extensive attention for their potential application in biochemical and medical fields. Elastin-like peptides (ELPs) are synthetic polypeptides derived from the hydrophobic domains of the elastic protein elastin, and exhibit lower critical solution temperature (LCST)-type behavior (also known as coacervation) in aqueous environments. Specifically, ELPs are soluble at low temperatures but undergo reversible phase separation and become insoluble upon heating. ELPs typically comprise repetitive pentapeptide motifs, most commonly $(Val\text{-}Pro\text{-}Gly\text{-}Xaa\text{-}Gly)_n$, where Xaa is a guest residue that can be any amino acid except Pro. The temperature-responsive behavior of ELPs has been extensively investigated with respect to intrinsic and extrinsic parameters that can tune their phase behavior, the mechanism behind the temperature-responsive self-assembly, and their potential for application in diverse fields. From this perspective, investigations of ELPs of varied compositions, chain lengths, and molecular architectures provide not only opportunities for developing more accessible and economical materials but also powerful platforms for clarifying the fundamental mechanisms of thermoresponsive self-assembly, thereby offering insight into the rational design of ELPs for practical applications. As a background of this thesis, this chapter first introduces the fundamental properties of ELPs, including their origin, temperature-responsive behavior, and synthesis. Then, this chapter provides an overview of the intrinsic and extrinsic factors that control their phase behavior and describes the current understanding of the molecular mechanisms underlying their phase behavior. Subsequently, the chapter highlights representative applications of ELPs in which their temperature-responsive self-assembling behavior is directly exploited to enable specific functionalities. Finally, this chapter concludes by outlining the aims of this thesis and its contributions to the field.

1. Overview of Elastin-like Peptides (ELPs)

Stimuli-responsive materials are substances that dynamically alter their physical or chemical properties in response to external or internal stimuli such as changes in temperature, pH, light, ionic strength, or mechanical force [1,2]. Among them, temperature-responsive systems have been attractive because the temperature can be precisely controlled easily and remotely. Temperature-responsive behavior is typically classified into two categories: lower critical solution temperature (LCST) and upper critical solution temperature (UCST) [3]. In LCST polymers, the polymers show phase transitions from soluble states to insoluble states upon heating, and the transition is generally triggered by an entropy-driven process. In contrast, UCST polymers exhibit the opposite behavior; they are insoluble at low temperatures but become soluble upon heating, and this transition is generally triggered by an enthalpy-driven process. In aqueous solutions, LCST behavior is more common, while UCST behavior is more frequently observed in organic environments [3].

Elastin-like peptides (ELPs) are synthetic peptides that exhibit LCST-like behavior (also known as coacervation) in aqueous solutions (Figure 1-1). ELPs mimic the primary sequence of the hydrophobic domain of (tropo)elastin. Tropoelastin is a soluble, 60–72 kDa precursor protein of elastin that consists of alternating hydrophobic domains and hydrophilic domains [4]. The hydrophobic domains are enriched in non-polar residues such as Gly, Val, and Pro, and often appear as repeating motifs. In contrast, hydrophilic domains are rich in Lys and Ala, which are responsible for covalent cross-linking via the formation of desmosine and isodesmosine linkages. As tropoelastin in aqueous solution shows LCST behavior (coacervation), ELPs show LCST behavior in aqueous environment: ELPs are water-soluble at low temperatures, but insoluble at high temperatures. ELPs are designed based on the amino acid sequences found in natural elastin, particularly the repetitive sequences in vertebrates represented by $(\text{Val-Pro-Gly-Val-Gly})_n$ [5–7]. Artificial ELPs are constructed by modification of this motif, typically using the generalized sequence $(\text{Val-Pro-Gly-Xaa-Gly})_n$, where Xaa is a guest residue that can be any amino acid except Pro. As shown in the following section, various intrinsic and extrinsic factors have been investigated for their influence on the phase behavior of ELPs.

(Figure 1-1)

Most commonly, ELPs have been produced with expression systems or chemical methods [8–15]. Notably, Chilkoti group developed recursive directional ligation (RDL) as a strategy to obtain repetitive polypeptides with desired chain lengths [11]. This approach oligomerizes a monomer DNA in a stepwise manner into oligomers of desired repetitions. They further developed recursive directional ligation by plasmid reconstruction (PRe-RDL), a method

commonly used for obtaining ELPs today, which can avoid background self-ligation of a vector and sequence limitations observed in RDL [12]. Advances in genetic code expansion techniques enabled the incorporation of non-canonical amino acids into ELP sequences. For example, Amiram group synthesized azobenzene- and arylazopyrazole-containing ELPs, which respond not only to temperature changes but also to light conditions [16,17]. Chemical synthetic approaches are also available to obtain ELPs. While limited to shorter chain length compared to expression systems, solid-phase peptide synthesis (SPPS) and liquid-phase peptide synthesis (LPPS) have been utilized to obtain ELPs with desired sequences and lengths [15]. SPPS has allowed the incorporation of unnatural amino acids at a desired position within the sequence. For instance, Shimizu *et al*. successfully compared the T_t values of variants of $(FPGVG)_5$, whose Phe at *N*-terminus was substituted with various unnatural amino acids including Phg, Cha, Phe(4-NO_2) to name a few [18]. In contrast to SPPS, which often requires excess reagents owing to the heterogeneity of the reaction system, LPPS allows homogenous reaction conditions and can reduce the amount of reagents and solvents. For its sustainable aspect, LPPS approach has been developed and used in the investigation of ELPs. Okada *et al.* achieved the synthesis of $(PGVGV)_2$ via high-pressure LPPS using hydrophobic benzyl alcohol as a soluble tag [19]. They also reported tag-assisted LPPS of ELPs using hydrophobic magnetic nanoparticles, wherein the target ELP-tag molecule precipitated with the nanoparticle and could be rapidly collected with a magnet [20]. Yoshida *et al.* also utilized the benzyl alcohol tag for the synthesis of $(FPGVG)_n$ and $(FPGV)_n$ [21]. Endo group used microwave irradiation for the condensation of GVGVP, and obtained polymeric products with a molecular weight of 7,000–40,000 [22]. Chemoenzymatic approach was performed by Gudeangadi *et al*. Using papain, they obtained poly(VPG-*co*-VG) from small peptide ethyl esters (VG-OEt, GPG-OEt, and VPG-OEt) [23].

While general methods to obtain linear ELPs were described above, these peptides could be used as a macromonomer to obtain dendrimers, multi-chain or brush-type polymers bearing ELP-based side chains, although these architectures can also be obtained by conjugating monomers onto the backbone or core molecule [24–31]. In these branched ELP molecules, while LCST behavior was generally observed, UCST behavior was observed in brush polymers with poly(phenylacetylene) backbone [32].

Generally, ELPs are regarded as biodegradable and biocompatible [33,34], and these properties have made them particularly attractive as responsive biomaterials. Applications wherein ELPs can be exploited include drug delivery, non-chromatographic protein purification (inverse transition cycling, ITC), protein conjugates, culture medium, hydrogel, toxic substance scavengers, reaction field, coating to name a few [35–48]. Additionally, owing to their simple primary structures and phase separating properties, they have served as artificial models to investigate the phase behavior of intrinsically disordered proteins [49,50], contributing to the

understanding of complex liquid-liquid phase separation (LLPS) of biomacromolecules. Representative examples of applications are introduced in section 4.

Although the temperature-responsive phase behavior and applications of ELPs have been extensively studied, the majority of previous studies have focused on relatively long-chain ELPs, typically consisting of several hundred amino acid residues. While short-chain ELPs enable facile chemical synthesis and sequence flexibility, their phase behavior remains insufficiently understood, particularly in relation to molecular architecture and intermolecular interactions.

2. Factors Controlling the Phase Behavior of ELPs

The phase behavior of ELPs is known to be influenced by intrinsic and extrinsic factors. Phase behavior refers to the temperature- and environment-dependent transition of ELPs between soluble and aggregated states. This section describes the factors that can modulate the phase behavior (Table 1-1).

(Table 1-1)

2.1. Intrinsic parameters

The LCST-like behavior of ELPs can be modified by varying intrinsic or extrinsic parameters. Intrinsic parameters that affect T_t values include amino acid composition, chain length, peptide concentration, molecular architecture, and conjugation with other molecules. Amino acid composition strongly affects the T_t values of ELPs. Incorporation of hydrophilic residues typically increases the solubility of ELPs and leads to higher T_t values or loss of LCST behavior (i.e., solution state over a measurable temperature range). In contrast, hydrophobic residues facilitate the self-assembly of ELPs and lower T_t values [51–56]. In addition to residue hydrophobicity, the size of side chains also modulates the temperature-responsiveness of ELPs. ELPs with bulky side chains at *N*-termini have lower T_t values than the otherwise counterpart [18]. This effect has been attributed to the larger surface areas of bulky side chains, which provided more sites for noncovalent intermolecular and intramolecular interactions.

The directionality of sequence affects the temperature-responsiveness of ELPs. For instance, Li *et al.* demonstrated poly(VPGVG) and its reverse sequence, poly(VGPVG), exhibited distinct thermal responses: while both peptides aggregate upon heating above T_t, only poly(VPGVG) resolubilizes upon cooling [57]. Their MD simulations indicated that sequence order affects the dynamics of the specific residues (especially Val), which lead to different secondary structure formation and overall structure. In case of these two sequences, poly(VPGVG) had more extended conformation and larger surface area, which led to formation of strong interchain hydrogen bonds and, consequently, stabilized aggregate and the thermal

hysteresis. Tatsubo *et al.* investigated the sequence-shuffled variants of short-chain ELPs $(FPGVG)_n$ [58]. Their study found that even short ELPs with identical composition and repeat number can show different T_t values and solubilities. They revealed that the secondary structures were different from each other even among the ones with the LCST-type behavior. These findings highlight the importance of sequence order in tuning the LCST behavior of ELPs.

Peptide chain length and peptide concentration are also intrinsic determinants of temperature-responsiveness. ELPs with longer peptide chains generally show lower T_t values compared to ones with shorter peptide chains. Higher peptide concentration leads to lower T_t values. Chilkoti group has reported equations that can predict the T_t as a function of ELP concentration, chain length, and/or amino acid compositions [53–55].

Furthermore, molecular architecture also plays an important role. While typical ELPs are linear peptides, dendric, branched, or multi-chain ELPs have been synthesized and investigated for their properties [24–31,59–61]. Ayres *et al.* synthesized brush polymers with elastin-based side chains by atom transfer radical polymerization and demonstrated their LCST behavior with varying T_t values based on polymer concentration, molecular weight, and pH [29]. Navon *et al.* used dendric ELPs with GLPGL pentamers and observed that T_t values of dendrimers were higher than those of linear ELPs [31]. While ELP-based branched molecules typically show LCST behavior, Arias *et al.* reported UCST behavior in ELP-based brush polymer, which was composed of poly(phenylacetylene) backbone and pentapeptide VPGVG side chains [32].

Conjugation of ELPs with other molecules such as hydrophobic/hydrophilic cores or functional molecules are a strategy that controls temperature-responsive behavior without altering the ELP sequence itself. Such conjugation enables tunability of T_t and combination of temperature-responsiveness of ELPs and functions originating from conjugated molecules. Lipidation is one of such modifications [62–67]. Garbay group synthesized a series of *N*-termini acylated ELP with myristic, palmitic, stearic, oleic or linoleic acid [65]. They showed that not only acylation could affect the T_t values but also the micelle sizes were largely determined by ELP blocks. Zhang *et al.* reported that longer lipid length leading to lower T_t is in a sigmoidal manner, and coalescence kinetics depend on the lipid length, which might be due to temperature-dependent interactions between lipids and the protein [66]. Moreover, the conjugates of ELP and other molecules offer unique nanostructures ranging from spherical micelles to fibers. Chilkoti group achieved cylindrical micelles using the ELPs fused with a short $(XG_y)_8$ assembly domain, where X was Tyr, Phe, or Trp, and y was the number of Gly [68]. Jeong *et al.* reported ELPs fused with tripeptides (WFF, FFF, YFF, LFF, VFF, and AFF) at their *N*-terminus as hydrophobic cores, showing that while these peptides form micelles, their T_t values differed even with a single amino acid substitution in the cores [69].

Conjugating ELP with other biopolymers is another intriguing example. One such

example is conjugates of ELP with resilin-like polypeptides (RLPs) [70–72]. RLPs are derived from resilin, which is an elastic protein found in insect cuticles and responsible for high energy storing for functions such as jumping and flying. RLPs show UCST behavior; they are soluble at high temperatures but insoluble at low temperatures. The fusion of ELP and RLP provides dual temperature responses of LCST and UCST behavior. Weitzhandler *et al.* reported that diblock copolypeptides of ELP and RLP showed LCST and UCST behavior and formed spherical or cylindrical micelles dictated by their chain length and hydrophilicity [70]. Basheer *et al.* also synthesized block copolymers of varying chain length of ELP and RLP [72]. Their copolymers showed both LCST and UCST behavior with varied nanostructures, and the phase behavior was dependent on peptide chain length and the ratio, polymer concentration, and salt concentration. Another conjugate of ELP and biopolymer is collagen-like peptide (CLP)-conjugated ELPs [73–76]. Kiick group reported that block copolymers of CLP and ELP showed reduced T_t values compared to the ELP domain owing to the triple-helix-forming CLP [73]. Additionally, their CLP-ELP showed well-defined vesicles at physiological temperature, but the vesicles were resolubilized at elevated temperatures owing to the unfolding of CLP domain. Furthermore, they achieved unique nanosized platelets morphology by simply varying the ELP sequences [75]. Polysaccharide-ELP conjugates are another example of hybrid ELP molecules [77–79]. Xiao *et al.* observed higher T_t values for the conjugates compared to the ELP because of the hydrophilicity of the polysaccharides [77]. Oligonucleotide-ELP conjugates have been also investigated [80–82]. For example, Wang *et al.* synthesized conjugates of oligonucleotide (21–38 bases) and short chain ELP $(VPGFG)_6$, and showed that the nanospheres formed by the conjugates shrunk upon heating [80].

2.2. Extrinsic parameters

In addition to intrinsic factors, extrinsic parameters influence the LCST behavior of ELPs. These parameters include pH, salt, solvent, pressure, and coexisting molecules.

pH: Changes in pH affect the ionization state of charged residues of ELPs and alter electrostatic repulsion and hydration; increased net charge leads to increased solubility and higher T_t values [83,84].

Salt concentration and ionic strength: T_t values of ELPs can be affected through salting-in and salting-out effects depending on the type of co-existing salts [51,55,85,86]. In terms of Hofmeister series of anions, Cho *et al.* reported that kosmotropic anions lowered the LCST of ELPs by increasing the polarization of interfacial water around amide groups, whereas chaotropic anions lowered the LCST via surface-tension effect and exhibited salting-in effect at low salt concentration [86]. In contrast, Aladini *et al.* reported that the effects of cations on the T_t of ELPs are related to the direct interaction between ions and ELPs rather than the order of the salting-out

effects in the Hofmeister series [51].

Solvents: Certain solvent combinations exhibit cononsolvency of ELPs [87,88]. Mills *et al.* investigated the effects of mixtures of water and alcohol (methanol, ethanol, isopropanol, or 1-propanol) on the phase behavior of an ELP [87]. They observed decreased T_t values in the mixed solvent. Furthermore, even UCST-like behavior was observed in the mixtures except for water/methanol mixture.

Pressure: Tamura *et al.* reported that the T_t of $(VPGIG)_{40}$-based ELP increased associated with pressure increased from atmospheric levels to approximately 100 MPa and then decreased with further pressure increases (> 200 MPa) [89].

The presence of protease: Wirz *et al*. synthesized block co-polypeptide of a hydrophilic ELP block $((VPGVG)(VPGAG)_8(VPGGG)_7)_6$ and a hydrophobic ELP block $(VPGVG)_{60}$ linked by a protease cleavage site [90]. Under an isothermal condition upon the cleavage, the hydrophobic block underwent phase separation.

The presence of other ELP components: The presence of other ELP components with different chain lengths or compositions can fluctuate the phase behavior of ELPs [60, 91–94]. Chilkoti group reported that binary mixtures of long-chain ELPs varied in both sequence composition and length (n = 150 and 160) underwent independent phase transitions [91]. Similarly, van Hest's group showed that two- and three-component mixtures of $(VPGVG)_n$ that differ only in chain length (n = 20, 40, and 90) also phase-separate independently upon heating [92]. Holland group used mixtures of linear ELP and three-armed ELP and found that concentration condition was an important factor in observing single transition and two-step transition: single transitions were observed in mixtures prepared at high concentration while two distinct transitions were observed under low concentration conditions [60]. In contrast, mixtures of two ELPs with nearly identical amino acid compositions, or with different compositions but substantially reduced molecular weight in one or both components were found to form mixed coacervates rather than undergoing separate transitions [94]. Together, these results indicate that chain length and sequence composition dictate whether the phase separation is independent or not.

3. Mechanism of Temperature-responsive Behavior

3.1. Experimental studies

The mechanism of the phase behavior of ELPs has been investigated primarily through experimental approaches. Urry *et al.* reported that ELPs are surrounded by ordered water molecules below T_t but the water molecules become less ordered above T_t [52]. Their studies based on experimental methods (such as NMR or CD spectroscopy) suggested that, above T_t, ELPs formed an ordered β-spiral structure, which is a helical conformation consisting of repeating VPGVG pentapeptide units linked by β-turns [95–101]. Importantly, such structural transitions

were observed even in short-chain elastin-like peptides $(VPGVG)_n$, where n = 1–5, indicating that these conformational changes are not limited to long polymeric peptides [102,103]. In a study on the oligopeptide GVG(VPGVG), it was reported that the peptide undergoes folding over a temperature range around 36 °C and unfolding at 90 °C [104]. In contrast, an ATR-FTIR study by Serrano *et al.* showed that the ELP undergoes a conformational transition in which the β-spiral decreases and β-sheet increases with increasing temperature [105]. Furthermore, Reichheld *et al.* reported that ELPs only formed transient β-turns in a highly dynamic and disordered chain and the disordered chains were retained after thermoresponsive phase separation [106]. Thus, the relationship between the temperature-responsive self-assembly and secondary structural changes in ELPs remains controversial.

Recently, NMR studies have provided residue-level insights into the thermoresponsive phase transition of ELPs. Brandis *et al.* reported that, upon aggregation, Pro residues become motionally restricted, which indicated their involvement in interchain contacts [107]. Furthermore, NMR experiments using hyperpolarized water enabled the acquisition of aggregate surface-selective NMR spectra and provided direct evidence that Gly residues are enriched at the coacervate surface while hydrophobic residues such as Ala and Val are buried [108]. Other studies have also demonstrated higher preferences for β-turn formation upon the self-assembly of ELPs, which emphasized the importance of Pro-Gly sequences [109,110].

3.2. Theoretical studies

Computational simulations also have been used to investigate the phase behavior and conformational changes of ELPs [111]. All-atom simulations of ELPs have provided varying insights into temperature-dependent structural changes. Li *et al.* simulated $(VPGVG)_{18}$ and reported that water plays a critical role in conformational behavior [112]. They showed that the polymer formed more turns and distorted β-structure at higher temperatures, largely in agreement with these experimental insights. They further reported that hydrophobic hydration is responsible for entropy-based elasticity of elastin [113]. Tarakanova *et al*. likewise observed a structural transition from extended to contracted structures in $(GVGVP)_3$, reflected by a reduced radius of gyration upon heating [114]. In contrast, long-time simulation (up to 350 ns) by Krukau *et al.* suggested that $GVG(VPGVG)_3$ had rigid conformation at low temperature and highly flexible structure at high temperature [115], while Zhao *et al.* also did not observe a transition in $GVG(VPGVG)_3$ [116]. Simulations on GVG(VPGVG) octapeptide even suggested that the peptide folded upon heating and unfolded upon further heating [117–119]. Taken together, these single-chain simulations have provided valuable but sometimes contradictory insights into the temperature-dependent phase behavior of ELPs, highlighting the complexity of their phase behavior.

More detailed mechanistic insight could be provided by MD simulation with multi-chain systems. Using $(VPGVG)_{18}$ in one-chain or two-chains system, Yingling *et al.* reported that increasing temperature led to more ordered secondary structures such as β-strands, accompanied by changes in hydrophobicity [120]. They concluded that the transition arose from thermal disruption of the hydration shell, a reduction in the solvent-accessible surface area, and an overall increase in hydrophobicity. Using ELPs of various chain lengths ($(GVG)(VPGVG)_3$, $(VPGVG)_{10}$, $(VPGVG)_{18}$, and $(VPGVG)_{30}$), they further reported that the hydrogen bonding tendencies of the pentamer motifs depend only on sequence rather than chain length [116]. Additionally, comparison of $(VPGVG)_{18}$ and compositionally identical $(VGPVG)_{18}$ revealed differences in hydrophobicity of aggregate surface, torsion angles, and secondary structure propensities that contributed to experimentally observed, distinct thermal hysteresis behavior [57, 121]. Effects of chain-length on self-assembly were also examined by Morozova *et al*. using $GVG(VPGVG)_3$ at varied concentrations and temperatures (below, near, and above the LCST) [122]. Their simulations showed that the ELP collapses moderately upon heating and that two chains become attractive at high temperature, which reflects LCST-like behavior. In multichain systems, the peptides formed dynamic, coil-like aggregates, with Val residues driving interpeptide contacts and with contact lifetimes increasing at higher temperatures. Higher temperatures and concentrations also reduced both translational and internal peptide mobility. Additionally, they reported that short-chain ELPs remain in coil-like conformations and form temporal intrapeptide hydrogen bonds, while the long-chain ELPs prefer globule states and form hundreds of long-lived (nanosecond-long) intrapeptide hydrogen bonds associated with ordered structures, demonstrating that the chain length modulates the material properties of elastin condensates [123]. Large-scale all-atom simulations were performed by Pomès group on $(GVPGV)_7$ in a single-chain and 27-chain systems with a combined sampling time exceeding 200 μs [124]. They found that aggregates were stabilized by hydrophobic effect but do not form a buried hydrophobic core. The aggregated peptides are highly hydrated and nearly maximally disordered, while exhibiting sparse, transient turn motifs.

Coarse-grained (CG) simulations have been also developed and used to better understand the multi-chain systems of ELPs. Baul *et al*. developed an explicitly temperature-dependent CG model for disordered, hydrophobic polypeptides [125]. Using a variety of polypeptides including $(VPGXG)_n$ (n = 20–150), they confirmed that the T_t values of ELPs decrease with increasing chain length. Mabuchi *et al.* showed that higher polymer concentration and longer chains promoted coacervate formation, whereas these conditions had little influence on the structural or dynamic properties within the coacervate [126]. CG simulation by Mukherjee *et al.* also examined the effects of temperature and concentration on coacervation [127]. Using $(VPGIG)_{20}$, they reported that higher temperatures lead to stronger interchain interactions and

weaker peptide-water interactions. They also showed that at low peptide concentration, cluster size increased with temperature whereas at high concentration, clusters form earlier and became more compact upon heating. Consistently, chains were extended during coacervation at low concentration but more collapsed at higher concentration in their conformational analysis.

Overall, computational simulations have provided important insights into the temperature-responsive behavior of ELPs. However, the discrepancies among reported results, particularly for short-chain ELPs, highlight the complexity of the phase behavior of ELPs and the continued need for systematic experimental and theoretical studies.

4. Applications of ELPs

Owing to the stimuli-responsive self-assembling properties, ELPs have been utilized in a wide range of applications, including drug delivery systems, protein purification and functionalization, culture media, hydrogels, toxic substance scavengers, reaction fields, biosensors, and coatings. This section focuses on representative examples in which the temperature-responsive self-assembling behavior of ELPs is directly exploited to enable desired functionalities.

4-1. Carriers for drug delivery

ELPs have been widely explored in drug delivery system (DDS) because of their stimuli-responsive self-assembling properties, drug incorporation capability, and ability to extend the half-life of therapeutic molecules [128–132]. Fusion of drugs or protein therapeutics to ELPs increases their effective molecular size, thereby reducing renal clearance and prolonging systemic circulation. This self-assembling behavior enables the incorporation of therapeutic molecules either through direct fusion or noncovalent complexation, which enables controlled drug localization and release profiles. For example, MacKay *et al.* prepared near-monodisperse nanoparticles of an ELP upon conjugation with doxorubicin and demonstrated improvement in antitumor efficacy and prolongation of half-life of doxorubicin [133]. By altering the amino acid sequence, chain length, and hydrophobicity of ELPs, the size, stability, and drug-loading capacity of the assemblies can be finely tuned [128]. The use of ELPs in drug delivery has been applied to a variety of pharmaceutical molecules including peptides [134–136], cytokines [137–142], nucleic acids [143–145], or antibodies/nanobodies [146–149], leading to improved pharmacokinetic profiles and enhanced therapeutic efficacy. Moreover, the self-assembling behavior of ELPs allows for the formation of depots at physiological temperatures, enabling sustained drug release at the target site [128,130]. Amiram *et al*. demonstrated that a glucagon-like peptide (GLP)-1-ELP fusion protein can form an injectable depot upon subcutaneous injection, reducing blood glucose levels in mice for five days (a 120-fold increase in duration

compared to the native peptide) [134]. Their study highlights the potential of ELPs as a reservoir that provides sustained therapeutic activity, contributing to improved bioavailability and reduced dosing frequency. Furthermore, the self-assembly of ELPs can also be exploited for drug activation. Recently, Vu and Arai reported controlled programmed cell death using ELP-fused human caspase 8 (CASP8) [150]. In their system, the heat-induced self-assembly of the ELP domain increased the local concentration of CASP8, which facilitated dimerization-induced activation and, consequently, death of HEK293T cells. This approach demonstrates that phase transitions of ELPs can be leveraged as a physical switch for spatiotemporal control of therapeutic activity in deep tissues.

Overall, the abilities of ELPs to self-assemble, contain drugs and extend drug half-life underscore their utility as multifunctional DDS platforms, positioning them as promising candidates for next-generation drug delivery applications.

4-2. Tags for nonchromatographic purification and functionalization of proteins

One of the major applications of ELPs is their use as tags for nonchromatographic purification of proteins. In addition, fusion of ELPs to proteins can improve expression levels, solubility, and thermal and storage stability without compromising proteins' functionalities [142,151–161].

A protein purification method in which ELPs are fused to a target protein and purified by temperature changes was proposed by Chilkoti and co-workers and is referred to as inverse transition cycling (ITC) [162,163]. In ITC, an increase in temperature induces a phase transition of the ELP, resulting in selective precipitation of the ELP-protein conjugate [164]. The precipitate is then collected and resolubilized by lowering the temperature, and the purity of the target protein can be progressively improved by repeating the heating-cooling cycle. Compared with conventional chromatographic methods, ITC only requires lower volumes of solvents and enables rapid purification, because this method does not involve column packing, equilibration, or elution steps. As an example of ITC purification, Addai *et al.* reported the fusion of *Lactobacillus sp.* B164 β-galactosidase modified with His tag (β-Gal-LH) and ELP $(VPGVG)_{50}$ expressed in *E. coli* [152]. The produced recombinant β-Gal-Linker-ELP-His (β-Gal-LEH) purified via ITC showed a higher recovery rate and purification fold and even enzymatic activity compared to the conjugates purified with nickel-nitrilotriacetic acid (Ni-NTA) resin. However, it should be noted that conjugation of ELP to proteins could affect the expression levels, yields of purified proteins, and activity of the target proteins, as well as the T_t values of ELPs [151,165]. In particular, the length of the ELP chain has been shown to significantly influence the expression yield of ELP fusion proteins, indicating that minimizing the ELP length is critical [164].

After the purification of ELP-protein conjugates, removal of the ELP tag after

purification is often required, and this has typically necessitated the use of protease [36,154,162,166,167] or transpeptidase [168]. Apart from these approaches, purification systems employing self-cleaving sequences (inteins) have been developed [169–171]. In this approach, the intein is inserted between the target protein and ELP, and a protein-intein-ELP fusion is first recovered by ITC. Then, subsequent addition of thiol compounds (such as β-mercaptoethanol, dithiothreitol, cysteine, etc.) triggers intein-mediated self-cleavage, releasing the target protein into solution. This strategy eliminates the need for enzyme treatment and separation of the enzyme and the target protein, thereby simplifying the purification process [170]. On the other hand, recent studies have demonstrated that, in some cases, target proteins retain their biological activity even when the ELP tag is not removed. Wang *et al.* reported the purification of an endoglucanase from *Thermotoga maritima*, showing that the ELP-fused enzyme exhibited little difference in activity compared with the untagged enzyme [153]. Moreover, ELP fusion has been shown to enhance the thermal stability and storage stability of the target protein [152,153,156]. These findings suggest that the necessity of the tag removal should be determined based on the functional requirements and intended applications of the target protein.

In addition to its use as purification tags covalently bonded to the target protein, ELP tags have also been employed for affinity precipitation-based protein purification [172–177]. In this method, ELP is fused to ligands that specifically bind target proteins, and changes in temperature or ionic strength induce precipitation of the complex of ELP-ligand conjugate and target protein. For example, Kim *et al.* reported the purification of monoclonal antibodies using ELP fused to Protein A or Z-domains [172]. In their system, the antibodies are first bound to the ELP-ligand conjugate, followed by precipitation and recovery of the complex. Then, the antibodies are subsequently isolated under acidic conditions. Furthermore, Mullerpatan *et al.* have demonstrated that, using peptide ligands fused to ELP, purification efficiency is influenced by both the type of ligand and the number of the ligand fused to the ELP [178]. When the affinity between the ligand and the target protein is weak, or when the ligand has high hydrophobicity, nonspecific interactions between the ligand and ELP chains may occur, which reduce purification efficiency. These challenges may be addressed through rational design of the ELP, including optimization of its amino acid composition and chain length. Thus, rational design of ELPs plays a key role in affinity precipitation-based protein purification.

As mentioned, ELPs can functionalize proteins not only by imparting temperature-responsiveness, but also by improving thermal, pH, and storage stability of the fused proteins without compromising their functionalities. For instance, several proteins, such as β-galactosidase and endoglucanase [152,153], have been reported to exhibit enhanced tolerance to broader temperature or pH ranges upon fusion with ELPs, compared to their wild-type counterparts. These works highlight the potential of ELP-proteins conjugates for industrial applications. In order to

rationally impart functionality to proteins by ELP fusion, it is essential to investigate the correlation between the structure of the ELP and its temperature-responsiveness in detail.

4-3. Scavengers for toxic and rare substances

ELPs have also attracted attention as scavengers or adsorbents for low-cost and effective removal or recovery of toxic substances or valuable substances. For example, ELPs with metal binding domains can form complexes with target metal ions and then be precipitated by external stimuli [40,179–185]. Choi *et al.* developed ELPs consisting of 64 repeats of VPGVG fused to synthetic phytochelatin of varying lengths and demonstrated their metal binding and removal abilities for Cd^{2+} in comparison with Co^{2+}, Hg^{2+}, and Mn^{2+} [182]. Sumiyoshi *et al.* utilized short-chain ELPs (26-mer and 22-mer) to remove Cd^{2+}, highlighting the potential of short-chain ELPs as easier-to-synthesize and cost-effective biomaterials for heavy metal remediation [184,185]. Apart from metal removal and recovery, ELPs have also been explored for the removal of harmful organic chemicals. Suyama *et al.* demonstrated that FPGVG-based linear and cyclic ELPs could remove aromatic compounds such as bisphenol A, an endocrine-disrupting chemical, through π-π and CH-π interactions [41]. Collectively, these studies highlight the utility of ELPs as scavengers, whose binding ability and stimuli-responsiveness can be tuned through the attached domains or incorporated amino acids.

4-4. Condensates as reaction fields

ELPs have also been explored as reaction platforms that provide unique microenvironments for biochemical reactions. Owing to their self-assembling properties, ELPs enable spatiotemporal confinement, concentration, and reversible assembly of functional molecules to facilitate diverse reactions. The Lampel group has designed minimalistic ELP-related peptides that can form coacervates [186] and used the biomolecular condensates (homotypic condensates and heterotypic condensates with RNA) for the regulation of compartmentalized enzymatic reactions [42]. They demonstrated the composition of the condensates affected the incorporation of substrate and product, and the kinetics of the enzymatic reaction. Moreover, the hydrophobicity of the peptide component was also shown to affect the reaction kinetics. In contrast to these *in vitro* systems, Shapiro *et al.* developed an ELP fused to an RNA-binding protein and demonstrated that its condensates can enhance translation from a target mRNA in *E. coli* by locally sequestrating the mRNA into the condensates [44].

Together, these studies highlight the potential of ELP-based condensates as versatile reaction fields for regulating biochemical reactions both *in vitro* and *in vivo*. However, most of these studies—ranging from mechanistic investigations to application-oriented designs—have focused on long-chain ELPs, and how the established principles governing phase behavior

translate to short-chain ELPs, particularly in branched or multicomponent systems, remains insufficiently understood.

5. Conclusion and Motivation of This Thesis

ELPs are temperature-responsive polypeptides that typically exhibit LCST-type phase behavior. Their phase behavior can be tuned by both intrinsic factors such as amino acid composition or chain length, and extrinsic factors including pH or ionic strength. Advances in synthetic methods of polypeptides have broadened the accessible ELPs in terms of chain-length or residue compositions including non-canonical amino acids. Both experimental and computational approaches have been used to investigate how temperature, concentration, and/or sequence affect the phase behavior, and have proposed varied mechanisms behind the temperature-responsiveness. Although early models suggested ordered β-spiral structures, accumulated evidence indicates that ELPs remain highly dynamic, hydrated, and predominantly disordered, adopting only sparse and transient secondary structural motifs. These insights have positioned ELPs as valuable model systems for exploring the phase behavior of IDPs. Moreover, ELPs have found utility across biomedical science, synthetic biology, and materials science. As mechanistic understanding becomes deeper, the rational design of ELP-based molecules would be possible, and those molecules would contribute even more significantly to the advanced applications.

As described above, the majority of both fundamental and applied studies on ELPs have been conducted using relatively long-chain ELPs so far. In contrast, short-chain ELPs have been far less explored, despite their practical advantages such as facile chemical synthesis and sequence/structural flexibility. As a result, a critical gap remains in our understanding of the temperature-responsive behavior, its underlying mechanisms, and the potential applications of short-chain ELPs. To fully exploit the advantages of short-chain ELPs, systematic investigations involving the design, synthesis, and characterization of novel short-chain ELP-based molecules are required to deepen understanding of their phase behavior. In light of these considerations, this thesis focuses on short-chain elastin-like peptides. Specifically, this thesis aims to develop short-chain ELPs with branched, multi-chain structures—a class of architectures uniquely accessible through chemical synthetic approaches—to elucidate their temperature-responsive phase behavior. Furthermore, because practical applications often involve multicomponent environments, this thesis also investigates the phase behavior of mixed systems composed of short-chain ELPs. Through these studies, focusing on (i) how branched short-chain ELPs behave, and (ii) how short-chain ELPs of either linear or branched structures behave in multicomponent systems, this thesis provides insights into the design of ELP-based molecules with tailored properties and the construction of ELP-based systems for advanced applications.

6. References

[1] Kim, Y.-J.; T. Matsunaga, Y. Thermo-Responsive Polymers and Their Application as Smart Biomaterials. *J. Mater. Chem. B* **2017**, *5* (23), 4307–4321.

[2] Alexander, C.; Shakesheff, K. M. Responsive Polymers at the Biology/Materials Science Interface. *Adv. Mater.* **2006**, *18* (24), 3321–3328.

[3] Zhao, C.; Ma, Z.; Zhu, X. X. Rational Design of Thermoresponsive Polymers in Aqueous Solutions: A Thermodynamics Map. *Prog. Polym. Sci.* **2019**, *90*, 269–291.

[4] Wise, S. G.; Weiss, A. S. Tropoelastin. *Int. J. Biochem. Cell Biol*. **2009**, *41* (3), 494–497.

[5] Indik, Z.; Yeh, H.; Ornstein-Goldstein, N.; Sheppard, P.; Anderson, N.; Rosenbloom, J. C.; Peltonen, L.; Rosenbloom, J. Alternative splicing of human elastin mRNA indicated by sequence analysis of cloned genomic and complementary DNA. *Proc. Natl. Acad. Sci. USA* **1987**, *84* (16), 5680–5684.

[6] Raju, K.; Anwar, R. A. Primary structures of bovine elastin a, b, and c deduced from the sequences of cDNA clones. *J. Biol. Chem.* **1987**, *262* (12), 5755–5762.

[7] Bressan, G. M.; Argos. P.; Stanley, K. K. Repeating Structure of Chick Tropoelastin Revealed by Complementary DNA Cloning. *Biochemistry* **1987**, *26* (6), 1497–1503.

[8] McPherson, D. T.; Morrow, C.; Minehan, D. S.; Wu, J.; Hunter, E.; Urry, D. W. Production and Purification of a Recombinant Elastomeric Polypeptide, G-$(VPGVG)_{19}$-VPGV, from *Escherichia coli*. *Biotechnol. Prog.* **1992**, *8*, 347–352.

[9] McPherson, D. T.; Xu, J.; Urry, D. W. Product Purification by Reversible Phase Transition Following *Escherichia coli* Expression of Genes Encoding up to 251 Repeats of the Elastomeric Pentapeptide GVGVP. *Protein Expr. Purif.* **1996**, *7* (1), 51–57.

[10] Guda, C.; Zhang, X.; McPherson, D. T.; Xu, J.; Cherry, J. H.; Urry, D. W.; Daniell, H. Hyper expression of an environmentally friendly synthetic polymer gene. *Biotechnol. Lett.* **1995**, *17*, 745–750.

[11] Meyer, D. E.; Chilkoti, A. Genetically Encoded Synthesis of Protein-Based Polymers with Precisely Specified Molecular Weight and Sequence by Recursive Directional Ligation: Examples from the Elastin-like Polypeptide System. *Biomacromolecules* **2002**, 3 (2), 357–367.

[12] McDaniel, J. R.; MacKay, J. A.; Quiroz, F. G.; Chilkoti, A. Recursive Directional Ligation by Plasmid Reconstruction Allows Rapid and Seamless Cloning of Oligomeric Genes. *Biomacromolecules* **2010**, *11* (4), 944–952.

[13] Amiram, M.; Quiroz, F. G.; Callahan, D. J.; Chilkoti, A. A highly parallel method for synthesizing DNA repeats enables the discovery of 'smart' protein polymers. *Nat. Mater.* **2011**, *10*, 141–148.

[14] Tang, N. C.; Chilkoti, A. Combinatorial codon scrambling enables scalable gene synthesis and amplification of repetitive proteins. *Nat. Mater.* **2016**, *15*, 419–424.

[15] Nose, T.; Suyama, K. Chapter 7 - Recent Advances and Applications in Self-Assembling Short-Chain Elastin-Like Peptide Analogs. In *Repeat Amino Acid Sequences in Proteins*; Uversky, V. N., Gupta M. N., Eds.; **2025**, 123–146.

[16] Israeli, B.; Strugach, D. S.; Gelkop, S.; Weber, S.; Gozlan, D. S.; Amiram, M. Genetically Encoding Light-Responsive Protein-Polymers Using Translation Machinery for the Multi-Site Incorporation of Photo-Switchable Unnatural Amino Acids. *Adv. Funct. Mater.* **2021**, *31*, 2011276

[17] Strugach, D. S.; Hadar, D.; Amiram, M. Robust Photocontrol of Elastin-like Polypeptide Phase Transition with a Genetically Encoded Arylazopyrazole. *ACS Synth. Biol.* **2023**, *12* (10), 2802–2811.

[18] Suyama, K.; Shimizu, M.; Maeda, I.; Nose T. Flexible customization of the self-assembling abilities of short elastin-like peptide Fn analogs by substituting *N*-terminal amino acids. *Biopolymers* **2022**, *113*, e23521.

[19] Okada, Y.; Hosoya, S.; Suzuki, H.; Chiba K. Total Synthesis of Elastin Peptide Using High Pressure-Liquid Phase Synthesis Assisted by a Soluble Tag Strategy. *Org. Lett.* **2014**, *16* (24), 6448–6451.

[20] Okada, Y.; Asama, H.; Wakamatsu, H.; Chiba, K.; Kamiya, H. Hydrophobic Magnetic Nanoparticle Assisted One-Pot Liquid-Phase Peptide Synthesis. Eur. *J. Org. Chem.* **2017**, *40*, 5961–5965.

[21] Yoshida, K.; Suyama, K.; Matsushita, S.; Maeda, I.; Nose, T. Development of the efficient preparation method for thermoresponsive elastin-like peptides using liquid-phase synthesis combined with fragment condensation strategy. *J. Pept. Sci.* **2023**, *29* (12), e3528.

[22] Goto, M.; Endo, T. High-molecular-weight poly(Gly-Val-Gly-Val-Pro) synthesis through microwave irradiation. *J. Pept. Sci.* **2016**, *22* (7), 452–460.

[23] Gudeangadi, P. G.; Tsuchiya, K.; Sakai, T.; Numata, K. Chemoenzymatic synthesis of polypeptides consisting of periodic di- and tri-peptide motifs similar to elastin. *Polym. Chem.* **2018**, *9* (17), 2336–2344.

[24] Kojima, C.; Irie, K. Synthesis of temperature-dependent elastin-like peptide-modified dendrimer for drug delivery. *Pept. Sci.* **2013**, *100* (6), 553–795.

[25] Bo, J.; Wang, L.; Li, W.; Zhang, X.; Zhang, A. Comb-like Polymers Pendanted with Elastin-like Peptides Showing Sharp and Tunable Thermoresponsiveness through Dynamic Covalent Chemistry. *J. Polym. Sci. Part Polym. Chem.* **2016**, *54* (20), 3379–3387.

[26] Kojima, C.; Sk, U. H.; Fukushima, D.; Irie, K.; Akazawa, N.; Umeda, M.; Niidome, T. Effect of Main Chain Conformation on Thermosensitivity in Elastin-like Peptide-Grafted

Polylysine. *RSC Adv.* **2015**, *5* (127), 104900–104906.

[27] Conrad, R. M.; Grubbs, R. H. Tunable, Temperature-Responsive Polynorbornenes with Side Chains Based on an Elastin Peptide Sequence. *Angew. Chem., Int. Ed.* **2009**, *48* (44), 8328–8330.

[28] Fernández-Trillo, F.; Duréault, A.; Bayley, J. P. M.; Van Hest, J. C. M.; Thies, J. C.; Michon, T.; Weberskirch, R.; Cameron, N. R. Elastin-Based Side-Chain Polymers: Improved Synthesis via RAFT and Stimulus Responsive Behavior. *Macromolecules* **2007**, *40* (17), 6094–6099.

[29] Ayres, L.; Koch, K.; Van Hest, J. C. M. Stimulus Responsive Behavior of Elastin-Based Side Chain Polymers. *Macromolecules* **2005**, *38* (5), 1699–1704.

[30] Weller, D.; McDaniel, J. R.; Fischer, K.; Chilkoti, A.; Schmidt, M. Cylindrical Polymer Brushes with Elastin-Like Polypeptide Side Chains. *Macromolecules* **2013**, *46* (12), 4966–4971

[31] Navon, Y.; Zhou, M.; Matson, J. B.; Bitton, R. Dendritic Elastin-like Peptides: The Effect of Branching on Thermoresponsiveness. *Biomacromolecules* **2016**, 17 (1), 262–270.

[32] Arias, S.; Freire, F.; Calderón, M.; Bergueiro, J. Unexpected Chiro-Thermoresponsive Behavior of Helical Poly(phenylacetylene)s Bearing Elastin-Based Side Chains. *Angew. Chem. Int. Ed.* **2017**, *56* (38), 11420–11425.

[33] Shah, M.; Hsueh, P. Y.: Sun, G.; Chang, H. Y.; Janib, S. M.; MacKay, J. A. Biodegradation of elastin-like polypeptide nanoparticles. *Protein Sci.* **2012**, *21* (6), 743–750.

[34] Rincón, A. C.; Molina-Martinez, I. T.; de las Heras, B.; Alonso, M.; Baílez, C.; Rodríguez-Cabello, J. C.; Herrero-Vanrell, R. Biocompatibility of elastin-like polymer poly(VPAVG) microparticles: *in vitro* and *in vivo* studies. *J. Biomed. Mater. Res. A* **2006**, *78* (2), 343–351.

[35] Kowalczyk, T.; Hnatuszko-Konka, K.; Gerszberg, A.; Kononowicz, A. K. Elastin-like polypeptides as a promising family of genetically-engineered protein based polymers. *World J. Microbiol. Biotechnol.* **2014**, *30* (8), 2141–2152.

[36] Trabbic-Carlson, K.; Liu, L.; Kim, B.; Chilkoti, A. Expression and purification of recombinant proteins from Escherichia coli: Comparison of an elastin-like polypeptide fusion with an oligohistidine fusion. *Protein Sci.* **2004**, *13* (12), 3274–3284.

[37] Varanko, A. K.; Su, J. C.; Chilkoti, A. Elastin-Like Polypeptides for Biomedical Applications. *Annu. Rev. Biomed. Eng.* **2020**, *22*, 343–369.

[38] Berckman, E. A.; Hartzell, E. J.; Mitkas, A. A.; Sun, Q.; Chen, W. Biological Assembly of Modular Protein Building Blocks as Sensing, Delivery, and Therapeutic Agents. *Annu. Rev. Chem. Biomol. Eng.* **2020**, *11*, 35–62.

[39] Hassouneh, W.; MacEwan, S. R.; Chilkoti, A. Fusions of Elastin-Like Polypeptides to Pharmaceutical Proteins. *Methods Enzymol.* **2012**, *502*, 215–237.

[40] Kostal, J.; Mulchandani, A.; Chen, W. Tunable Biopolymers for Heavy Metal Removal. *Macromolecules* **2001**, *34*, 2257–2261.

[41] Suyama, K.; Murashima, M.; Maeda, I.; Nose, T. Enhancement of Aggregate Formation Through Aromatic Compound Adsorption in Elastin-like Peptide $(FPGVG)_5$ Analogs. *Biomacromolecules* **2023**, *24* (11), 5265–5276.

[42] Harris, R.; Veretnik, S.; Dewan, S.; Leshem, A. B.; Lampel, A. Regulation of enzymatic reactions by chemical composition of peptide biomolecular condensates. *Commun. Chem.* **2024**, *7*, 90.

[43] Lim, S.; Clark, D. S. Phase-separated biomolecular condensates for biocatalysis. *Trends Biotechnol.* **2024**, *42* (4), 496–509.

[44] Shapiro, D. M.; Deshpande, S.; Eghtesadi, S. A.; Zhong, M.; Fontes, C. M.; Fiflis, D.; Rohm, D.; Min, J.; Kaur, T.; Peng, J.; Ney, M.; Su, J.; Dai, Y.; Asokan, A.; Gersbach, C. A.; Chilkoti, A. Synthetic biomolecular condensates enhance translation from a target mRNA in living cells. *Nat. Chem.* **2025**, *17*, 448–456.

[45] Nath, N.; Chilkoti, A. Creating "Smart" Surfaces Using Stimuli Responsive Polymers. *Adv. Mater.* **2002**, *14*, 1243–1247.

[46] Hyun, J.; Lee, W.-K.; Nath, N.; Chilkoti, A.; Zauscher, S. Capture and Release of Proteins on the Nanoscale by Stimuli-Responsive Elastin-Like Polypeptide "Switches". *J. Am. Chem. Soc.* 2004, *126* (23), 7330–7335.

[47] Atefyekta, S.; Pihl, M.; Lindsay, C.; Heilshorn, S. C.; Andersson, M. Antibiofilm elastin-like polypeptide coatings: functionality, stability, and selectivity. *Acta Biomater.* **2019**, *83*, 245–256.

[48] Acosta, S.; Chaskovska, V.; El-Maachi, I.; Englert, J.; Puertas-Bartolomé, M.; Jockenhoevel, S.; Rodríguez-Cabello, J. C.; Rodriguez-Emmenegger, C.; Fernández-Colino, A. Bioorthogonal Mussel-Inspired Elastin-like Nanocoatings for Indwelling Devices. *ACS Appl. Mater. Interfaces* **2025**, 17 (36), 50279–50291.

[49] Roberts, S.; Dzuricky, M.; Chilkoti, A. Elastin-like Polypeptides as Models of Intrinsically Disordered Proteins. *FEBS Lett.* **2015**, *589*, 2477–2486.

[50] Juanes-Gusano, D.; Santos, M.; Reboto, V.; Alonso, M.; Rodríguez-Cabello, J. C. Self-Assembling Systems Comprising Intrinsically Disordered Protein Polymers like Elastin-like Recombinamers. *J. Pept. Sci.* **2022**, *28* (1), e3362

[51] Aladini, F.; Araman, C.; Becker, C. F. W. Chemical synthesis and characterization of elastin-like polypeptides (ELPs) with variable guest residues. *J. Pept. Sci.* **2016**, *22*, 334–342.

[52] Urry, D. W.; Gowda, D. C.; Parker, T. M.; Luan, C.-H.; Reid, M. C.; Harris, C. M.; Pattanaik, A.; Harris, R. D. Hydrophobicity scale for proteins based on inverse temperature transitions. *Biopolymers* **1992**, *32* (9), 1243–1250.

[53] Meyer, D. E.; Chilkoti A. Quantification of the Effects of Chain Length and Concentration on the Thermal Behavior of Elastin-like Polypeptides. *Biomacromolecules* **2004**, 5 (3), 846–851.

[54] McDaniel, J. R.; Radford, D. C.; Chilkoti, A. A Unified Model for *De Novo* Design of Elastin-like Polypeptides with Tunable Inverse Transition Temperatures. *Biomacromolecules* **2013**, *14* (8), 2866–2872.

[55] Nuhn, H.; Klok, H.-A. Secondary Structure Formation and LCST Behavior of Short Elastin-Like Peptides. *Biomacromolecules* **2008**, 9 (10), 2755–2763.

[56] Ibrahimova, V.; González-Delgado, J. A.; Levêque, M.; Torres, T.; Garanger, E.; Lecommandoux, S. Photooxidation Responsive Elastin-Like Polypeptide Conjugates for Photodynamic Therapy Application. *Bioconjugate Chem.* **2021**, *32* (8), 1719–1728.

[57] Li, N. K.; Roberts, S.; Quiroz, F. G.; Chilkoti, A.; Yingling, Y. G. Sequence Directionality Dramatically Affects LCST Behavior of Elastin-Like Polypeptides. *Biomacromolecules* **2018**, *19* (7), 2496–2505.

[58] Tatsubo, D.; Suyama, K.; Sakamoto, N.; Tomohara, K.; Taniguchi, S.; Maeda, I.; Nose, T. Determining the Sequence Dependency of Self-Assembly of Elastin-Like Peptides Using Short Peptide Analogues with Shuffled Repetitive Sequences. *Biochemistry* **2023**, *62* (17), 2559–2570.

[59] Ghoorchian, A.; Cole, J. T.; Holland, N. B. Thermoreversible Micelle Formation Using a Three-Armed Star Elastin-like Polypeptide. *Macromolecules* **2010**, *43* (9), 4340–4345.

[60] Ghoorchian, A.; Holland, N. B. Molecular Architecture Influences the Thermally Induced Aggregation Behavior of Elastin-like Polypeptides. *Biomacromolecules* **2011**, *12* (11), 4022–4029.

[61] Ghoorchian, A.; Vandemark, K.; Freeman, K.; Kambow, S.; Holland, N. B.; Streletzky, K. A. Size and Shape Characterization of Thermoreversible Micelles of Three-Armed Star Elastin-Like Polypeptides. *J. Phys. Chem. B* **2013**, *117* (29), 8865–8874.

[62] Mozhdehi, D.; Luginbuhl, K. M.; Dzuricky, M.; Costa, S. A.; Xiong, S.; Huang, F. C.; Lewis, M. M.; Zelenetz, S. R.; Colby, C. D.; Chilkoti, A. Genetically Encoded Cholesterol-Modified Polypeptides. *J. Am. Chem. Soc.* **2019**, *141* (2), 945–951.

[63] Mozhdehi, D.; Luginbuhl, K. M.; Simon, J. R.; Dzuricky, M.; Berger, R.; Varol, H. S.; Huang, F. C.; Buehne, K. L.; Mayne, N. R.; Weitzhandler, I.; Bonn, M.; Parekh, S. H.; Chilkoti, A. Genetically encoded lipid–polypeptide hybrid biomaterials that exhibit temperature-triggered hierarchical self-assembly. *Nat. Chem.* **2018**, *10* (5), 496–505.

[64] Hossain, M. S.; Alam, M. M.; Huang, Z.; Mousazadeh, F.; Sarangi, R.; de Jong, E.; Kolamunna, K. C.; Adhya, A. L.; Hougland, J. L.; Acharya, A.; Mozhdehi, D. Scalable One-Pot Production of Geranylgeranylated Proteins in Engineered Prokaryotes. *Bioconjugate*

Chem. **2025**, *36* (3), 415–423.

[65] Zhang, T.; Peruch, F.; Weber, A.; Bathany, K.; Fauquignon, M.; Mutschler, A.; Schatz, C.; Garbay, B. Solution behavior and encapsulation properties of fatty acid–elastin-like polypeptide conjugates. *RSC Adv.* **2023**, *13*, 2190–2201.

[66] Zhang, Z.; Lynch, C. J.; Huo, Y.; Chakraborty, S.; Cremer, P. S.; Mozhdehi, D. Modulating Phase Behavior in Fatty Acid-Modified Elastin-like Polypeptides (FAMEs): Insights into the Impact of Lipid Length on Thermodynamics and Kinetics of Phase Separation. *J. Am. Chem. Soc.* **2024**, *146* (8), 5383–5392.

[67] Hossain, M. S.; Wang, A.; Anika, S.; Zhang, Z.; Mozhdehi, D. Genetically Engineered Liposwitch-Based Nanomaterials. *Biomacromolecules* **2024**, *25* (12), 8058–8068.

[68] McDaniel, J. R.; Weitzhandler, I.; Prevost, S.; Vargo, K. B.; Appavou, M. S.; Hammer, D. A.; Gradzielski, M.; Chilkoti, A. Noncanonical Self-Assembly of Highly Asymmetric Genetically Encoded Polypeptide Amphiphiles into Cylindrical Micelles. *Nano Lett.* **2014**, *14* (11), 6590–6598.

[69] Jeong, W. J.; Kwon, S. H.; Lim, Y. Modular Self-Assembling Peptide Platform with a Tunable Thermoresponsiveness via a Single Amino Acid Substitution. *Adv. Funct. Mater.* **2018**, *28* (35), 1803114.

[70] Weitzhandler, I.; Dzuricky, M.; Hoffmann, I.; Quiroz, F. G.; Gradzielski, M.; Chilkoti, A. Micellar Self-Assembly of Recombinant Resilin-/Elastin-Like Block Copolypeptides. *Biomacromolecules* **2017**, *18* (8), 2419–2426.

[71] Navarro, L. A.; Ryan, J. J.; Dzuricky, M.; Gradzielski, M.; Chilkoti, A.; Zauscher, S. Microphase Separation of Resilin-like and Elastin-like Diblock Copolypeptides in Concentrated Solutions. *Biomacromolecules* **2021**, *22* (9), 3827–3838.

[72] Basheer, A.; Shahid, S.; Kang, M. J.; Lee, J. H.; Lee, J. S.; Lim, D. W. Switchable Self-Assembly of Elastin- and Resilin-Based Block Copolypeptides with Converse Phase Transition Behaviors. *ACS Appl. Mater. Interfaces* **2021**, 13 (21), 24385–24400.

[73] Luo, T.; Kiick, K. L. Noncovalent Modulation of the Inverse Temperature Transition and Self-Assembly of Elastin-*b*-Collagen-like Peptide Bioconjugates. *J. Am. Chem. Soc.* **2015**, *137* (49), 15362–15365.

[74] Luo, T.; David, M. A.; Dunshee, L. C.; Scott, R. A.; Urello, M. A.; Price, C.; Kiick, K. L. Thermoresponsive Elastin-*b*-Collagen-Like Peptide Bioconjugate Nanovesicles for Targeted Drug Delivery to Collagen-Containing Matrices. *Biomacromolecules* **2017**, *18* (8), 2539–2551.

[75] Qin, J.; Luo, T.; Kiick, K. L. Self-Assembly of Stable Nanoscale Platelets from Designed Elastin-like Peptide–Collagen-like Peptide Bioconjugates. *Biomacromolecules* **2019**, 20 (4), 1514–1521.

[76] Prhashanna, A.; Taylor, P. A.; Qin, J.; Kiick, K. L.; Jayaraman, A. Effect of Peptide Sequence on the LCST-Like Transition of Elastin-Like Peptides and Elastin-Like Peptide–Collagen-Like Peptide Conjugates: Simulations and Experiments. *Biomacromolecules* **2019**, 20 (3), 1178–1189.

[77] Xiao, Y.; Chinoy, Z. S.; Pecastaings, G.; Bathany, K.; Garanger, E.; Lecommandoux, S. Design of Polysaccharide-*b*-Elastin-Like Polypeptide Bioconjugates and Their Thermoresponsive Self-Assembly. *Biomacromolecules* **2020**, *21* (1), 114–125.

[78] Levêque, M.; Xiao, Y.; Durand, L.; Massé, L.; Garanger, E.; Lecommandoux, S. Aqueous synthesis and self-assembly of bioactive and thermo-responsive HA-*b*-ELP bioconjugates. *Biomater. Sci.* **2022**, *10* (22), 6365–6376.

[79] Levêque, M.; Lecommandoux, S.; Garanger, E. Thermoresponsive Core-cross-linked Nanoparticles from HA-*b*-ELP Diblock Copolymers. *Biomacromolecules* **2024**, 25 (5), 3011–3017.

[80] Wang, B.; Pan, R.; Zhu, W.; Xu, Y.; Tian, Y.; Endo, M.; Sugiyama, H.; Yang, Y.; Qian, X. Short intrinsically disordered polypeptide–oligonucleotide conjugates for programmed self-assembly of nanospheres with temperature-dependent size controllability. *Soft Matter* **2021**, *17* (5), 1184–1188.

[81] Wang, B.; Fang, H.; Zhu, W.; Xu, Y.; Yang, Y.; Qian, X. Dynamic Compartmentalization of Peptide–Oligonucleotide Conjugates with Reversible Nanovesicle–Microdroplet Phase Transition Behaviors. *ACS Appl. Mater. Interfaces* **2022**, *14* (32), 36998–37008.

[82] Grazon, C.; Garanger, E.; Lalanne, P.; Ibarboure, E.; Galagan, J. E.; Grinstaff, M. W.; Lecommandoux, S. Transcription-Factor-Induced Aggregation of Biomimetic Oligonucleotide-*b*-Protein Micelles. *Biomacromolecules* **2023**, *24* (11), 5027–5034.

[83] MacKay, J. A.; Callahan, D. J.; FitzGerald, K. N.; Chilkoti, A. Quantitative Model of the Phase Behavior of Recombinant pH-Responsive Elastin-Like Polypeptides. *Biomacromolecules* **2010**, *11* (11), 2873–2879.

[84] de Haas, R. J.; Ganar, K. A.; Deshpande, S.; de Vries, R. pH-Responsive Elastin-Like Polypeptide Designer Condensates. *ACS Appl. Mater. Interfaces* **2023**, *15* (38), 45336–45344.

[85] Luan, C. H.; Parker, T. M.; Prasad, K. U.; Urry, D. W. Differential scanning calorimetry studies of NaCl effect on the inverse temperature transition of some elastin-based polytetra-, polypenta-, and polynonapeptides. *Biopolymers* **1991**, *31* (5), 465–475.

[86] Cho, Y.; Zhang, Y.; Christensen, T.; Sagle, L. B.; Chilkoti, A.; Cremer, P. S. Effects of Hofmeister Anions on the Phase Transition Temperature of Elastin-like Polypeptides. *J. Phys. Chem. B* **2008**, *112* (44), 13765–13771.

[87] Mills, C. E.; Ding, E.; Olsen, B. D. Cononsolvency of Elastin-like Polypeptides in

Water/Alcohol Solutions. *Biomacromolecules* **2019**, *20* (6), 2167–2173.

[88] Zhao, Y.; Singh, M. K.; Kremer, K.; Cortes-Huerto, R.; Mukherji, D. Why Do Elastin-Like Polypeptides Possibly Have Different Solvation Behaviors in Water–Ethanol and Water–Urea Mixtures? *Macromolecules* **2020**, *53* (6), 2101–2110.

[89] Tamura, T.; Yamaoka, T.; Kunugi, S.; Panitch, A.; Tirrell, D. A. Effects of Temperature and Pressure on the Aggregation Properties of an Engineered Elastin Model Polypeptide in Aqueous Solution. *Biomacromolecules* **2000**, 1 (4), 552–555.

[90] Wirtz, B. M.; Yun, A. G.; Wick, C.; Gao, X. J.; Mai, D. J. Protease-Driven Phase Separation of Elastin-Like Polypeptides. *Biomacromolecules* **2024**, 25 (8), 4898–4904.

[91] Meyer, D. E.; Kong, G. A.; Dewhirst, M. W.; Zalutsky, M. R.; Chilkoti, A. Targeting a Genetically Engineered Elastin-like Polypeptide to Solid Tumors by Local Hyperthermia. *Cancer Res.* **2001**, *61* (4), 1548–1554.

[92] Teeuwen, R. L. M.; de Wolf, F. A.; Zuilhof, H.; van Hest, J. C. M. Elastin-like polypeptides of different molecular weights show independent transition temperatures when mixed. *Soft Matter* **2009**, *5*, 4305–4310.

[93] Ge, X.; Hoare, T.; Filipe, C. D. M. Protein-Based Aqueous−Multiphasic Systems. *Langmuir* **2010**, *26* (6), 4087–4094.

[94] Simon, J. R.; Carroll, N. J.; Rubinstein, M.; Chilkoti, A.; López, G. P. Programming molecular self-assembly of intrinsically disordered proteins containing sequences of low complexity. *Nat. Chem.* **2017**, *9*, 509–515.

[95] Cook, W. J.; Einspahr, H.; Trapane, T. L.; Urry, D. W.; Bugg, C. E. Crystal Structure and Conformation of the Cyclic Trimer of a Repeat Pentapeptide of Elastin, *cyclo*-(L-Valyl-L-prolylglycyl-L-valylglycyl)$_3$. *J. Am. Chem. Soc.* **1980**, *102*, 5502–5505.

[96] Urry, D. W.; Shaw, R. G.; Prasad, K. U. Polypentapeptide of elastin: temperature dependence of ellipticity and correlation with elastomeric force. *Biochem. Biophys. Res. Commun*. **1985**, *130* (1), 50–57.

[97] Urry, D. W.; Mitchell, L. W.; Ohnishi, T.; Long, M. M. Proton and carbon magnetic resonance studies of the synthetic polypentapeptide of elastin. *J. Mol. Biol.* **1975**, *96* (1), 101–117.

[98] Urry, D. W.; Trapane, T. L.; Sugano, H.; Prasad, K. U. Sequential Polypeptides of Elastin: Cyclic Conformational Correlates of the Linear Polypentapeptide, *J. Am. Chem. Soc.* **1981**, *103*, 2080–2089.

[99] Venkatachalam, C. M.; Urry, D. M. Development of a Linear Helical Conformation from Its Cyclic Correlate. β-Spiral Model of the Elastin Poly(pentapeptide) (VPGVG)$_n$. *Macromolecules* **1981**, *14* (5), 1225–1229.

[100] Urry, D. W. Entropic elastic processes in protein mechanisms. I. Elastic structure due to

an inverse temperature transition and elasticity due to internal chain dynamics. *J. Protein Chem.* **1988**, *7* (1), 1–34.

[101] Urry, D. W. Entropic elastic processes in protein mechanisms. II. Simple (passive) and coupled (active) development of elastic forces. *J. Protein Chem.* **1988**, *7* (2), 81–114.

[102] Reiersen, H.; Clarke, A. R.; and Anthony R. Rees, Short Elastin-like Peptides Exhibit the Same Temperature-induced Structural Transitions as Elastin Polymers: Implications for Protein Engineering. *J. Mol. Biol.* **1998**, *283*, 255–264.

[103] Glaves, R.; Baer, M.; Schreiner, E.; Stoll, R.; Marx, D. Conformational Dynamics of Minimal Elastin-Like Polypeptides: The Role of Proline Revealed by Molecular Dynamics and Nuclear Magnetic Resonance. *ChemPhysChem* **2008**, *9* (18), 2633–2859.

[104] Nicolini, C.; Ravindra, R.; Ludolph, B.; Winter, R. Characterization of the Temperature- and Pressure-Induced Inverse and Reentrant Transition of the Minimum Elastin-Like Polypeptide GVG(VPGVG) by DSC, PPC, CD, and FT-IR Spectroscopy. *Biophys. J.* **2004**, *86* (3), 1385–1392.

[105] Serrano, V.; Liu, W.; Franzen, S. An Infrared Spectroscopic Study of the Conformational Transition of Elastin-Like Polypeptides. *Biophys J.* **2007**, *93* (7), 2429–2435.

[106] Reichheld, S. E.; Muiznieks, L. D.; Keeley, F. W.; Sharpe, S. Direct Observation of Structure and Dynamics during Phase Separation of an Elastomeric Protein. *Proc. Natl. Acad. Sci. USA* **2017**, *114* (22), E4408–E4415.

[107] Brandis, D.; Kaderavek, P.; Kurzbach, D. The Internal Structural Dynamics of Elastin-Like Polypeptide Assemblies by ^{13}C-Direct Detected NMR Spectroscopy. *Anal. Chem.* **2025**, *97* (7), 3937–3944.

[108] Brandis, D.; Turhan, E.; Zachrdla, M.; Kurzbach, D. Residue-Resolved Liquid-State Hyperpolarized NMR of Peptide Condensate Surfaces. *J. Am. Chem. Soc.* **2025**, *147* (40), 36920–36927.

[109] Maeda, I.; Fukumoto, Y.; Nose, T.; Shimohigashi, Y.; Nezu, T.; Terada, Y.; Kodama, H.; Kaibara, K.; Okamoto, K. Structural Requirements Essential for Elastin Coacervation: Favorable Spatial Arrangements of Valine Ridges on the Three-Dimensional Structure of Elastin-Derived Polypeptide $(VPGVG)_n$. *J. Pept. Sci.* **2011**, *17* (11), 735–743.

[110] Zhang, Y.; Zai-Rose, V.; Price, C. J.; Ezzell, N. A.; Bidwell, G. L.; Correia, J. J.; Fitzkee, N. C. Modeling the Early Stages of Phase Separation in Disordered Elastin-like Proteins. *Biophys. J.* **2018**, *114* (7), 1563–1578.

[111] Barreiro, D. L.; Minten, I. J.; Thies, J. C.; Sagt, C. M. J. Structure–Property Relationships of Elastin-like Polypeptides: A Review of Experimental and Computational Studies. *ACS Biomater. Sci. Eng.* **2023**, *9* (7), 3796–3809.

[112] Li, B.; Alonso, D. O.; Daggett, V. The molecular basis for the inverse temperature

transition of elastin. *J. Mol. Biol.* **2001**, *305* (3), 581–592.

[113] Li, B.; Alonso, D. O. V.; Bennion, B. J.; Daggett, V. Hydrophobic Hydration Is an Important Source of Elasticity in Elastin-Based Biopolymers. *J. Am. Chem. Soc.* **2001**, *123* (48), 11991–11998.

[114] Tarakanova, A.; Huang, W.; Weiss, A. S.; Kaplan, D. L.; Buehler, M. J. Computational smart polymer design based on elastin protein mutability. *Biomaterials* **2017**, *127*, 49–60.

[115] Krukau, A.; Brovchenko, I.; Geiger, A. Temperature-Induced Conformational Transition of a Model Elastin-like Peptide GVG(VPGVG)$_3$ in Water. *Biomacromolecules* **2007**, 8 (7), 2196–2202.

[116] Zhao, B.; Li, N. K.; Yingling, Y. G.; Hall, C. K. LCST Behavior is Manifested in a Single Molecule: Elastin-Like polypeptide (VPGVG)$_n$. *Biomacromolecules* **2016**, 17 (1), 111–118.

[117] Schreiner, E.; Nicolini, C.; Ludolph, B.; Ravindra, R.; Otte, N.; Kohlmeyer, A.; Rousseau, R.; Winter, R.; Marx, D. Folding and Unfolding of an Elastinlike Oligopeptide: "Inverse Temperature Transition," Reentrance, and Hydrogen-Bond Dynamics. *Phys. Rev. Lett.* **2004**, *92* (14), 148101.

[118] Rousseau, R.; Schreiner, E.; Kohlmeyer, A.; Marx, D. Temperature-Dependent Conformational Transitions and Hydrogen-Bond Dynamics of the Elastin-Like Octapeptide GVG(VPGVG): A Molecular-Dynamics Study. *Biophys. J.* **2004**, *86* (3), 1393–1407.

[119] Baer, M.; Schreiner, E.; Kohlmeyer, A.; Rousseau, R.; Marx, D. Inverse Temperature Transition of a Biomimetic Elastin Model: Reactive Flux Analysis of Folding/Unfolding and Its Coupling to Solvent Dielectric Relaxation. *J. Phys. Chem. B* **2006**, *110* (8), 3576–3587.

[120] Li, N. K.; Quiroz, F. G.; Hall, C. K.; Chilkoti, A.; Yingling, Y. G. Molecular Description of the LCST Behavior of an Elastin-Like Polypeptide. *Biomacromolecules* **2014**, *15* (10), 3522–3530.

[121] Li, N. K.; Xie, Y.; Yingling, Y. G. Insights into Structure and Aggregation Behavior of Elastin-like Polypeptide Coacervates: All-Atom Molecular Dynamics Simulations. *J. Phys. Chem. B* **2021**, *125* (30), 30, 8627–8635.

[122] Morozova, T. I.; García, N. A.; Matsarskaia, O.; Roosen-Runge, F.; Barrat, J. L. Structural and Dynamical Properties of Elastin-Like Peptides near Their Lower Critical Solution Temperature. *Biomacromolecules* **2023**, *24* (4), 1912–1923.

[123] Morozova, T. I.; García, N. A.; Barrat, J. L. Sequence Length Controls Coil-to-Globule Transition in Elastin-like Polypeptides. *J. Phys. Chem. Lett.* **2024**, *15* (43), 10757–10762.

[124] Rauscher, S.; Pomès, R. The Liquid Structure of Elastin. *eLife* **2017**, *6*, e26526.

[125] Baul, U.; Bley, M.; Dzubiella, J. Thermal Compaction of Disordered and Elastin-like Polypeptides: A Temperature-Dependent, Sequence-Specific Coarse-Grained Simulation Model. *Biomacromolecules* **2020**, *21* (9), 3523–3538.

[126] Mabuchi, T.; Kijima, J.; Yamashita, Y.; Miura, E.; Muraoka, T. Coacervate Formation of Elastin-like Polypeptides in Explicit Aqueous Solution Using Coarse-Grained Molecular Dynamics Simulations. *Macromolecules* **2023**, *56* (3), 794–805.

[127] Mukherjee, P.; Nanavare, P.; Chakrabarti, R. Coacervation of Elastin-Like Polypeptides: A Coarse-Grained Perspective. *J. Chem. Theory Comput.* **2025**, *21* (15), 7701–7710.

[128] MacEwan, S. R.; Chilkoti, A. Applications of elastin-like polypeptides in drug delivery. *J. Control. Release* **2014**, *190*, 314–330.

[129] Jenkins, I. C.; Milligan, J. J.; Chilkoti, A. Genetically Encoded Elastin-Like Polypeptides for Drug Delivery. *Adv. Healthc. Mater.* **2021**, *10* (13), 2100209.

[130] Rodríguez-Cabello, J. C.; Arias, F. J.; Rodrigo, M. A.; Girotti, A. Elastin-like polypeptides in drug delivery. *Adv. Drug Deliv. Rev.* **2016**, *97*, 85–100.

[131] Strohl, W. R. Fusion Proteins for Half-Life Extension of Biologics as a Strategy to Make Biobetters. *BioDrugs* **2015**, *29* (4), 215–239.

[132] Phan, A.; MacKay, J. A. Steric stabilization of bioactive nanoparticles using elastin-like polypeptides. *Adv. Drug Deliv. Rev.* **2024**, *206*, 115189.

[133] MacKay, J. A.; Chen, M.; McDaniel, J. R.; Liu, W.; Simnick, A. J.; Chilkoti, A. Self-assembling chimeric polypeptide–doxorubicin conjugate nanoparticles that abolish tumours after a single injection. *Nat. Mater.* **2009**, *8*, 993–999.

[134] Amiram, M.; Luginbuhl, K. M.; Li, X.; Feinglos, M. N.; Chilkoti, A. A depot-forming glucagon-like peptide-1 fusion protein reduces blood glucose for five days with a single injection. *J. Control. Release* **2013**, *172* (1), 144–151.

[135] Li, Z.; Sreekumar, P. G.; Peddi, S.; Hinton, D. R.; Kannan, R.; MacKay, J. A. The humanin peptide mediates ELP nanoassembly and protects human retinal pigment epithelial cells from oxidative stress. *Nanomed.: Nanotechnol. Biol. Med.* **2020**, *24*, 102111.

[136] Bidwell III, G. L.; Raucher, D. Cell penetrating elastin-like polypeptides for therapeutic peptide delivery. *Adv. Drug Deliv. Rev.* **2010**, *62* (15), 1486–1496.

[137] Kim, D. W.; Smith, J. T.; Chilkoti, A.; Reichert, W. M. The effect of covalently immobilized rhIL-1ra-ELP fusion protein on the inflammatory profile of LPS-stimulated human monocytes. *Biomaterials* **2007**, *28* (23), 3369–3377.

[138] Patel, J.; Zhu, H.; Menassa, R.; Gyenis, L.; Richman, A.; Brandle, J. Elastin-like polypeptide fusions enhance the accumulation of recombinant proteins in tobacco leaves. *Transgenic Res.* **2007**, *16*, 239–249.

[139] Shamji,M. F.; Betre, H.; Kraus, V. B.; Chen, J.; Chilkoti, A.; Pichika, R.; Masuda, L.; Setton, L. A. Development and characterization of a fusion protein between thermally responsive elastin-like polypeptide and interleukin-1 receptor antagonist: Sustained release of a local antiinflammatory therapeutic. *Arthritis Rheum.* **2007**, *56* (11), 3650–3661.

[140] Kaldis, A.; Ahmad, A.; Reid, A.; McGarvey, B.; Brandle, J.; Ma, S.; Jevnikar, A.; Kohalmi, S. E.; Menassa, R. High-level production of human interleukin-10 fusions in tobacco cell suspension cultures. *Plant Biotechnol. J.* **2013**, *11* (5), 535–545.

[141] Gonçalves, A.; Pinho, V.; da Costa, A.; Ribeiro, A.; Gomes, A. C.; Machado, R. Elastin-like Recombinamers as a Biotechnological Platform for the Development of Cytokine-Functionalized Materials. *ACS Omega* **2024**, *9* (47), 46733–46742.

[142] Gong, L.; Yang, Z.; Zhang, F.; Gao, W. Cytokine conjugates to elastin-like polypeptides, *Adv. Drug Deliv. Rev.* **2022**, *190*, 114541

[143] Li, F.; Wang, Q.; Wang, T.; Xiong, C.; Chen, Z.; Ouyang, H.; Lou, X.; Xia, F.; Wang, S.; Wu, M.; Dai, J. Elastin-like peptides for efficient and safe delivery of mRNA. *J. Control. Release* **2025**, *388*, 114337.

[144] Yi, A.; Sim, D.; Lee, Y. J.; Sarangthem, V.; Park, R. W. Development of elastin-like polypeptide for targeted specific gene delivery in vivo. *J. Nanobiotechnol.* **2020**, *18*, 15.

[145] Aayush, A.; Darji, S.; Estes, K. M.; Yeh, E.; Thompson, D. H. Development of an Elastin-like Polypeptide-Based Nucleic Acid Delivery System Targeted to EGFR+ Bladder Cancer Cells Using a Layer-by-Layer Approach. *Biomacromolecules* **2024**, *25* (9), 5729–5744.

[146] Conrad, U.; Plagmann, I.; Malchow, S.; Sack, M.; Floss, D. M.; Kruglov, A. A.; Nedospasov, S. A.; Rose-John, S.; Scheller, J. ELPylated anti-human TNF therapeutic single-domain antibodies for prevention of lethal septic shock. *Plant Biotechnol. J.* **2011**, *9*, 22–31.

[147] Floss, D. M.; Sack, M.; Arcalis, E.; Stadlmann, J.; Quendler, H.; Rademacher, T.; Stoger, E.; Scheller, J.; Fischer, R.; Conrad, U. Influence of elastin-like peptide fusions on the quantity and quality of a tobacco-derived human immunodeficiency virus-neutralizing antibody. *Plant Biotechnol. J.* **2009**, *7*, 899–913.

[148] Pille, J.; van Lith, S. A. M.; van Hest, J. C. M.; Leenders, W. P. J. Self-Assembling VHH-Elastin-Like Peptides for Photodynamic Nanomedicine. *Biomacromolecules* **2017**, *18* (4), 1302–1310.

[149] Yao, Q.; Zhang, F.; Yang, Z.; Sun, Y.; Gao, W. A super-long-acting anti-PD-L1 nanobody fused to elastin-like polypeptide for triple-negative breast cancer immunotherapy. *J. Control. Release* **2025**, *385*, 114002.

[150] Vu, C. Q.; Arai, S. A Thermogenetic Tool Employing Elastin-like Polypeptides for Controlling Programmed Cell Death. *ACS Nano* **2025**, *19* (36), 32280–32290.

[151] Christensen, T.; Hassouneh, W.; Trabbic-Carlson, K.; Chilkoti, A. Predicting Transition Temperatures of Elastin-Like Polypeptide Fusion Proteins. *Biomacromolecules* **2013**, *14* (5), 1514–1519.

[152] Addai, F. P.; Wang, T.; Kosiba, A. A.; Lin, F.; Zhen, R.; Chen, D.; Gu, J.; Shi, H.; Zhou,

Y. Integration of elastin-like polypeptide fusion system into the expression and purification of *Lactobacillus* sp. B164 β-galactosidase for lactose hydrolysis. *Bioresour. Technol*. **2020**, *311*, 123513.

[153] Wang, S.; Lin, R.; Ren, Y.; Zhang, T.; Lu, H.; Wang, L.; Fan, D. Non-chromatographic purification of thermostable endoglucanase from *Thermotoga maritima* by fusion with a hydrophobic elastin-like polypeptide. *Protein Expr. Purif.* **2020**, *173*, 105634.

[154] Yang, K.; Su, Y.; Li, J.; Sun, J.; Yang, Y. Expression and purification of the antimicrobial peptide cecropin AD by fusion with cationic elastin-like polypeptides. *Protein Expr. Purif.* **2012**, *85* (2), 200–203.

[155] Conley, A. J.; Joensuu, J. J.; Jevnikar, A. M.; Menassa, R.; Brandle, J. E. Optimization of elastin-like polypeptide fusions for expression and purification of recombinant proteins in plants. *Biotechnol. Bioeng.* **2009**, *103* (3), 562–573.

[156] Heidari-Japelaghi, R.; Haddad, R.; Valizadeh, M.; Dorani-Uliaie, E.; Jalali-Javaran, M. Elastin-like polypeptide fusions for high-level expression and purification of human IFN-γ in *Escherichia coli*. *Anal. Biochem.* **2019**, *585*, 113401.

[157] Heidari-Japelaghi, R.; Valizadeh, M.; Haddad, R.; Dorani-Uliaie, E.; Jalali-Javaran, M. Fusion to elastin-like polypeptide increases production of bioactive human IFN-γ in tobacco. *Transgenic Res.* **2020**, *29*, 381–394.

[158] Akbari, N.; Haddad, R.; Heidari-Japelaghi, R; Gheibi, N. Improving the Accumulation and Solubility of Human Interferon-γ (hIFN-γ) in *Escherichia coli*: A Fusion Protein-Based Method and Network Pharmacology Analysis. *Appl. Biochem. Biotechnol.* **2025**, *197*, 6169–6201.

[159] Yang, C. G.; Lang, M. F.; Fu, X.; Lin, H.; Zhang, L. C.; Ge, G. S.; Sun, J.; Hu, X. J. Application of short hydrophobic elastin-like polypeptides for expression and purification of active proteins. *3 Biotech* **2020**, *10*, 156.

[160] Wang, W.; Wang, Y.; Xia, Z.; Hao, G.; Tuffour, A.; Yan, L.; Chen, J.; Zhu, Y.; Lin, F.; Zhou, Y. Enhancing the Purification and Stability of Superoxide Dismutase by Fusion with Thermoresponsive Self-Assembly of Elastin Like Polypeptide. *ChemistrySelect* **2024**, *9* (4), e202401100.

[161] Bhardwaj, R.; Mishra, P. Multiresponsive Nanoscale Self-Assembly of Azurin-Elastin-like Polypeptide Fusion Protein for Enhanced Prostate Cancer Therapy. *Biomacromolecules* **2024**, *25* (1), 508–521.

[162] Meyer, D. E.; Chilkoti, A. Purification of recombinant proteins by fusion with thermally-responsive polypeptides. *Nat. Biotechnol.* **1999**, *17*, 1112–1115.

[163] Trabbic-Carlson, K.; Meyer, D. E.; Liu, L.; Piervincenzi, R.; Nath, N.; LaBean, T.; Chilkoti, A. Effect of protein fusion on the transition temperature of an environmentally

responsive elastin-like polypeptide: a role for surface hydrophobicity? *Protein Eng. Des. Sel.* **2004**, *17* (1), 57–66.

[164] Meyer, D. E.; Trabbic-Carlson, K.; Chilkoti, A. Protein Purification by Fusion with an Environmentally Responsive Elastin-Like Polypeptide: Effect of Polypeptide Length on the Purification of Thioredoxin. *Biotechnol. Prog.* **2001**, *17* (4), 720–728.

[165] Christensen, T.; Amiram, M.; Dagher, S.; Trabbic-Carlson, K.; Shamji, M. F.; Setton, L. A.; Chilkoti, A. Fusion order controls expression level and activity of elastin-like polypeptide fusion proteins. *Protein Sci.* **2009**, *18* (7), 1377–1387.

[166] Lan, D.; Huang, G.; Shao, H.; Zhang, L.; Ma, L.; Chen, S.; Xu. A. An improved nonchromatographic method for the purification of recombinant proteins using elastin-like polypeptide-tagged proteases. *Anal. Biochem.* **2011**, *415* (2), 200–202.

[167] Zhang, J.; Ma, L.; Zhang, S. Q. Expression and purification of soluble human APRIL in Escherichia coli using ELP-SUMO tag. *Protein Expr. Purif.* **2014**, *95*, 177–181.

[168] Bellucci, J. J.; Amiram, M.; Bhattacharyya, J.; McCafferty, D.;Chilkoti, A. Three-in-One Chromatography-Free Purification, Tag Removal, and Site-Specific Modification of Recombinant Fusion Proteins Using Sortase A and Elastin-like Polypeptides. *Angew. Chem. Int. Ed.* **2013**, *52* (13), 3703–3708.

[169] Ge, X.; Yang, D. S. C.; Trabbic-Carlson, K.; Kim, B.; Chilkoti, A.; Filipe, C. D. M. Self-Cleavable Stimulus Responsive Tags for Protein Purification without Chromatography. *J. Am. Chem. Soc.* **2005**, *127* (32), 11228–11229.

[170] Mee, C.; Banki, M. R.; Wood, D. W. Towards the elimination of chromatography in protein purification: Expressing proteins engineered to purify themselves. *Chem. Eng. J.* **2008**, *135*, 56–62.

[171] Chong, S.; Mersha, F. B.; Comb, D. G.; Scott, M. E.; Landry, D.; Vence, L. M.; Perler, F. B.; Benner, J.; Kucera, R. B.; Hirvonen, C. A.; Pelletier, J. J.; Paulus, H.; Xu, M. Q. Single-column purification of free recombinant proteins using a self-cleavable affinity tag derived from a protein splicing element. *Gene* **1997**, *192* (2), 271–281.

[172] Kim, J. Y.; O'Malley, S.; Mulchandani, A.; Chen, W. Genetically Engineered Elastin-Protein A Fusion as a Universal Platform for Homogeneous, Phase-separation Immunoassay. *Anal. Chem*. **2005**, *77* (8), 2318–2322.

[173] Sheth, R. D.; Madan, B.; Chen, W.; Cramer, S. M. High-throughput screening for the development of a monoclonal antibody affinity precipitation step using ELP-z stimuli responsive biopolymers. *Biotechnol. Bioeng.* **2013**, *110* (10), 2664–2676.

[174] Sheth, R. D.; Jin, M. Bhut, B. V.; Li, Z.; Chen, W.; Cramer, S. M. Affinity precipitation of a monoclonal antibody from an industrial harvest feedstock using an ELP-Z stimuli responsive biopolymer. *Biotechnol. Bioeng.* **2014**, *111* (8), 1595–1603.

[175] Sheth, R. D.; Bhut, B. V.; Jin, M.; Li, Z.; Chen, W.; Cramer, S. M. Development of an ELP-Z based mAb affinity precipitation process using scaled-down filtration techniques. *J. Biotechnol.* **2014**, *192*, 11–19.

[176] Swartz, A. R.; Xu, X.; Traylor, S. J.; Li, Z. J.; Chen, W. High-efficiency affinity precipitation of multiple industrial mAbs and Fc-fusion proteins from cell culture harvests using Z-ELP-E2 nanocages. *Biotechnol. Bioeng.* **2018**, *115* (8), 2039–2047.

[177] Swartz, A. R.; Xu, X.; Traylor, S. J.; Li, Z. J.; Chen, W. One-step affinity capture and precipitation for improved purification of an industrial monoclonal antibody using Z-ELP functionalized nanocages. *Biotechnol. Bioeng.* **2018**, *115* (2), 423–432.

[178] Mullerpatan, A.; Chandra, D.; Kane, E.; Karande, P.; Cramer, S. Purification of proteins using peptide-ELP based affinity precipitation. *J. Biotechnol*. **2020**, *309*, 59–67.

[179] Kostal, J.; Mulchandani, A.; Gropp, K. E.; Chen, W. A Temperature Responsive Biopolymer for Mercury Remediation. *Environ. Sci. Technol.* **2003**, *37* (19), 4457–4462.

[180] Prabhukumar, G.; Matsumoto, M.; Mulchandani, A.; Chen, W. Cadmium Removal from Contaminated Soil by Tunable Biopolymers. *Environ. Sci. Technol.* **2004**, *38* (11), 3148–3152.

[181] Chu, H. S.; Ryum, J.; Won, J, I. Cadmium detection by a thermally responsive elastin copolymer with metal-binding functionality. *Enzyme Microb. Technol.* **2013**, *53* (3), 189–193.

[182] Choi, H.; Han, S. J.; Won, J. I. Thermal characteristics and cadmium binding behavior of EC-ELP fusion polypeptides. *Enzyme Microb. Technol.* **2020**, *140*, 109628.

[183] Suyama, K.; Mawatari, M.; Tatsubo, D.; Maeda, I.; Nose, T. Simple Regulation of the Self-Assembling Ability by Multimerization of Elastin-Derived Peptide $(FPGVG)_n$ Using Nitrilotriacetic Acid as a Building Block. *ACS Omega* **2021**, 6 (8), 5705–5716.

[184] Sumiyoshi, S.; Suyama, K.; Tatsubo, D.; Tanaka, N.; Tomohara, K.; Taniguchi, S.; Maeda, I.; Nose, T. Metal ion scavenging activity of elastin-like peptide analogues containing a cadmium ion binding sequence. *Sci. Rep.* **2022**, *12*, 1861.

[185] Sumiyoshi, S.; Suyama, K.; Tanaka, N.; Andoh, T.; Nagata, A.; Tomohara, K.; Taniguchi, S.; Maeda, I.; Nose, T. Development of truncated elastin-like peptide analogues with improved temperature-response and self-assembling properties. *Sci. Rep.* **2022**, *12*, 19414.

[186] Leshem, A. B.; Sloan-Dennison, S.; Massarano, T.; Ben-David, S.; Graham, D.; Faulds, K.; Gottlieb, H. E.; Chill, J. H.; Lampel, A. Biomolecular condensates formed by designer minimalistic peptides. *Nat. Commun*. **2023**, *14*, 421.

Table 1-1. Effects of representative factors and variations on T_t of ELPs.

Category	Factor	Typical variation	Effect on T_t or temperature-responsiveness	Representative references	Related chapters in this study
Intrinsic factors	Amino acid composition	Higher hydrophobicity	Lower T_t	[18, 51−56]	
		Higher hydrophilicity	Higher T_t		
	Chain length	Longer chains	Lower T_t	[53−55]	Chapter 2−5
		Shorter chains	Higher T_t		
	ELP concentration	Higher ELP concentration	Lower T_t	[53−55]	Chapter 2−4
	Sequence patterns	Regular repeats of (Val-Pro-Gly-Val-Gly) or variants	LCST-type behavior	[57,58,121]	
		Randomized sequences	LCST-type behavior or loss of reversibility		
	Molecular architecture	Branched architectures	LCST- and/or UCST-type behavior	[24–32,59–61]	Chapter 2−5
	End-group modification	Hydrophobic groups	Lower T_t	[62−82]	Chapter 2
		Hydrophilic groups	Higher T_t		
		Conjugation with other polymers	Varied thermoresponsive behavior depending on the conjugated molecule		

Table 1-1. Effects of representative factors and variations on T_t of ELPs (continued).

Category	Factor	Typical variation	Effect on T_t or temperature-responsiveness	Representative references	Related chapters in this study
Extrinsic factors	pH	Higher net charge	Higher T_t	[83,84]	Chapter 2
	Salt	Salt type, concentration	Varied T_t	[51,55,85,86]	Chapter 2 and 4
		High concentration	Lower T_t		
	Solvent	Use of organic cosolvent	Varied T_t, emergence of UCST-type behavior	[87,88]	
	Coexisting ELPs	Mixtures of ELPs with similar composition or chain length	Mixed coacervates	[60, 91–94]	Chapter 4
		Mixtures of ELPs with dissimilar composition or chain length	Stepwise LCST-type behavior		

Representative factors and their variations influencing the temperature-responsive behavior of ELPs are summarized. Factors particularly relevant to this study are indicated with chapter numbers.

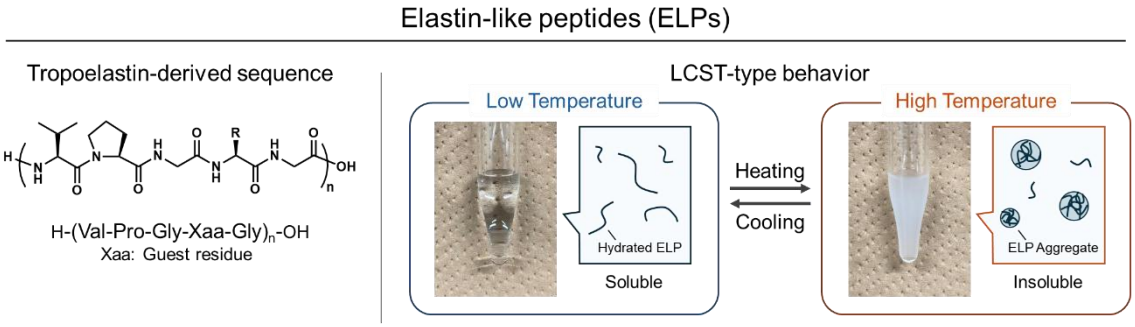

Figure 1-1. Schematic illustration of the LCST-type behavior of ELPs.

A representative structure of ELPs, photographs, and schematic illustrations of their reversible phase behavior are shown.

Chapter 2

Development of covalent two- to four-armed short-chain ELPs via EDTA-mediated multimerization and investigation of their temperature-responsive behavior

This chapter is based on the manuscript published in *J. Pept. Sci.* **2023**, *29* (2), e3449.

Abstract

Elastin-like peptides (ELPs) are artificial polypeptides inspired by amino acid sequences of elastin and are widely used as thermoresponsive building blocks because they undergo a reversible lower critical solution temperature (LCST)-type phase transition (coacervation), remaining soluble at low temperatures and forming coacervates upon heating. Short-chain ELPs are particularly attractive because they are readily accessible by chemical synthesis, which enables position-specific incorporation of canonical and noncanonical residues (including D-amino acids) and allows rapid sequence optimization. At the same time, however, very short ELPs often fail to show apparent LCST-type behavior under practical conditions, limiting their direct use. Here, we address this limitation by covalently multimerizing the short $(FPGVG)_n$ as motifs (n = 1 or 2; termed F1 and F2) with ethylenediaminetetraacetic acid (EDTA), a tetracarboxylate scaffold, to generate branched two- to four-armed ELP analogs. Turbidity measurements demonstrated that the EDTA-linked multimers (four F1 arms or two to four F2 arms) exhibited coacervation in aqueous media, whereas the corresponding linear F1 and F2 building blocks did not. Circular dichroism spectroscopy indicated reversible temperature-dependent secondary structural changes that were comparable to those of linear $(FPGVG)_4$. Dynamic light scattering and microscopy further revealed a stepwise aggregation pathway in which small aggregates formed at lower temperatures matured into larger spherical particles upon heating. Together, these results show that the EDTA-mediated simple multimerization converts nonresponsive short ELP motifs into practical thermoresponsive molecules, providing an accessible route to peptide tags for engineering thermoresponsive biomaterials with diverse functionalities.

1. Introduction

Stimuli-responsive materials can alter their structure and macroscopic properties in response to internal or external environmental stimuli, and they are therefore of broad interest for bioengineering and biomedical applications [1,2]. One of the prominent examples is elastin-like peptides (ELPs), synthetic polypeptides that mimic the repeating motifs found in (tropo)elastin. ELPs show a reversible soluble-to-insoluble transition upon temperature changes, which is commonly described as an LCST-type phase transition or coacervation: at low temperatures they are soluble while at high temperature they become insoluble. This thermally triggered assembly/disassembly has enabled ELP-based platforms for a range of applications, including temperature-responsive drug delivery, metal scavenging, and protein separation [3–10].

For such applications, it is essential to tune their LCST-type behavior so that phase transitions occur at desired temperatures (for example, near physiological temperature for drug delivery systems). The LCST-type behavior of ELPs depends on multiple parameters, including repeat number, amino acid composition, peptide concentration, pH, and ionic strength [11–18]. Compared to long-chain ELPs, short-chain variants offer practical advantages, that is, they can be synthesized efficiently by solid-phase methods, allowing site-specific substitutions or incorporations at any position (including noncanonical residues), and the effects of these changes are often reflected clearly in their temperature-responsive properties. However, expanding the utility of short-chain ELPs requires both new molecular designs and a deeper understanding of how their sequence and architecture govern coacervation.

The most prevalent elastin motif in vertebrates is Val-Pro-Gly-Val-Gly (VPGVG) [19–21], and its repetition, $(VPGVG)_n$, is commonly used as long-chain ELPs with n on the order of 40 (approximately 200 residues) to achieve robust LCST-type transitions for ELP-fused recombinant proteins [22–25]. In contrast, Maeda and co-workers developed an analog based on the Phe-Pro-Gly-Val-Gly motif and showed that $H\text{-}(FPGVG)_n\text{-}NH_2$ (Fn, where n represents repetition number) can exhibit apparent coacervation with fewer repeats (n = 5) than typical VPGVG-based ELPs [26]. Subsequent studies demonstrated that branched, dimeric and trimeric Fn analogs exhibited coacervation at lower temperatures and concentrations compared to the monomeric building block peptides [27,28]. Importantly, such multimerization represents a convergent strategy that can reduce repetitive coupling/deprotection steps compared with synthesizing a linear chain of the same overall length, offering a potentially greener and more economical route to temperature-responsive materials [29].

Because the self-assembly propensity of multichain ELPs increases with the number of peptide arms [28], it was hypothesized that even short Fn chains could be rendered thermoresponsive through covalent multimerization. Therefore, in this chapter, F1 and F2 (n = 1 and 2, respectively), which are shorter than those used in previous research, are multimerized

using ethylenediaminetetraacetic acid (EDTA) as a four-arm linker to prepare dimeric, trimeric, and tetrameric short-chain Fn analogs. The temperature-responsive behavior of the synthesized multimers is characterized by turbidimetry and further examined for their temperature-dependent secondary structure, size distributions, and aggregate morphology using circular dichroism spectroscopy, dynamic light scattering, and microscopy.

2. Materials and Methods

Chemicals. 9-Fluorenylmethyloxycarbonyl (Fmoc)-protected amino acids, Fmoc-NH-SAL-MBHA resin (100–200 mesh), *N,N*-diisopropylethylamine (DIPEA), piperidine, trifluoroacetic acid (TFA), 4-(4,6-dimethoxy-1,3,5-triazin-2-yl)-4-methylmorpholinium chloride (DMT-MM), and 1-[(1-(cyano-2-ethoxy-2-oxoethylideneaminooxy) dimethylamino-morpholino)] uronium hexafluorophosphate (COMU) were obtained from Watanabe Chemical Industries (Hiroshima, Japan). 2-(1H-benzotriazole-1-yl)-1,1,3,3-tetramethyl uronium hexafluorophosphate (HBTU) and 1-hydroxybenzotriazole (HOBt) were purchased from Kokusan Chemical (Tokyo, Japan). Triisopropylsilane (TIS), EDTA, and 4-dimethylaminopyridine (DMAP) were purchased from Tokyo Chemical Industry (Tokyo, Japan). Triethylamine (TEA) was purchased from Wako Pure Chemical Industries (Osaka, Japan). *N*,*N*-dimethylformamide (DMF) was purchased from Nacalai Tesque (Kyoto, Japan). Ultrapure water was prepared using a Milli-Q Integral 3 (Merck Millipore, Darmstadt, Germany). All other solvents and reagents were obtained from commercial suppliers and used as received.

Peptide synthesis. Linear short-chain ELPs, H-(FPGVG)$_n$-NH$_2$ (n = 1 or 2; denoted as F1 and F2, respectively), were synthesized by the Fmoc-based solid-phase peptide synthesis using an ABI 433A peptide synthesizer (Applied Biosystems, Foster City, CA), using HBTU/HOBt for coupling. After cleavage of the target peptides with 5 mL of a mixture of 95% TFA, 2.5% TIS, and 2.5% H_2O, the resulting TFA solution was purified using a Sep-Pak Vac 35 cc C8 cartridge (Waters Co., Milford, MA) with MeCN/H_2O as the eluent, and then the ELPs were lyophilized. The purity and molecular weight of the ELPs were confirmed by UPLC (ACQUITY UPLC H-Class, Waters) equipped with an ACQUITY UPLC BEH C-18 column (100 mm; flow rate 0.6 mL/min). The UPLC mobile phases were 0.1% formic acid in water (v/v, solvent A) and 0.1% formic acid in MeCN (v/v, solvent B), and the gradient was 10–50% solvent B over 4.51 min. The resulting F1 and F2 were used as building blocks for EDTA-linked multimers. In addition, *N*-acetylated F2 (AcF2) was prepared by stirring F2 with acetic anhydride and DIPEA, followed by quenching with water. AcF2 was purified by a Sep-Pak C8 cartridge and reverse-phase HPLC (RP-HPLC). For the solvent system of RP-HPLC, 0.1% TFA in water (v/v, solvent C) and a

mixture of 80% MeCN/20% solvent C (v/v, solvent D) were used. Purity and molecular weight of AcF2 were confirmed by UPLC-MS.

Tetrameric F1 (EDTA-4F1) was obtained by conjugating EDTA (0.035 mmol, 1 eq) and F1 (0.17 mmol, 4.9 eq) in DMF using COMU (0.28 mmol, 8.0 eq) and TEA (0.25 mmol, 7.1 eq). The mixture was stirred at 0 °C for 1 h and then at 25 °C overnight, followed by purification using a Sep-Pak Vac 35 cc C8 cartridge and RP-HPLC. Multimeric F2 analogs, EDTA-mF2 (m = 2–4, where m is the number of F2 chains conjugated to an EDTA molecule), were synthesized as follows. For EDTA-4F2 and EDTA-3F2, EDTA (0.014 mmol, 1 eq), F2 (0.065 mmol, 4.6 eq), COMU (0.067 mmol, 4.8 eq), and TEA (0.078 mmol, 5.6 eq) were stirred in DMF at 0 °C for 1 h and then at 25 °C overnight, and products were purified by Sep-Pak and RP-HPLC. For EDTA-2F2, EDTA (0.010 mmol, 1.0 eq), F2 (0.020 mmol, 2.0 eq), DMT-MM (0.040 mmol, 4.0 eq), TEA (0.040 mmol, 4.0 eq), and DMAP (0.49 mg) were stirred in water at 25 °C overnight. The solution was concentrated and purified using a Sep-Pak Vac 12 cc C18 cartridge followed by RP-HPLC. Molecular weights and purities of the multimers were analyzed by UPLC-MS using a 24–56% solvent B gradient over 4.23 min. To assist structural assignment of EDTA-derived EDTA-2F2, a dimer was synthesized from EDTA dianhydride (0.021 mmol, 1 eq) and F2 (0.045 mmol, 2.1 eq) in DMF at 25 °C overnight, and the product was isolated by RP-HPLC (62% yield). For UPLC-MS comparison, equal volumes of aqueous solutions (0.1 mg/mL) of the dimers prepared from EDTA and EDTA dianhydride were mixed.

Turbidity measurement. LCST-type behavior and its reversibility were evaluated by monitoring turbidity at 400 nm with a JASCO V-660 spectrophotometer (JASCO, Tokyo, Japan). Peptides were dissolved in phosphate buffer (pH 2.0, 7.4, or 12; $\mu = 0.100$) or in phosphate buffer (pH 7.0) containing 3.5% NaCl (w/v) corresponding to seawater salinity (0.60 M NaCl). To examine the influence of divalent ions, turbidity was also measured for EDTA-2F2 in saline containing Cu^{2+} (14 mM; equimolar to EDTA-2F2 at 30 mg/mL). Concentrations were set based on the solubility of each peptide. Temperature was ramped at 0.5 °C/min during both heating and cooling, starting from 0 °C for EDTA-4F2 and from 5 °C for the other peptides. The transition temperature (T_t) was defined as the temperature at which turbidity reached half of its maximum value on heating. The measurements were performed at least three times.

Circular dichroism (CD) measurement. CD spectra were collected on a J-725 spectropolarimeter (JASCO) using a 1.0 mm path-length cuvette. Samples (0.1 mg/mL) were prepared in phosphate buffer (pH 7.4; $\mu = 0.100$), under which no obvious aggregation occurred. Spectra were recorded from 190 to 260 nm at temperatures between 5 and 45 °C with 10 °C

intervals, after 3 min equilibration at the target temperature. After subtracting the background spectra, the resulting spectra were smoothed using Savitzky–Golay filtering.

Dynamic light scattering (DLS) measurement. Hydrodynamic size distributions of EDTA-mF2 in phosphate buffer (pH 7.4; μ = 0.100) were measured using a Zetasizer Nano ZS (Malvern Instruments, Worcestershire, U.K.) with ZEN0112 cells. Temperature was increased in 10 °C steps from 5 to 35 °C for EDTA-4F2 (3 mg/mL, 0.76 mM) and from 15 to 55 °C for EDTA-3F2 (10 mg/mL, 3.3 mM) and EDTA-2F2 (30 mg/mL, 14 mM). The measurement duration and attenuation were automatically selected. The 'protein' material parameters (refractive index 1.450; absorption 0.001) and 'water' dispersant parameters (refractive index 1.330; viscosity 0.8872) were used.

Bright-field microscopy. Aggregate formation was visualized on a Leica DM IL LED microscope (Leica Microsystems, Wetzlar, Germany) equipped with a HI PLAN 40× oil objective and an HC PLAN 10× eyepiece. Samples were prepared in phosphate buffer at 3 mg/mL (0.76 mM) for EDTA-4F2, 10 mg/mL (3.3 mM) for EDTA-3F2, and 30 mg/mL (14 mM) for EDTA-2F2. Then, 40 μL of the sample was placed on a glass slide and observed below and above T_t using a temperature-controlled stage (Thermo Plate TP-CHSQM; Tokai Hit, Shizuoka, Japan).

Scanning electron microscopy (SEM) analysis. Morphologies of air-dried aggregates/residuals were examined using a JSM-IT700HR InTouchScope (JEOL, Tokyo, Japan) at an operating voltage of 10.0 kV. EDTA-4F2 and F2 were dissolved in phosphate buffer (pH 7.4) at 3 mg/mL (0.76 mM) and 30 mg/mL (32 mM), respectively, deposited onto cover glass, and dried at 24 °C. Samples were osmium-coated using an HPC-1SW osmium plasma coater (Vacuum Device Co., Ibaraki, Japan) prior to imaging.

3. Results and Discussion

Synthesis of ELPs. The monomeric building blocks (F1, F2, and AcF2) and the EDTA-linked multimers (EDTA-mF2 and EDTA-4F1) were prepared as described in Section 2. AcF2 served as an alternative linear counterpart of F2 because EDTA-linked F2 multimers lack free amino groups. Their molecular structures are shown in Figure 2-1. Analytical UPLC-MS traces demonstrating the purity of each peptide are shown in Figure 2-2a–d, and the isolated yields, retention times, and observed *m/z* values are summarized in Table 2-1. Although two structural isomers are possible for the dimeric F2, a single dimer was obtained as the major product in this study. This major dimer was assigned to the less sterically hindered structure (Figure 2-1e), based on a comparison of its UPLC-MS elution time with that of a reference dimer independently

synthesized by condensation of F2 with EDTA dianhydride in DMF (Figure 2-2e).

(Figures 2-1 and 2-2)
(Table 2-1)

Temperature-responsive behavior of ELPs. Thermoresponsive phase behavior of the linear Fn peptides and their EDTA-linked multimers was evaluated by turbidimetry. The concentrations of the peptide solutions varied depending on the solubility of each peptide (Table 2-2).

Under the tested conditions, the linear short peptides F1, F2, and AcF2 remained optically clear and did not exhibit LCST-type transitions (Figure 2-3a; Table 2-2). F2 did not show LCST-type behavior at 30 mg/mL (32 mM) even in a phosphate buffer containing 3.5 % NaCl (0.60 M, Figure 2-3b). In contrast, EDTA-linked F2 multimers (EDTA-mF2) exhibited reversible turbidity changes upon temperature changes. For example, EDTA-4F2 (3.0 mg/mL, 0.76 mM) exhibited LCST-type behavior with a T_t value of 9.1 °C (Figure 2-3c). Lower concentrations of EDTA-4F2 shifted T_t at higher temperatures, yielding T_t values of 21 °C at 1.0 mg/mL (0.25 mM) and 32 °C at 0.5 mg/mL (0.13 mM). EDTA-3F2 and EDTA-2F2 also underwent coacervation near 40 °C at 10 mg/mL (3.3 mM) and 30 mg/mL (14 mM), respectively (Figure 2-3d, e). Moreover, both peptides displayed concentration-dependent T_t values under the measured conditions of 10–20 mg/mL (3.3–6.6 mM) for EDTA-3F2 and 30–60 mg/mL (14–28 mM) for EDTA-2F2 in phosphate buffer (pH 7.4). The observed T_t-concentration relationships were well described by the empirical form $T_t = a \ln(C) + b$ reported by Meyer and Chilkoti, where C is ELP concentration, and a and b represent constants (Figure 2-3f) [13], enabling estimation of the concentration required to trigger coacervation at a target temperature, or vice versa. Consistent with increased multivalency enhancing self-assembly [28], the concentration ranges required for LCST-type behavior decreased as the number of F2 chains per molecule increased.

In phosphate buffer (pH 7.4; $\mu = 0.100$), EDTA-4F1 did not show a detectable transition within the concentration range examined (Figure 2-3g). However, in phosphate buffer containing 3.5% NaCl (0.60 M NaCl), EDTA-4F1 showed LCST-type behavior in a concentration-dependent manner (Figure 2-3h, i). As commonly observed for ELP systems [17], increasing ionic strength lowered the T_t of EDTA-4F1. Although relatively higher peptide and/or salt concentrations appear necessary for F1-based multimers, these results nonetheless demonstrate that even the F1 block can be converted into a thermoresponsive molecule via multimerization. Taken together, the turbidity data indicate that covalent multimerization of short-chain, easy-to-synthesize Fn chains into multichain architectures provides a straightforward route to LCST-type behavior, whereas the corresponding monomers remain nonresponsive under comparable conditions. The apparent self-assembling properties of EDTA-mFn could be attributed to the conjugation with EDTA,

which capped the free *N*-terminals of Fn chains and increased the hydrophobicity, and to the proximity of Fn chains linked by EDTA, which might enhance the inter- and intra-molecular chain-chain interactions.

Influence of ionizable groups and pH. Among the F2 multimers, EDTA-3F2 and EDTA-2F2 retain one or two carboxyl groups derived from EDTA. Such charged/hydrophilic functional groups, whether or not they derive from ELP sequences or non-ELP moieties, can affect the LCST-type behavior by altering hydration and overall polarity. Therefore, the turbidity profiles of EDTA-2F2 (30 mg/mL, 14 mM) were examined at pH 2.0, 7.4, and 12 (Figure 2-3e, j). At both pH 2.0 and 12, EDTA-2F2 transitioned at lower temperatures than at pH 7.4 (Table 2-2). This discrepancy could be attributed to the hydration states of EDTA-2F2: near neutral pH, both carboxyl and amine groups are ionized, resulting in a higher population of charged species compared to pH 2.0 or 12, which enhanced solvation and thus elevated T_t. Despite these variations in T_t values, these results demonstrated that EDTA-2F2 retained LCST-type behavior over a broad pH range. At the same time, the pH-dependent changes in T_t values of EDTA-2F2 highlight the potential that its aggregation behavior can be controlled by pH. Similar charge-mediated modulation of ELP assembly has been reported for ELPs bearing short, charged peptide tags (e.g., YKV sequences) [15]. These results therefore suggest the potential of multimers as useful temperature-responsive and/or pH-responsive materials. From an application standpoint, the remaining carboxyl groups in EDTA-2F2 (and, analogously, EDTA-3F2) would offer opportunities for modification with functional molecules, although such derivatization is beyond the scope of this chapter.

Effect of metal ions. Metal chelation can also influence ELP phase behavior. A Cd^{2+}-binding short-chain ELP was previously reported to show a reduced T_t upon chelation [30], and ELPs conjugated with nitrilotriacetic acid displayed increased T_t values in the presence of excess Cu^{2+} or Ni^{2+} while retaining metal-binding capacity [28]. Because EDTA is a multidentate chelator, the phase behavior of EDTA-2F2 in saline containing Cu^{2+} (1 eq; 14 mM) was examined. In the presence of Cu^{2+}, T_t increased to approximately 27.9 °C compared with ~25.9 °C in the absence of Cu^{2+} (Figure 2-3k). LCST-type behavior of ELPs is known to be sensitive to ionic conditions; for example, Hofmeister anions can modulate T_t through effects on interfacial water and hydrophobic hydration [18]. While cation trends can be less systematic, divalent cations have been reported to increase protein/colloid solubility [31,32], and cation 'salting-out' in ELP systems can depend on specific ion-ELP interactions rather than strictly following the Hofmeister series [33]. These considerations suggest that Cu^{2+} may enhance EDTA-2F2 solvation via direct interactions with the ELP, shifting the T_t to a higher temperature.

(Figure 2-3)

(Table 2-2)

CD spectra. To investigate whether EDTA-mediated multimerization affects the intrinsic conformational preferences of the Fn chains, CD spectroscopy was performed for EDTA-2F2, EDTA-4F1, $(FPGVG)_4$ (abbreviated as F4), F2, and F1 over a temperature range of 5–45 °C. EDTA-2F2, EDTA-4F1, and F4 share the same number of pentapeptide units, whereas F2 and F1 represent the monomeric building blocks. Measurements were conducted under dilute conditions (0.1 mg/mL, phosphate buffer pH 7.4) where no macroscopic LCST-type transition was observed.

All peptides exhibited closely similar spectral signatures (Figure 2-4). At low temperature, spectra featured a weak negative band near 234 nm, a positive band around 220 nm, and a pronounced negative band at approximately 198 nm, a characteristic of polyproline type II (PPII)-like conformations [34]. Upon heating, the intensities of these bands decreased and a shoulder emerged near 205 nm, consistent with an increased contribution from β-turn and/or β-sheet-like structures (Figure 2-4a–e). Cooling restored the original spectral patterns, demonstrating the reversibility of these conformational changes (Figure 2-4f–j). The close agreement between the spectra of the multimers and those of their corresponding linear counterparts indicates that the multimerization via EDTA does not substantially alter the secondary structural response of the Fn segments. Similar preservation of conformational behavior has been reported for other branched $(FPGVG)_n$-based oligomers [27,28]. Moreover, the temperature-dependent spectral changes of F1 and F2 closely resembled those of longer $(FPGVG)_n$ peptides (n = 4–5) [35]. These results support the notion that multimerization can endow short-chain ELPs with LCST-type behavior without requiring major changes in chain-level secondary structure.

(Figure 2-4)

Size distribution analysis. Aggregate growth during coacervation of EDTA-mF2 was monitored by DLS. Size distributions (Figure 2-5) were obtained from the autocorrelation functions (Figure 2-6) using the cumulant analysis implemented in the Zetasizer software. EDTA-4F2 and EDTA-3F2 showed clear temperature-dependent aggregate growth. Specifically, both samples showed bimodal size distributions below T_t and large particles (> 1 μm) above T_t (Figure 2-5a, b), consistent with a stepwise pathway in which submicron assemblies form first and then mature into larger coacervate droplets upon further heating [28,36,37]. EDTA-2F2 also displayed a bimodal distribution at lower temperature; however, particle sizes exceeding 1 μm were already

observed at 35 °C, i.e., below its macroscopic T_t (~40 °C; Figure 2-5c). At 45 °C, the DLS correlogram exhibited a tail extending to long delay times (~100,000 μs; Figure 2-6c), indicating the presence of very large aggregates. These observations suggest that EDTA-2F2 undergoes rapid coalescence near the T_t, producing large assemblies that continue to grow and ultimately precipitate.

(Figures 2-5 and 2-6)

Morphological properties. Aggregate morphology was examined by bright-field microscopy and SEM. In microscopy experiments performed in phosphate buffer, no discernible particles were observed for EDTA-mF2 below T_t, whereas droplet-like aggregates appeared above T_t (Figure 2-7). The observed droplets were generally larger than the dominant sizes detected by DLS. This discrepancy likely reflects the limitations of DLS in detecting particles larger than 10 μm, and the tendency of droplets to settle and fuse on the glass slide during observation.

SEM was also employed to examine the morphological differences in the multimer and its building block after drying. The air-dried sample of EDTA-4F2 showed three-dimensional spherical features with diameters of approximately 1–20 μm (Figure 2-8a), consistent with the droplet sizes observed by optical microscopy. Although the SEM samples were formed by drying rather than by temperature-changes, the retention of a spherical morphology suggests robust droplet-like assembly of the tetramer. In contrast, the linear F2 control produced only planar, paste-like residues upon drying (Figure 2-8b). Collectively, these results show that EDTA-mediated multimers show coacervate formation and temperature-dependent growth upon heating, which are common features of ELPs [26].

(Figures 2-7 and 2-8)

4. Conclusion

In this chapter, multimeric ELPs were synthesized from EDTA and short-chain ELPs (F2 or F1) as starting materials. While the linear F1 and F2 building blocks did not exhibit apparent LCST-type behavior under the examined conditions, the EDTA-linked multimers (EDTA-mFn) underwent concentration- and salt-dependent coacervation. The multimers also exhibited reversible temperature-dependent secondary structural changes between PPII-like helical structures and β-structures. Consistent with the phase behavior of previously reported FPGVG-based ELPs, the multimers self-assembled into spherical aggregates, and the size distribution analyses suggested a stepwise pathway in which small aggregates formed below T_t matured into larger particles above T_t. Overall, these findings demonstrate that simple

multimerization can transform otherwise nonresponsive short-chain ELPs into temperature-responsive materials.

From the perspective of possible applications, free functional groups (in this study, carboxyl groups derived from EDTA) on ELPs may offer opportunities for modification with functional molecules, allowing the fused molecules to acquire temperature-responsiveness. Thus, by multimerizing easily accessible short-chain ELPs with a central linker and introducing additional functional molecules, it would be possible to design and create responsive biomaterials with tailored functions.

5. References

[1] Sun, J.; Han, J.; Wang, F.; Liu, K.; Zhang, H. Bioengineered Protein-based Adhesives for Biomedical Applications. *Chemistry* **2022**, *28* (1), e202102902.

[2] Kim, Y. J.; Matsunaga, Y. T. Thermo-responsive polymers and their application as smart biomaterials. *J. Mater. Chem. B* **2017**, *5* (23), 4307–4321.

[3] Kowalczyk, T.; Hnatuszko-Konka, K.; Gerszberg, A.; Kononowicz, A. K. Elastin-like polypeptides as a promising family of genetically-engineered protein based polymers. *World J. Microbiol. Biotechnol.* **2014**, *30* (8), 2141–2152.

[4] Varanko, A. K.; Su, J. C.; Chilkoti, A. Elastin-Like Polypeptides for Biomedical Applications. *Annu. Rev. Biomed. Eng.* **2020**, *22*, 343–369.

[5] Berckman, E. A.; Hartzell, E. J.; Mitkas, A. A.; Sun, Q.; Chen, W. Biological Assembly of Modular Protein Building Blocks as Sensing, Delivery, and Therapeutic Agents. *Annu. Rev. Chem. Biomol. Eng.* **2020**, *11*, 35–62.

[6] Kostal, J.; Mulchandani, A.; Chen, W. Tunable biopolymers for heavy metal removal. *Macromolecules* **2001**, *34*, 2257–2261.

[7] Mahmoodi, S.; Pourhassan-Moghaddam, M.; Wood, D. W.; Majdi, H.; Zarghami, N. Current affinity approaches for purification of recombinant proteins. *Cogent Biol*. **2019**, *5* (1), 1665406.

[8] Wright, E. R.; Conticello, V. P. Self-assembly of block copolymers derived from elastin-mimetic polypeptide sequences. *Adv. Drug. Deliv. Rev.* **2002**, *54* (8), 1057–1073.

[9] Mills, C. E.; Ding, E.; Olsen, B. Protein purification by ethanol-induced phase transitions of the elastin-like polypeptide (ELP). *Ind. Eng. Chem. Res.* **2019**, *58* (27), 11698–11709.

[10] Hollingshead, S.; Lin, C. Y.; Liu, J. C. Designing Smart Materials with Recombinant Proteins. *Macromol Biosci.* **2017**, *17* (7), 1600554.

[11] Urry, D. W.; Gowda, D. C.; Parker, T. M.; Luan, C. H.; Reid, M. C.; Harris, C. M.; Pattanaik, A.; Harris, R. D. Hydrophobicity scale for proteins based on inverse temperature transitions. *Biopolymers* **1992**, *32* (9), 1243–1250.

[12] McDaniel, J. R.; Radford, D. C.; Chilkoti, A. A unified model for de novo design of elastin-like polypeptides with tunable inverse transition temperatures. *Biomacromolecules* **2013**, *14* (8), 2866–2872.

[13] Meyer, D. E.; Chilkoti, A. Quantification of the effects of chain length and concentration on the thermal behavior of elastin-like polypeptides. *Biomacromolecules* **2004**, *5* (3), 846–851.

[14] Mackay, J. A.; Callahan, D. J.; Fitzgerald, K. N.; Chilkoti, A. Quantitative model of the phase behavior of recombinant pH-responsive elastin-like polypeptides. *Biomacromolecules* **2010**, *11*(11), 2873–2879.

[15] Lin, C. Y.; Liu, J. C. Incorporation of short, charged peptide tags affects the temperature responsiveness of positively-charged elastin-like polypeptides. *J. Mater. Chem. B* **2019**, *7* (34), 5245–5256.

[16] Hollingshead, S.; Liu, J. C. pH-Sensitive Mechanical Properties of Elastin-Based Hydrogels. *Macromol. Biosci.* **2020**, *20* (4), e1900369.

[17] Nuhn, H.; Klok, H. A. Secondary structure formation and LCST behavior of short elastin-like peptides. *Biomacromolecules* **2008**, 9 (10), 2755–2763.

[18] Cho, Y.; Zhang, Y.; Christensen, T.; Sagle, L. B.; Chilkoti, A.; Cremer, P. S. Effects of Hofmeister anions on the phase transition temperature of elastin-like polypeptides. *J. Phys. Chem. B* **2008**, *112* (44), 13765–13771.

[19] Indik, Z.; Yeh, H.; Ornstein-Goldstein, N.; Sheppard, P.; Anderson, N.; Rosenbloom, J. C.; Peltonen, L.; Rosenbloom, J. Alternative splicing of human elastin mRNA indicated by sequence analysis of cloned genomic and complementary DNA. *Proc. Natl. Acad. Sci. U S A.* **1987**, *84* (16), 5680–5684.

[20] Raju, K.; Anwar, R. A. Primary structures of bovine elastin a, b, and c deduced from the sequences of cDNA clones. *J. Biol. Chem.* **1987**, *262* (12), 5755–5762.

[21] Bressan, G. M.; Argos, P.; Stanley, K. K. Repeating structure of chick tropoelastin revealed by complementary DNA cloning. *Biochemistry* **1987**, *26* (6), 1497–1503.

[22] Maeda, I.; Taniguchi, S.; Ebina, J.; Watanabe, N.; Hattori, T.; Nose, T. Comparison between coacervation property and secondary structure of synthetic peptides, Ile-containing elastin-derived pentapeptide repeats. *Protein Pept. Lett.* **2013**, *20* (8), 905–910.

[23] Kaibara, K.; Akinari, Y.; Okamoto, K.; Uemura, Y.; Yamamoto, S.; Kodama, H.; Kondo, M. Characteristic interaction of Ca^{2+} ions with elastin coacervate: ion transport study across coacervate layers of α-elastin and elastin model polypeptide, $(Val\text{-}Pro\text{-}Gly\text{-}Val\text{-}Gly)_n$. *Biopolymers* **1996**, *39* (2), 189–198.

[24] Maeda, I.; Fukumoto, Y.; Nose, T.; Shimohigashi, Y.; Nezu, T.; Terada, Y.; Kodama, H.; Kaibara, K.; Okamoto, K. Structural requirements essential for elastin coacervation:

favorable spatial arrangements of valine ridges on the three-dimensional structure of elastin-derived polypeptide $(VPGVG)_n$. *J. Pept. Sci.* **2011**, *17* (11), 735–743.

[25] Hassouneh, W.; MacEwan, S. R.; Chilkoti, A. Fusions of elastin-like polypeptides to pharmaceutical proteins. *Methods Enzymol.* **2012**, *502*, 215–237.

[26] Maeda, I.; Taniguchi, S.; Watanabe, N,; Inoue, A.; Yamasaki, Y.; Nose, T. Design of Phenylalanine-Containing Elastin-Derived Peptides Exhibiting Highly Potent Self-Assembling Capability. *Protein Pept. Lett.* **2015**, *22* (10), 934–939.

[27] Suyama, K.; Taniguchi, S.; Tatsubo, D.; Maeda, I.; Nose, T. Dimerization effects on coacervation property of an elastin-derived synthetic peptide $(FPGVG)_5$. *J. Pept. Sci.* **2016**, *22* (4), 236–243.

[28] Suyama, K.; Mawatari, M.; Tatsubo, D.; Maeda, I.; Nose, T. Simple Regulation of the Self-Assembling Ability by Multimerization of Elastin-Derived Peptide $(FPGVG)_n$ Using Nitrilotriacetic Acid as a Building Block. *ACS Omega* **2021**, *6* (8), 5705–5716.

[29] Dias, A. P.; da Silva Santos S.; da Silva J. V.; Parise-Filho, R.; Ferreira, E. I.; El Seoud, O.; Giarolla, J. Dendrimers in the context of nanomedicine. *Int. J. Pharm.* **2020**, *573*, 118814.

[30] Sumiyoshi, S.; Suyama, K.; Tatsubo, D.; Tanaka, N.; Tomohara, K.; Taniguchi, S.; Maeda, I.; Nose, T. Metal ion scavenging activity of elastin-like peptide analogues containing a cadmium ion binding sequence. *Sci. Rep*. **2022**, *12* (1), 1861.

[31] Kang, B.; Tang, H.; Zhao, Z.; Song, S. Hofmeister Series: Insights of Ion Specificity from Amphiphilic Assembly and Interface Property. *ACS Omega* **2020**, *5* (12), 6229–6239.

[32] Moghaddam, S. Z.; Thormann, E. The Hofmeister series: Specific ion effects in aqueous polymer solutions. *J. Colloid. Interface Sci.* **2019**, *555*, 615–635.

[33] Aladini, F.; Araman, C.; Becker, C. F. Chemical synthesis and characterization of elastin-like polypeptides (ELPs) with variable guest residues. *J. Pept. Sci.* **2016**, *22* (5), 334–342.

[34] Lopes, J. L.; Miles, A. J.; Whitmore, L.; Wallace, B. A. Distinct circular dichroism spectroscopic signatures of polyproline II and unordered secondary structures: applications in secondary structure analyses. *Protein Sci.* **2014**, *23* (12), 1765–1772.

[35] Taniguchi, S.; Watanabe, N.; Nose, T.; Maeda, I. Development of short and highly potent self-assembling elastin-derived pentapeptide repeats containing aromatic amino acid residues. *J. Pept. Sci.* **2016**, *22* (1), 36–42.

[36] Shmidov, Y.; Zhou, M.; Yosefi, G.; Bitton, R.; Matson, J. B. Hydrogels composed of hyaluronic acid and dendritic ELPs: hierarchical structure and physical properties. *Soft Matter* **2019**, *15* (5), 917–925.

[37] Tatsubo, D.; Suyama, K.; Miyazaki, M.; Maeda, I.; Nose, T. Stepwise Mechanism of Temperature-Dependent Coacervation of the Elastin-like Peptide Analogue Dimer, $(C(WPGVG)_3)_2$. *Biochemistry* **2018**, *57* (10), 1582–1590.

Table 2-1. Retention time, yield, and *m/z* of the ELPs.

Peptide	Retention time (min)	Yield (%)	MS (ESI) *m/z*	
			Calculated	Found
EDTA-4F2	3.357[a]	22	987.51 $[M+4H]^{4+}$	988.09
EDTA-3F2	3.000[a]	11	1011.85 $[M+3H]^{3+}$	1012.55
EDTA-2F2	2.294[a]	46	1060.54 $[M+2H]^{2+}$	1061.04
EDTA-4F1	2.444[a]	21	1059.55 $[M+2H]^{2+}$	1060.03
F1	1.564[b]	95	476.25 $[M + H]^{+}$	475.47
F2	2.553[b]	71	466.76 $[M + 2H]^{2+}$	467.06
AcF2	3.502[b]	75	487.76 $[M + 2H]^{2+}$	488.04

[a] Retention times of each peptide were determined by RP-UPLC-MS with a linear gradient of solvent A in solvent B (24% to 56%) over 4.23 min.

[b] Retention times of each peptide were determined by RP-UPLC-MS with a linear gradient of solvent A in solvent B (10% to 50%) over 4.51 min.

Table 2-2. Conditions of the turbidity measurements and obtained T_t values.

Peptide	Concentration [mg/mL]	Concentration [mM]	pH	T_t [°C]
EDTA-4F2	3.0	0.76	7.4	9.11 ± 0.12
EDTA-4F2	1.0	0.25	7.4	20.90 ± 0.40
EDTA-4F2	0.5	0.13	7.4	32.40 ± 0.95
EDTA-3F2	20	6.6	7.4	14.74 ± 2.06
EDTA-3F2	15	4.9	7.4	28.14 ± 5.39
EDTA-3F2	10	3.3	7.4	40.19 ± 1.29
EDTA-2F2	60	28	7.4	16.31 ± 0.04
EDTA-2F2	45	21	7.4	22.87 ± 0.52
EDTA-2F2	30	14	7.4	40.31 ± 1.19
EDTA-2F2	30	14	2.0	29.27 ± 0.38
EDTA-2F2	30	14	12	36.12 ± 0.41
EDTA-2F2	30[a]	14	-	27.91 ± 0.52
EDTA-2F2	30[b]	14	-	25.89 ± 0.15
EDTA-4F1	30	14	7.4	N.D.[d]
EDTA-4F1	30[c]	14	7.0	22.42 ± 0.03
EDTA-4F1	20[c]	9.4	7.0	34.72 ± 0.08
EDTA-4F1	10[c]	4.7	7.0	55.75 ± 0.01
F2	30	32	7.4	N.D.[d]
F2	30[c]	32	7.0	N.D.[d]
AcF2	30	31	7.4	N.D.[d]
F1	30	63	7.4	N.D.[d]

The T_t values are shown with standard errors. The peptide concentrations were determined based on the solubility of each peptide.

[a] Measurements were performed in saline solution containing Cu^{2+}.

[b] Measurements were performed in saline solution.

[c] Measurements were performed in phosphate buffer containing 3.5% NaCl.

[d] T_t could not be determined since increase in turbidity was not observed in this study.

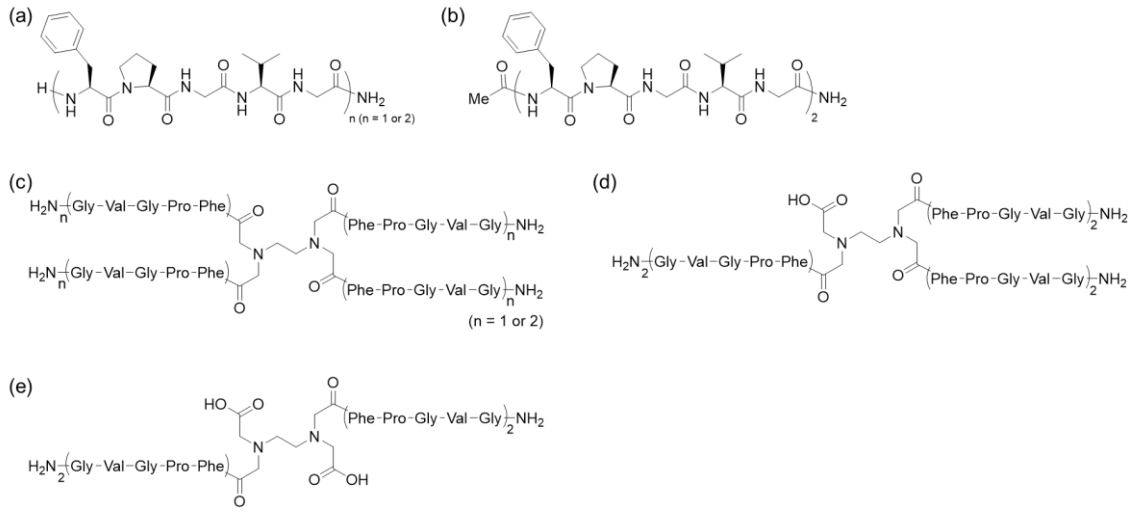

Figure 2-1. Chemical structures of linear ELPs and EDTA-mFn.

(a) Fn (H-(FPGVG)$_n$-NH$_2$ (Fn, where n stands for the number of repetitions), n = 1 or 2), (b) AcF2 (acetylated F2), (c) EDTA-4Fn (n = 1 or 2), (d) EDTA-3F2, and (e) EDTA-2F2.

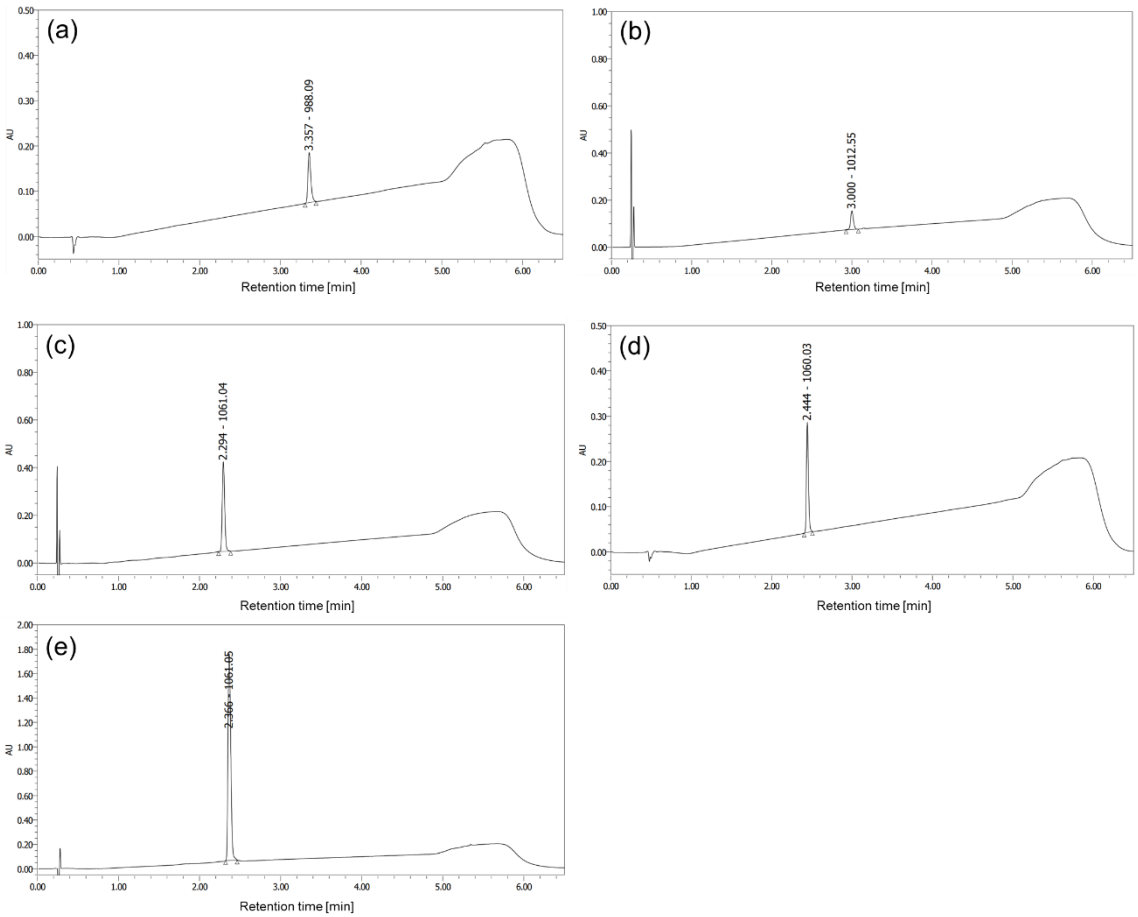

Figure 2-2. UPLC-MS analysis of EDTA-mFn.

UPLC-MS analysis of (a) EDTA-4F2, (b) EDTA-3F2, (c) EDTA-2F2, (d) EDTA-4F1, and (e) a mixture of EDTA-2F2 obtained from EDTA and from EDTA dianhydride showing only one peak. The subscripts for each peak indicate the retention time and the *m/z* detected. The peptides were monitored in a linear gradient of solvent B in solvent A (24% to 56%) over 4.23 min.

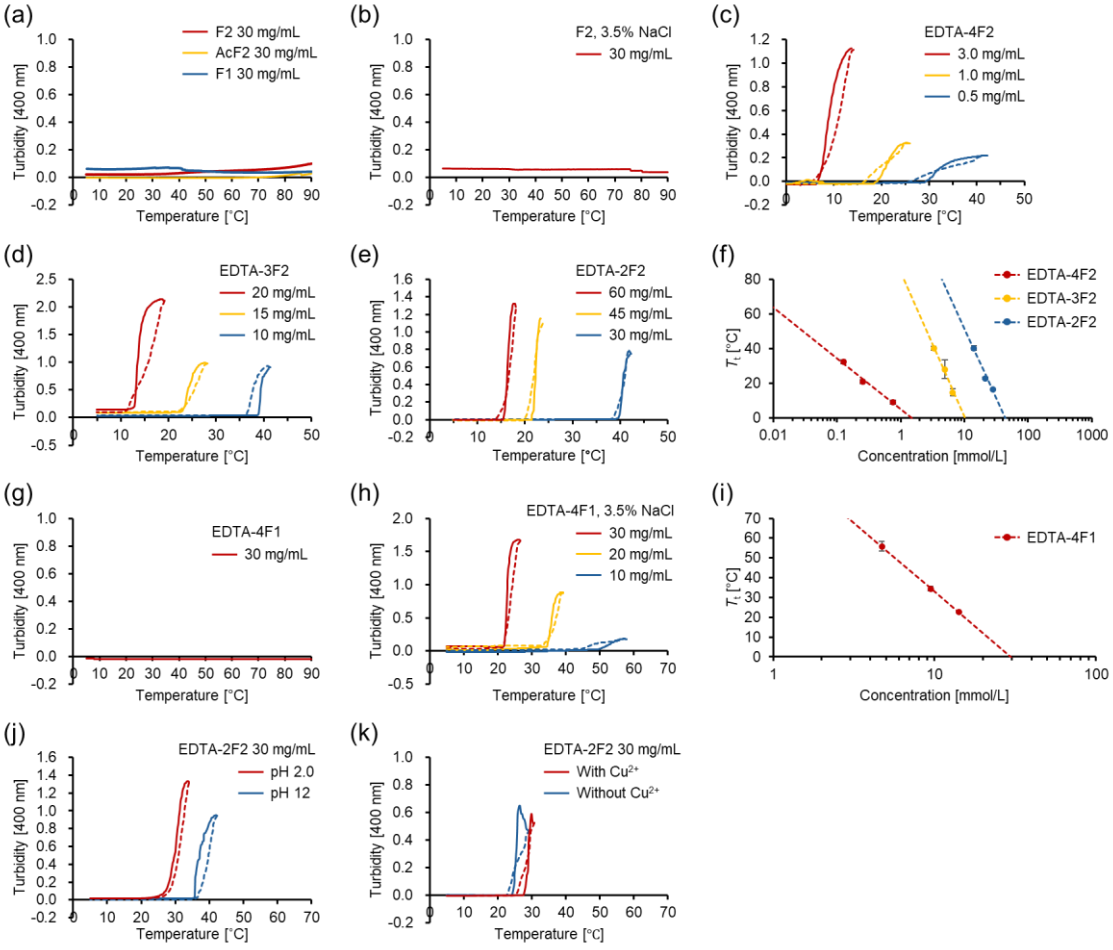

Figure 2-3. Turbidity profiles of linear Fn and EDTA-mFn.

Turbidity profiles of (a) F2, AcF2, and F1 at 30 mg/mL in phosphate buffer, (b) F2 in phosphate buffer containing 3.5% NaCl, (c) EDTA-4F2 in phosphate buffer, (d) EDTA-3F2 in phosphate buffer, and (e) EDTA-2F2 in phosphate buffer. (f) T_t-concentration relationships of EDTA-4F2, EDTA-3F2, and EDTA-2F2 in phosphate buffer. Turbidity profiles of (g) EDTA-4F1 (30 mg/mL) in phosphate buffer and (h) EDTA-4F1 in phosphate buffer containing 3.5% NaCl. (i) T_t-concentration relationship of EDTA-4F1 in phosphate buffer containing 3.5% NaCl. Turbidity profiles of (j) EDTA-2F2 (30 mg/mL) in phosphate buffer of pH 2.0 or pH 12, and (k) EDTA-2F2 (30 mg/mL) in saline with or without Cu^{2+}. Solid and dashed lines represent the change in turbidity upon heating and cooling, respectively in panels (c), (d), (e), (h), (j), and (k).

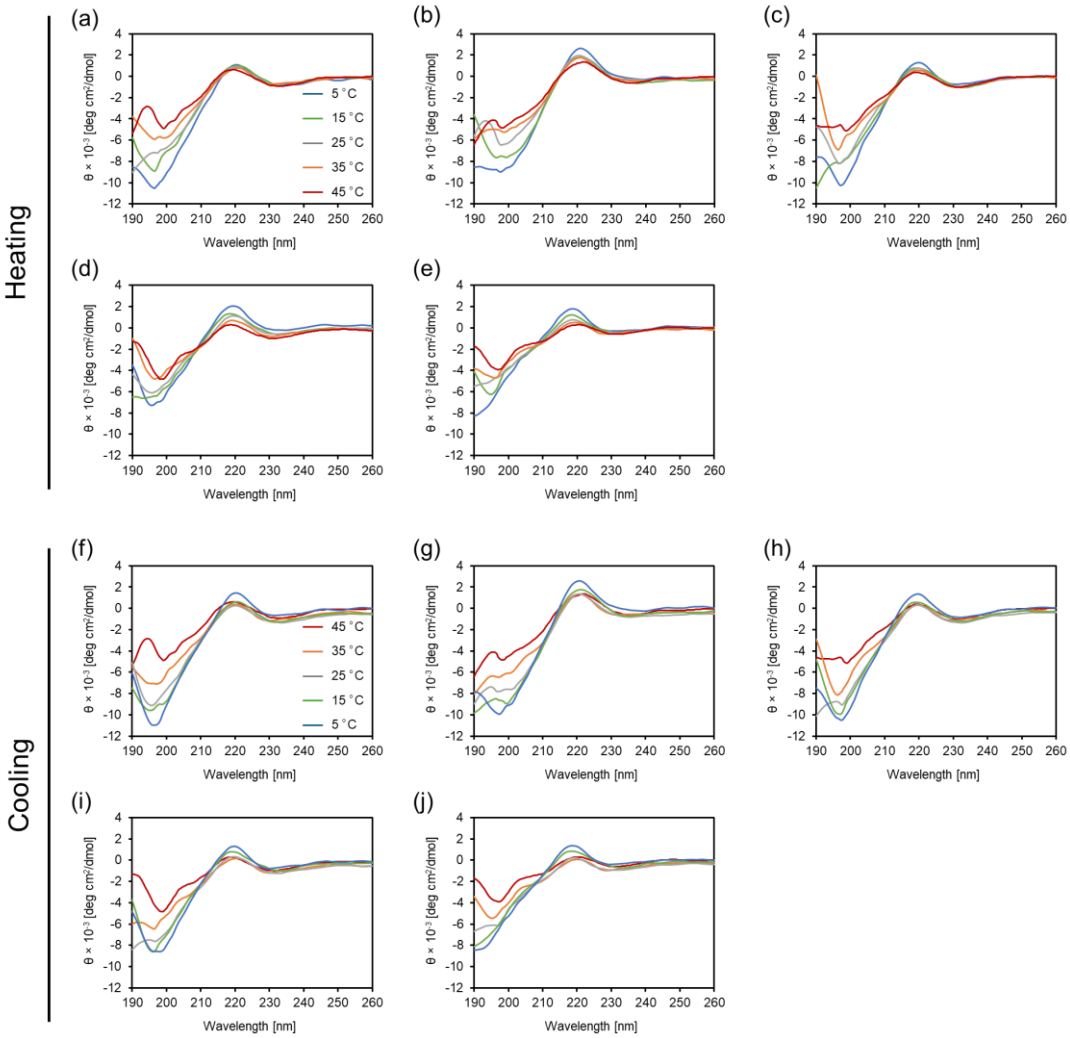

Figure 2-4. CD spectra of multimeric and linear Fn.

Spectra obtained upon heating for (a) EDTA-2F2, (b) EDTA-4F1, (c) F4, (d) F2, and (e) F1. Spectra obtained upon cooling for (f) EDTA-2F2, (g) EDTA-4F1, (h) F4, (i) F2, and (j) F1. Spectra were obtained over a temperature range of 5–45 °C. The colors of the spectra representing the temperatures are consistent among the panels.

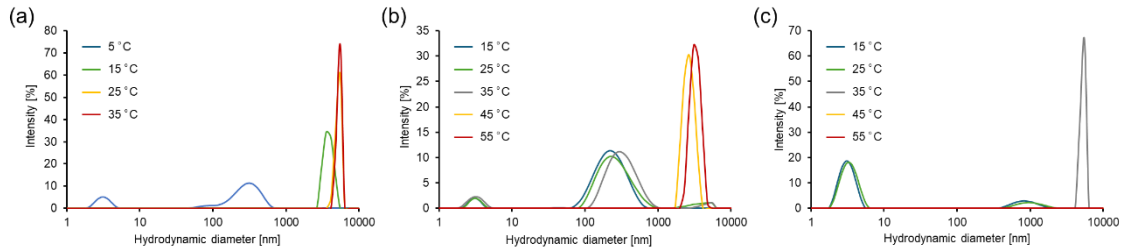

Figure 2-5. Size distribution analysis by DLS.

(a) EDTA-4F2 (3.0 mg/mL, T_t around 9 °C), (b) EDTA-3F2 (10 mg/mL, T_t around 40 °C), and (c) EDTA-2F2 (30 mg/mL, T_t around 40 °C) in phosphate buffer.

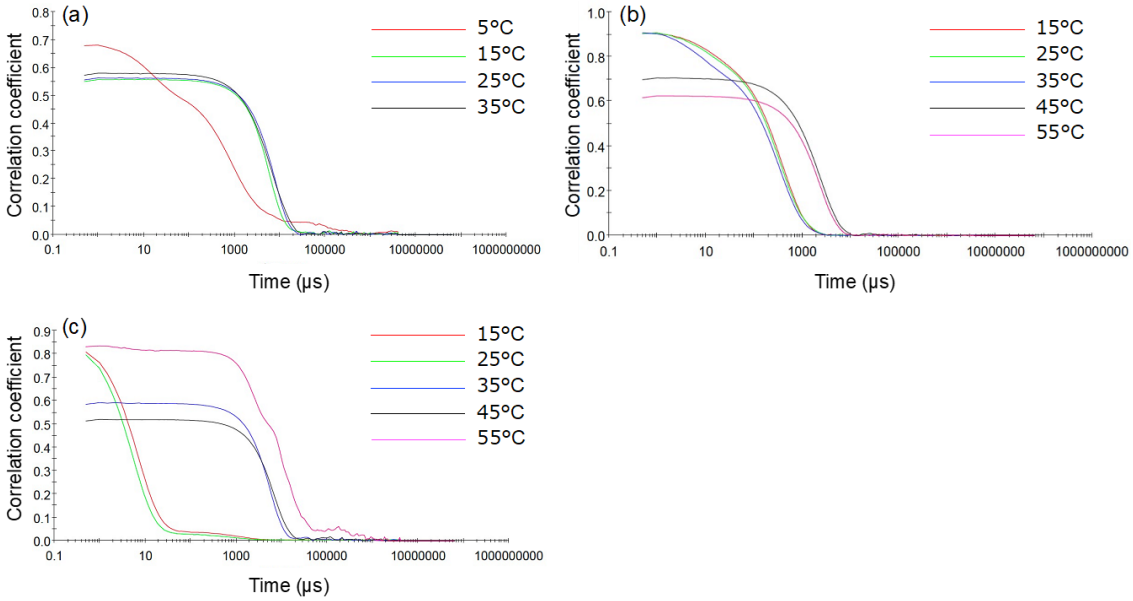

Figure 2-6. Autocorrelation curves of DLS.

(a) EDTA-4F2 (3 mg/mL), (b) EDTA-3F2 (10 mg/mL), and (c) EDTA-2F2 (30 mg/mL).

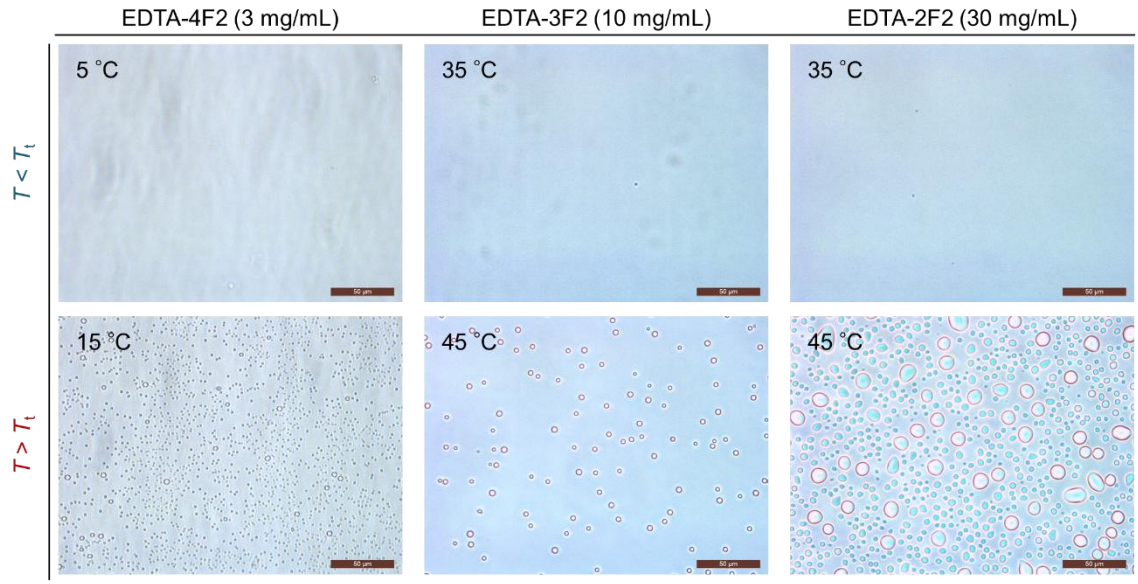

Figure 2-7. Bright-field microscopy images of EDTA-mF2.
Scale bars indicate 50 μm.

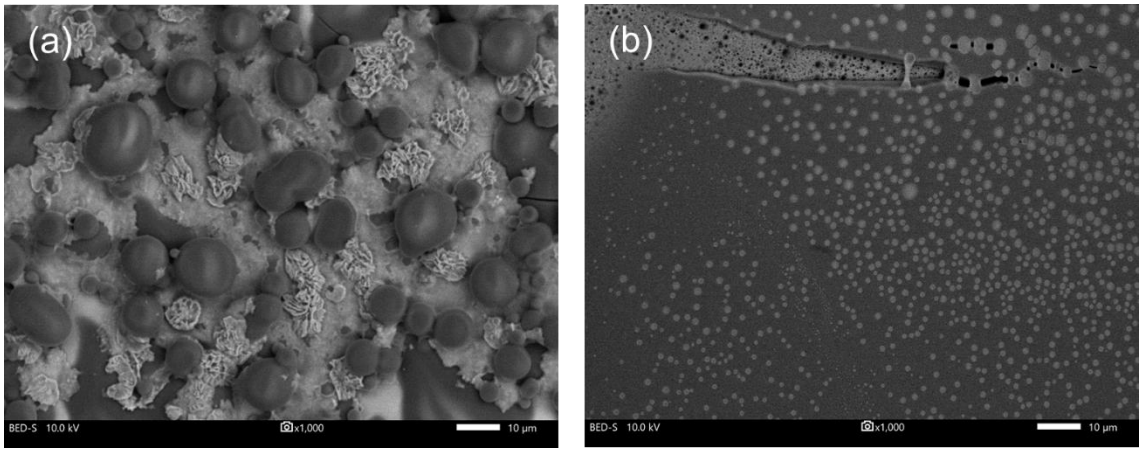

Figure 2-8. SEM images.
(a) EDTA-4F2, and (b) F2. Scale bars indicate 10 μm.

Chapter 3

Investigation of temperature-responsive behavior of branched molecules containing repeat units of elastin-like peptide FPGVG as side components

This chapter is based on the manuscript published in *Biomacromolecules* **2024**, *25* (11), 7156–7166.

Abstract

Elastin-like peptides (ELPs) exhibit lower critical solution temperature (LCST)-type phase behavior: they are soluble at low temperatures and insoluble at high temperatures. Because of this property, ELPs have attracted broad interest as thermoresponsive materials for diverse applications. Although the properties of linear, long-chain ELPs have been extensively characterized, much less is known about short-chain ELPs, particularly those with branched architectures. In this chapter, to extend the understanding of multimeric short ELPs, branched molecules consisting of a repeating pentapeptide unit of short-chain ELPs, Phe-Pro-Gly-Val-Gly (F1), as side components and oligo(Glu) as backbone structures were synthesized and investigated for their temperature-responsive properties. The molecular design was motivated by the observation that F1 undergoes temperature-dependent conformational changes similar to coacervation-competent FPGVG-based ELPs, despite the monomeric F1 itself not exhibiting LCST-type behavior. Turbidimetry showed that the branched ELPs undergo concentration-dependent LCST-like behavior, similar to conventional ELPs. Notably, in addition to LCST-like behavior, the branched molecules bearing six F1 chains exhibited upper critical solution temperature (UCST)-like behavior at 0.5 mM, an uncommon feature among ELP-based molecules. Spectroscopic and microscopic analyses demonstrated reversible secondary structural changes and the formation of spherical assemblies upon aggregation. Molecular dynamics simulations suggested that the unusual thermoresponsive profiles arise from temperature-dependent fluctuations in peptide conformation and hydration states across the temperature range of 5–90 °C. Overall, these results highlight the unique temperature-responsiveness of branched short-chain ELPs and provide new insights for the design and application of ELP-based materials with tailored properties.

1. Introduction

Stimuli-responsive materials undergo changes in their physicochemical properties in response to environmental stimuli such as temperature, pH, light, ionic strength, or mechanical force [1,2]. Among these triggers, temperature is particularly attractive because it can be controlled precisely and noninvasively, enabling on-demand switching of material functions [1,3,4]. Thermoresponsive phase behavior is commonly classified into lower critical solution temperature (LCST) or upper critical solution temperature (UCST) types [5]. LCST polymers are soluble at low temperature and phase-separate upon heating, whereas UCST polymers are soluble at high temperatures and phase-separate upon cooling.

Elastin-like peptides (ELPs) exhibit LCST-type phase separation (coacervation), and this property, combined with their potential biocompatibility and biodegradability [6,7], has been applied in protein purification, drug delivery, and sequestration of harmful substances [8–11]. They are typically composed of the vertebrate-derived motif $(Val\text{-}Pro\text{-}Gly\text{-}Xaa\text{-}Gly)_n$, where Xaa can be any residue except Pro [12–14]. Their transition temperature (T_t) can be tuned by sequence composition, chain length, concentration, and solution conditions [15–23].

Among the strategies for tuning the T_t of ELPs, short-chain ELPs offer a unique advantage in that their sequences can be precisely edited during chemical synthesis, enabling insertion, deletion, or substitution of residues at desired positions [24]. The high sequence customizability enables precise control over the phase behavior of ELPs. Previously, an ELP analog composed of $(Phe\text{-}Pro\text{-}Gly\text{-}Val\text{-}Gly)_n$ (Fn) was reported to exhibit LCST-like behavior with n of approximately 5, and subsequent studies showed that dimeric to tetrameric Fn molecules ($n \leq 5$), including tetrameric F2 and F1 described in Chapter 2, exhibited enhanced coacervation ability relative to their constituent monomers [24–27]. Nevertheless, the temperature-responsive behavior of branched short-chain ELPs, especially those composed of the minimal units ($n = 1$), remains less investigated compared with that of linear long-chain polypentapeptide ELPs.

In Chapter 2, it was revealed that multimeric, branched ELPs comprising four F1 chains exhibited LCST-like behavior even though the monomeric F1 did not show coacervation because of its short chain length [24]. However, it was found that temperature-dependent structural changes in the coacervation-competent branched multimer and linear F4 closely resembled those of monomeric F1: they adopted polyproline type II (PPII)-like helical conformations at low temperatures and showed a higher preference for β-turn/β-sheet structures at high temperatures. Previous studies have likewise reported that short-chain ELPs based on a $(VPGVG)_n$ sequence show the same structural changes upon temperature change as long-chain $(VPGVG)_n$ [28], and brush-like polymers bearing VPGVG units have been investigated [29–33]. Although ELPs of different sequences can show different structural features, the observed structural similarities between a pentapeptide unit and its polymer suggest that branched polymers bearing the

pentapeptide chains as side groups would exhibit LCST-like behavior similar to linear ELPs. These results motivated the working hypothesis of this chapter: conjugation of multiple F1 chains to a scaffold as side groups can yield branched molecules that can exhibit ELP-like thermoresponsiveness even though the individual F1 chain is too short to phase-separate on its own.

Accordingly, a series of branched peptides consisting of oligo(Glu) as the backbone and F1 chains as side components were synthesized and investigated for their temperature-responsive behavior to expand our understanding of branched short-chain ELPs. Turbidimetry revealed that the branched ELPs exhibit concentration-dependent LCST-like behavior over 0.5–4 mM. Notably, the branched ELPs with six F1 chains exhibited UCST-like behavior at 0.5 mM, a rare temperature-responsiveness for ELP-derived molecules. The mechanistic origins of these responses were examined using circular dichroism (CD) spectroscopy, thioflavin T (ThT) fluorescence assays, and molecular dynamics (MD) simulations.

2. Materials and Methods

Chemicals. 9-Fluorenylmethyloxycarbonyl (Fmoc)-Phe-OH, Fmoc-Pro-OH, Fmoc-Gly-OH, Fmoc-Val-OH, Fmoc-NH-SAL-MBHA resin (100–200 mesh), *N,N*-diisopropylethylamine (DIPEA), piperidine, trifluoroacetic acid (TFA), 1-[(1-(cyano-2-ethoxy-2-oxoethylideneaminooxy) dimethylamino-morpholino)] uronium hexafluorophosphate (COMU), 2-(1H-benzotriazole-1-yl)-1,1,3,3-tetramethyl uronium hexafluorophosphate (HBTU), and OxymaPure were purchased from Watanabe Chemical Industries (Hiroshima, Japan). Fmoc-Glu(O^{t}Bu)-OH, Fmoc-Glu-O^{t}Bu, and triisopropylsilane (TIS) were obtained from Tokyo Chemical Industry (Tokyo, Japan). *N,N*-dimethylformamide (DMF) was purchased from Kanto Chemical (Tokyo, Japan). Ultrapure water was prepared using a Milli-Q Integral 3 system (Merck Millipore, Darmstadt, Germany). Other reagents and solvents were obtained from commercial suppliers and used without further purification.

Peptide synthesis. Linear peptides were prepared by Fmoc-based solid-phase synthesis on a CSBio II automated peptide synthesizer (Menlo Park, CA), using HBTU/OxymaPure as coupling reagents. The pentapeptide H-FPGVG-NH_2 (F1) was synthesized on resin, cleaved with a cocktail of 95% TFA, 2.5% TIS, and 2.5% H_2O, and purified by Sep-Pak (C18, 10 g) using MeCN/H_2O as eluent before lyophilization. Backbone oligopeptides (Fmoc-α-(E(OH))$_n$-FPGVG-NH_2 and Fmoc-γ-(E(OH))$_n$-FPGVG-NH_2; n = 4–6) were synthesized similarly. After cleavage with 95% TFA/2.5% TIS/2.5% H_2O, the products were precipitated with cold diethyl ether and dried under vacuum.

Branched molecules bearing FPGVG side chains were obtained by conjugating Fmoc-

$(E(OH))_n$-FPGVG-NH_2 (0.02 mmol) with F1 (n × 0.03 mmol; 1.5 equiv per carboxyl group) using COMU (n × 0.04 mmol) and DIPEA (n × 0.04 mmol) in 200 μL of DMF. The reaction mixture was stirred at room temperature for a day, then an additional COMU/DIPEA (n × 0.04 mmol each) was added and stirring was continued for two more days. Water (200 μL) was added, and the mixture was stirred for 1 h, followed by addition of piperidine to give 20% (v/v) piperidine to remove Fmoc groups, and the mixture was kept stirred overnight. The crude reaction mixture was filtered, pre-purified by Sep-Pak (C8, 2 g), and purified by RP-HPLC (JASCO PU-2089 with UV-2075 or JASCO PU-4180 with UV-4075) using C8 columns (COSMOSIL 5C8-AR-300, 20 mm I.D. × 150 mm; Nacalai Tesque). The RP-HPLC mobile phases were 0.1% TFA in water (v/v; solvent C) and a mixture of 80% acetonitrile/20% solvent C (v/v; solvent D). After evaporation and lyophilization, the target branched peptide [α- or γ-$E(F1)]_n$-F1 (H-$[E(FPGVG\text{-}NH_2)]_n$-FPGVG-NH_2) was obtained as a colorless solid.

Peptide purity and molecular weight were confirmed on an ACQUITY UPLC H-Class system (Waters, Milford, MA) equipped with an ACQUITY UPLC BEH C-18 column (100 mm). The UPLC mobile phases were 0.1% formic acid in water (v/v; solvent A) and 0.1% formic acid in acetonitrile (v/v; solvent B).

Turbidity measurement. LCST/UCST-like behavior and reversibility were investigated by monitoring turbidity at 400 nm using a JASCO V-660 spectrophotometer (JASCO, Tokyo, Japan). Peptides were dissolved in phosphate buffer containing NaCl (pH 7.4; 27.4 mM Na_2HPO_4, 17.8 mM NaH_2PO_4, 1 M NaCl). This ionic strength was chosen because similar NaCl concentrations are used to induce ELP phase transitions in inverse transition cycling protocols for purification of ELP-fused proteins [9]. Turbidity traces were recorded during heating and cooling at 0.5 °C/min; samples at 0.5 mM were cycled at 1 °C/min. For 0.5 mM samples, after reaching 90 °C or 5 °C the solutions were vortexed to minimize possible concentration gradients arising from precipitation, held at the set temperature for 30 min, and then subjected to the subsequent cooling/heating step. The transition temperature (T_t) for LCST-like behavior was defined as the temperature at which turbidity reached half of its maximum value on heating. The measurements were performed at least three times.

Dynamic light scattering (DLS) measurement. Particle-size distributions were analyzed using a Zetasizer Nano ZS (Malvern Instruments, Worcestershire, U.K.) in filtered phosphate buffer (pH 7.4; 27.4 mM Na_2HPO_4, 17.8 mM NaH_2PO_4) containing 1 M NaCl. Measurements were performed from 15 to 55 °C in 10 °C increments for [α-$E(F1)]_n$-F1 and [γ-$E(F1)]_n$-F1 under conditions where the ELPs showed T_t values near 30 °C for LCST-like behavior (n = 4, 2.5 mM; n = 5, 1 mM; n = 6, 0.5 mM). In addition, [α-$E(F1)]_5$-F1 at 0.5 mM was analyzed at 20, 60, and

90 °C. Measurement duration was selected automatically. The “protein” parameter set (refractive index 1.450; absorption 0.001) and the “water” dispersant set (refractive index 1.330; viscosity 0.8872) were used, and attenuation was selected automatically.

Bright-field microscopy. Aggregate morphology was examined using a Leica DM IL LED microscope (Leica Microsystems, Wetzlar, Germany) equipped with a HI PLAN 40× oil objective and an HC PLAN 10 × eyepiece. Samples of $[\alpha\text{-E(F1)}]_n$-F1 and $[\gamma\text{-E(F1)}]_n$-F1 were prepared in phosphate buffer (pH 7.4; 27.4 mM Na_2HPO_4, 17.8 mM NaH_2PO_4) containing 1 M NaCl under conditions where the ELPs showed LCST-like behavior with T_t values around 30 °C. Imaging was performed at 15 °C and 45 °C using a temperature-controlled stage (Thermo Plate TP-CHSQM; Tokai Hit, Shizuoka, Japan). Additionally, a 0.5 mM solution of $[\alpha\text{-E(F1)}]_5$-F1 was prepared, and images were acquired at 60 °C either after heating from 15 °C (LCST-like behavior) or after cooling from 90 °C (UCST-like behavior). After 2 min of equilibration, images were recorded over 5 min at 1 min intervals, focusing on objects at the bottom surface of the glass slide. White balance was adjusted on Leica Application Suite X.

Circular dichroism (CD) measurement. CD spectra of $[\alpha\text{-E(F1)}]_5$-F1 and $[\gamma\text{-E(F1)}]_5$-F1 were obtained on a J-725 spectropolarimeter (JASCO) using a 1.0 mm path-length cuvette. Each peptide was dissolved in filtered phosphate buffer (pH 7.4; 27.4 mM Na_2HPO_4, 17.8 mM NaH_2PO_4) at 0.1 mg/mL. At this peptide concentration and ionic strength, no obvious aggregation was observed. Spectra were recorded from 190 to 260 nm between 10 and 90 °C with 20 °C intervals after 3 min of equilibration at each temperature. After subtracting background spectra, Savitzky–Golay filters were used to smooth the spectra.

Thioflavin T (ThT) fluorescence assay. ThT fluorescence measurements were performed on an FP-8500 spectrofluorometer (JASCO). Solutions of $[\alpha\text{-E(F1)}]_5$-F1 (1 mM or 0.5 mM) were prepared in phosphate buffer (pH 7.4; 27.4 mM Na_2HPO_4, 17.8 mM NaH_2PO_4) containing 1 M NaCl and 50 μM ThT. The temperature change rates were identical to those in the turbidity measurements. Using excitation at 446 nm, emission intensities at 483 nm were monitored during temperature changes or over time under fixed temperature conditions.

Molecular dynamics (MD) simulation. MD simulations were performed using GROMACS 2019 with the AMBER99SB-ILDN force field on a DELL PRECISION T3610 workstation (Dell Inc., Round Rock, TX, USA) [34]. Single-molecule trajectories were generated for $[\alpha\text{-E(F1)}]_5$-F1, $[\gamma\text{-E(F1)}]_5$-F1, and Ac-FPGVG-NH_2 (AcF1) using the TIP3P explicit solvent model. Initial structures were built in Discovery Studio 4.0 (Dassault Systèmes BIOVIA) and converted to .gro

file with gmx pdb2gmx command in GROMACS. The multimer models were placed in a 7 × 7 × 7 nm^3 box, solvated, and neutralized with 206 Na^+ and 207 Cl^- ions to mimic the experimental condition (1 M NaCl). AcF1 was simulated in a 3 × 3 × 3 nm^3 box with 16 Na^+ and 16 Cl^-. Simulations were run at 278, 303, 333, and 363 K (5, 30, 60, and 90 °C). These systems contained two minimizations, heating step, equilibrium step, and production step. The first minimization was performed by steepest descent algorithm, using a maximum of 10,000 steps, the maximum step size (emstep) of 0.01 nm, the tolerance (emtol) of 10.0 kJ mol^{-1} nm^{-1}, and no constraints; the second minimization was performed by conjugate gradient algorithm, using a maximum of 20,000 steps, emstep of 0.01 nm, emtol of 10.0 kJ mol^{-1} nm^{-1}, and no constraints; heating step: parameters are 500,000 steps, time step 2 fs, initial temperature 0 K, target temperature (278/303/333/363 K), LINCS constraint to h-bond atoms, annealing type single, annealing npoints 2, and annealing time 200 ps; an equilibration step: parameters are 500,000 steps with a time step of 2 fs, target temperature (278/303/333/363 K), LINCS constraint to h-bond atoms, and reference pressure 1.0 bar; and finally, a production step consisting of 15,000,000 steps (30 ns) for the multimers, and 50,000,000 steps (100 ns) for AcF1, time step 2 fs, target temperature (278/303/333/363 K), pressure coupling decay time (tau-p) = 1.0, LINCS constraint to h-bond atoms, nonbond list radius (rcoulomb, rvdw) = 1.0 nm, nonbond lower cutoff distance (rlist) = 1.0 nm, electrostatics = particle-mesh Ewald (PME) method, dynamics integrator = leapfrog, and random number seed = 1732. Trajectories (30,000 frames for the multimers, and 100,000 frames for AcF1) were processed by gmx trjcomv to correct the break in the molecular structure due to periodic boundary condition. During this process, the number of frames was reduced to 1/10 (3,000 or 10,000 frames). Then, the dihedral angles, radius of gyration (Rg), solvent accessible surface areas (SASA), the number of intramolecular hydrogen bonds (n_{PP}), and the number of hydrogen bonds between water and peptide (n_{PW}) were analyzed using the processed trajectory files by omitting the first 10 ns.

3. Results and Discussion

Synthesis of branched ELPs. The branched molecules were prepared via a grafting-onto strategy in which the backbone Fmoc-$[E(OH)]_n$-F1 (n = 4–6) was coupled with F1 side chains [35]. After deprotection, the target *N*-terminal free branched, multimeric ELPs, $[\alpha\text{-}E(F1)]_n$-F1 and $[\gamma\text{-}E(F1)]_n$-F1, were obtained (Figure 3-1). UPLC profiles confirming peptide purity are shown in Figure 3-2, and yields, retention times, and *m/z* values are summarized in Table 3-1. In general, $[\alpha\text{-}E(F1)]_n$-F1 was isolated in higher yield than the corresponding $[\gamma\text{-}E(F1)]_n$-F1, which may reflect differences in the accessibility of backbone carboxyl groups for side-chain modification.

(Figures 3-1 and 3-2)

(Table 3-1)

Temperature-responsive behavior. LCST-like phase behavior of the branched ELPs was first evaluated by turbidimetry in phosphate buffer containing 1 M NaCl. Under these conditions, all branched peptides composed of F1 side chains exhibited clear LCST-like transitions (Figure 3-3a–f, i, j). For example, at 1 mM, [α-E(F1)]$_5$-F1 and [γ-E(F1)]$_5$-F1 transitioned near 30 °C and 35 °C, respectively (Figure 3-3b, e). The T_t values determined at various peptide concentrations are shown in Table 3-2 and Figure 3-3g, h. For a given n value, [α-E(F1)]$_n$-F1 and [γ-E(F1)]$_n$-F1 exhibited comparable T_t values, indicating that the linkage position (α vs γ) has only a minor effect on the T_t values. The relationships between concentration and T_t of each branched ELP followed the equation $T_t = a \ln(C) + b$ originally established for linear ELPs, where C is ELP concentration, and a and b represent constants (Figure 3-3g, h) [19]. These results showed that increasing peptide concentration lowered T_t values, and increasing the number of F1 chains resulted in reduced peptide concentrations required for LCST-like behavior. These T_t-concentration relationships would be useful in selecting appropriate peptide and concentration conditions to achieve LCST-like behavior with a desired T_t value. Taken together, these results demonstrated that the branched ELPs behave in a similar manner to conventional linear ELPs with respect to their LCST-like behavior.

In addition to LCST-like behavior, [α-E(F1)]$_5$-F1 and [γ-E(F1)]$_5$-F1 at 0.5 mM became soluble again at high temperature after the LCST-type transition (Figure 3-3i–k). Upon cooling from 90 °C, turbidity increased, indicating a UCST-like transition. Thus, at 0.5 mM these branched peptides exhibit dual LCST- and UCST-like behavior. Regarding brush-type polymers, poly(phenylacetylene) bearing VPGVG side chains has been reported to exhibit UCST-like behavior [36]. At concentrations higher than 0.5 mM, however, insoluble aggregates formed at 90 °C, precipitated to the bottom of the measurement cell, and did not redissolve even after mixing (Figure 3-3l). This result underscored that peptide concentration is an important factor that determines peptide solubility for the appearance of UCST-like behavior. Because polymers with UCST-like behavior in aqueous systems are relatively rare [37–39], the branched ELPs synthesized here may contribute to the design and use of molecules with UCST-like behavior. Molecules capable of both LCST- and UCST-like behavior may offer distinct temperature regimes for solubilization and, conversely, for insolubilization by setting the temperature above the LCST or below the UCST, which potentially enable applications such as separation and purification. Collectively, these findings highlight the potential of branched ELPs to access unique and tunable thermoresponsive properties.

(Figure 3-3)

(Table 3-2)

Morphological properties. Bright-field microscopy was used to examine the morphology of aggregates formed by the branched short-chain ELPs. First, samples showing LCST-like behavior with T_t around 30 °C were examined (n = 4, 2.5 mM; n = 5, 1 mM; n = 6, 0.5 mM). For all the peptides, few or no coacervates were observed at 15 °C (below T_t), whereas spherical droplets were observed at 45 °C (above T_t) (Figures 3-4 and 3-5). Upon returning to 15 °C, these droplets disappeared, consistent with the reversible phase behavior. In addition, for [α-E(F1)]$_5$-F1 at 0.5 mM, aggregates formed through both LCST- and UCST-like transitions were observed at 60 °C (Figure 3-6). Together, these results show that branched F1-based ELPs form spherical assemblies upon aggregation.

(Figures 3-4–3-6)

Size distribution analysis. DLS measurements were carried out to quantify temperature-dependent changes in particle size distribution. Autocorrelation curves are shown in Figure 3-7. As temperature approached T_t (around 30 °C), the hydrodynamic diameters increased (Figure 3-8). At 15–25 °C, size distributions spanned from several nanometers to several micrometers; however, DLS results shown in number (%) demonstrated that the majority of the aggregates were in nanometer ranges. Given that single-molecule MD simulations shown below yield Rg values of 0.88–0.96 nm, the peaks at nanometer-scale are likely attributable to monomeric species. Upon heating to around or above T_t, the hydrodynamic diameters shifted predominantly to several micrometers. These results indicate that hydrated monomers and small pre-assemblies present below T_t undergo further association into larger particles above T_t. Such stepwise growth in aggregate size has also been reported for linear ELPs [40], confirming another similarity in LCST-like behavior between branched and linear ELPs.

For [α-E(F1)]$_5$-F1 at 0.5 mM, DLS results revealed that hydrodynamic diameters were larger at 60 °C than at 20 °C or 90 °C. This profile confirms that the formation of larger particles occurred within a specific temperature range through LCST- and UCST-like behavior (Figure 3-9).

(Figures 3-7–3-9)

Structural analysis by CD measurement. To elucidate temperature-dependent secondary structural changes, CD spectra were recorded for [α-E(F1)]$_5$-F1 and [γ-E(F1)]$_5$-F1 at 0.1 mg/mL. Although spectra were obtained over the range of 10–90 °C, they were interpreted as primarily

reflecting structural changes associated with LCST-like behavior, given that lower concentration and ionic strength increase its T_t value and may result in the absence of the macroscopic transition. At low temperatures, the branched ELPs exhibited a negative band near 200 nm and a positive band around 220 nm, which were attributed to PPII-like helical conformations (Figure 3-10a, b) [41]. Upon heating, the intensity of these bands decreased, and a shoulder peak emerged at 205 nm, indicating an increase in β-sheet and β-turn structures. An isodichroic point at 208 nm further indicated a structural transition upon temperature changes. Additionally, cooling restored the original spectral patterns (Figure 3-10c, d), demonstrating reversible conformational changes. Furthermore, the CD intensity of $[\alpha\text{-E(F1)}]_5$-F1 was higher than that of $[\gamma\text{-E(F1)}]_5$-F1 at each temperature, implying greater rigidity for $[\alpha\text{-E(F1)}]_5$-F1 [42]. This result could stem from the difference in the backbone flexibility, and was consistent with the temperature-dependent changes in the Rg values obtained in the MD simulations shown below.

(Figure 3-10)

Structural analysis by ThT assay. ThT fluorescence was used to further investigate the structural changes. For $[\alpha\text{-E(F1)}]_5$-F1 at 1 mM, fluorescence sharply increased around T_t upon heating, indicating that the formation of β-sheet structure and amyloid-like structures are involved in the aggregation through LCST-like behavior (Figure 3-11a) [43]. When the temperature was shifted to above and below the T_t, the fluorescence intensity showed rapid and reversible increases and decreases, correspondingly (Figure 3-11b), demonstrating the reversible formation and loss of β-sheet structure. These results aligned with the CD data and with previous observations for both branched and linear FPGVG-based ELPs [24, 26, 27, 44–46]. Below the T_t, slight decreases in fluorescence intensity were observed upon heating (Figure 3-11a, b), suggesting a decrease in β-sheet structures prior to macroscopic aggregation.

At 0.5 mM, where the branched peptides exhibit both LCST- and UCST-like behavior, ThT fluorescence intensity increased around the T_t for LCST-like behavior upon heating, reached a maximum around 60 °C, and then decreased upon further heating to 90 °C (Figure 3-11c, d). This trend corresponds to the aggregation and disaggregation behavior observed by turbidimetry. Upon cooling from 90 °C, the fluorescence intensity increased again, peaked around 60 °C, and then decreased around the T_t for LCST-like behavior. These data suggest that both LCST- and UCST-like transitions of the branched ELPs involve formation and denaturation of β-sheet-rich structures associated with aggregation and disaggregation, respectively. The LCST-type phase transition is typically regarded as an entropy-driven process. In the case of ELPs, heating reduces the structural ordering of water molecules surrounding the hydrophobic residues, resulting in a favorable entropy change above the LCST [15]. In contrast, UCST behavior is considered to be

an enthalpy-driven process, in which hydrogen bonds or electrostatic interactions are crucial in the association and dissociation properties [37,38]. While the observed LCST- and UCST-like behavior might be entropy- and enthalpy-driven processes, respectively, the ThT assay suggested that the formation and denaturation of β-sheet structures contribute to both processes in the present branched ELPs.

(Figure 3-11)

Structural and conformational insights from MD simulations. To further investigate temperature-dependent structural and conformational changes, MD simulations were conducted at 5, 30, 60, and 90 °C. First, Ramachandran plots were obtained by collecting the dihedral angles of the backbone Glu residues of $[\alpha\text{-E(F1)}]_5$-F1 to analyze the structural changes of the backbone (Figure 3-12a). The plots revealed a highly populated region around (φ, ψ) = (−60, +150) and a moderately populated region near (−100, −20) at 5 °C, corresponding to PPII and helical conformations, respectively (Figure 3-12a) [47]. At 30 °C, these populations diminished and β-sheet regions around (−150, +175) became populated. At 60 °C, β-sheet content decreased but helical content increased, which in turn indicated that the structural changes in the F1 chains caused the increase in ThT fluorescence intensity. Upon further heating to 90 °C, the helix structures decreased, and PPII structures increased again. These temperature-dependent changes in backbone conformations may contribute to the unique macroscopic thermoresponsive profile in combination with conformational changes in the F1 side chains.

To gain further insight into the mechanisms of temperature-responsive behavior, the peptide conformation and the interactions both within the peptide itself and in the solvent were investigated by analyzing the Rg, SASA, n_{PP}, and n_{PW} from the MD simulations performed for a single peptide molecule. These parameters were obtained for three peptides, $[\alpha\text{-E(F1)}]_5$-F1, $[\gamma\text{-E(F1)}]_5$-F1, and Ac-F1-NH_2 (AcF1). AcF1 represents the side component of the branched ELPs.

For $[\alpha\text{-E(F1)}]_5$-F1 and $[\gamma\text{-E(F1)}]_5$-F1, the Rg decreased upon heating to intermediate temperatures (30–60 °C) and increased at higher temperatures (Figure 3-12b, c). SASA displayed a similar trend, indicating that the branched ELPs fold at intermediate temperatures, reducing their solubility and promoting self-assembly, while they unfold upon further heating, enhancing their solubility and causing disaggregation of aggregates. The n_{PP} decreased upon heating from 5 °C to 30 °C, increased at 60 °C, and decreased again at 90 °C (Figure 3-12e, f). The high n_{PP} observed for $[\gamma\text{-E(F1)}]_5$-F1 at 5 °C likely reflects the low kinetic energy, which allows the F1 chains and backbone within the molecule to stay closer and maintain stable hydrogen bonds. With this exception, these parameters of the branched ELPs commonly featured the extremum values around medium temperatures (30–60 °C). Because the fluctuation of n_{PP} might positively correlate

with the formation of β-structures affecting peptide solubility, the n_{PP} changes at 5–60 °C could correspond to the aggregation and disaggregation of LCST-like behavior and those at 60–90 °C would reflect the disaggregation and aggregation of UCST-like behavior. Similarly, the n_{PW} decreased upon heating to 60 °C, but slightly increased at 90 °C. Taken together, the profiles of n_{PP} and n_{PW} indicate that the branched ELPs expose more hydrophilic sites to water upon heating from 60 °C to 90 °C, which leads to the peptide hydration and ultimately results in the UCST-like behavior.

Regarding AcF1, three of the four parameters likewise showed the extremum values at medium temperatures. Among the four temperature conditions simulated, Rg and SASA showed the lowest values and n_{PP} showed the highest value at 60 °C (Figure 3-12d, g). These results indicate that temperature-dependent changes in a single F1 molecule are preserved in the side components (F1 chains) of the branched ELPs and contribute to their parameter fluctuations. Notably, similar behavior, with folding at approximately 40–60 °C and unfolding at higher temperature (> 60 °C), has also been reported for the octapeptide GVG(VPGVG) [48].

Overall, these MD results indicated that the branched ELPs undergo changes in conformation and solvation over a range of 5–90 °C, with several parameters reaching extremum values at medium temperatures. These fluctuations likely account for the characteristic temperature-responsive behavior observed in these short-chain branched ELPs (Figure 3-13). Based on these findings, it is suggested that maintaining a moderately weak self-assembling property would be crucial to achieving dual LCST- and UCST-like behavior in ELP-based molecules. This is because a strong self-assembling property would result in insolubility at high temperatures and lack of UCST-like re-dissolution. For this reason, ELPs may be less likely to exhibit dual-responsive behavior under conditions that employ long peptide chains, highly hydrophobic amino acid compositions, or high peptide concentrations, which typically lowers T_t values for LCST-like behavior.

(Figures 3-12 and 3-13)

4. Conclusion

In this chapter, branched ELPs composed of F1 side components and oligo(Glu) backbone structures were synthesized and investigated for their temperature-responsive behavior. The obtained branched ELPs exhibited LCST-like behavior with concentration-dependent T_t values. The branched ELPs exhibited temperature-dependent reversible secondary structural changes and formed spherical aggregates in a stepwise manner. Notably, the branched ELPs with six F1 units showed UCST-like behavior at 0.5 mM in addition to LCST-like behavior, a phenomenon that has rarely been reported for ELPs. The unique responsive behavior was

attributed primarily to the temperature-dependent changes in peptide conformation and hydration states over a temperature range of 5–90 °C. Overall, these findings demonstrated the unique temperature-responsiveness of branched short ELPs, and provided new insights for the design and application of ELPs with desired properties.

Future studies will be required to determine whether similar dual temperature-responsive behavior can be observed in ELPs of other structural designs, including not only branched short-chain ELPs but also branched long-chain, linear short-chain, and linear long-chain variants. This point is important because turbidity measurements, a widely used method to examine temperature-responsive behavior, cannot distinguish between dissolution and precipitation of aggregates at high temperatures, meaning that similar dual temperature responsiveness might have been overlooked. Therefore, it will be crucial to elucidate the structural requirements and the detailed mechanism underlying the temperature-responsiveness. Advancing these investigations would further broaden the opportunities for designing and applying ELP-based materials.

5. References

[1] Kim, Y.-J.; T. Matsunaga, Y. Thermo-Responsive Polymers and Their Application as Smart Biomaterials. *J. Mater. Chem. B* **2017**, *5* (23), 4307–4321.

[2] Alexander, C.; Shakesheff, K. M. Responsive Polymers at the Biology/Materials Science Interface. *Adv. Mater.* **2006**, *18* (24), 3321–3328.

[3] Du, F.-S.; Huang, X.-N.; Chen, G.-T.; Lin, S.-S.; Liang, D.; Li, Z.-C. Aqueous Solution Properties of the Acid-Labile Thermoresponsive Poly(Meth)Acrylamides with Pendent Cyclic Orthoester Groups. *Macromolecules* **2010**, *43* (5), 2474–2483.

[4] Haq, M. A.; Su, Y.; Wang, D. Mechanical Properties of PNIPAM Based Hydrogels: A Review. *Mater. Sci. Eng. C* **2017**, *70*, 842–855.

[5] Zhao, C.; Ma, Z.; Zhu, X. X. Rational Design of Thermoresponsive Polymers in Aqueous Solutions: A Thermodynamics Map. *Prog. Polym. Sci.* **2019**, *90*, 269–291.

[6] Nair, L. S.; Laurencin, C. T. Biodegradable Polymers as Biomaterials. *Prog. Polym. Sci.* **2007**, *32* (8), 762–798.

[7] Despanie, J.; Dhandhukia, J. P.; Hamm-Alvarez, S. F.; MacKay, J. A. Elastin-like Polypeptides: Therapeutic Applications for an Emerging Class of Nanomedicines. *J. Controlled Release* **2016**, *240*, 93–108.

[8] Hassouneh, W.; MacEwan, S. R.; Chilkoti, A. Chapter Nine - Fusions of Elastin-Like Polypeptides to Pharmaceutical Proteins. In *Methods in Enzymology*; Wittrup, K. D., Verdine, G. L., Eds.; Protein Engineering for Therapeutics, Part A; Academic Press, 2012, 502, 215–237.

[9] Hassouneh, W.; Christensen, T.; Chilkoti, A. Elastin-Like Polypeptides as a Purification Tag for Recombinant Proteins. *Curr. Protoc. Protein Sci.* **2010**, *61* (1), 6.11.1–6.11.16.

[10] Rodríguez-Cabello, J. C.; Arias, F. J.; Rodrigo, M. A.; Girotti, A. Elastin-like Polypeptides in Drug Delivery. *Adv. Drug Deliv. Rev.* **2016**, *97*, 85–100.

[11] Kostal, J.; Mulchandani, A.; Chen, W. Tunable Biopolymers for Heavy Metal Removal. *Macromolecules* **2001**, *34* (7), 2257–2261.

[12] Indik, Z.; Yeh, H.; Ornstein-Goldstein, N.; Sheppard, P.; Anderson, N.; Rosenbloom, J. C.; Peltonen, L.; Rosenbloom, J. Alternative Splicing of Human Elastin mRNA Indicated by Sequence Analysis of Cloned Genomic and Complementary DNA. *Proc. Natl. Acad. Sci.* **1987**, *84* (16), 5680–5684.

[13] Bressan, G. M.; Argos, P.; Stanley, K. K. Repeating Structure of Chick Tropoelastin Revealed by Complementary DNA Cloning. *Biochemistry* **1987**, *26* (6), 1497–1503.

[14] Vrhovski, B.; Weiss, A. S. Biochemistry of Tropoelastin. *Eur. J. Biochem.* **1998**, *258* (1), 1–18.

[15] Urry, D. W.; Gowda, D. C.; Parker, T. M.; Luan, C.-H.; Reid, M. C.; Harris, C. M.; Pattanaik, A.; Harris, R. D. Hydrophobicity Scale for Proteins Based on Inverse Temperature Transitions. *Biopolymers* **1992**, *32* (9), 1243–1250.

[16] Nuhn, H.; Klok, H.-A. Secondary Structure Formation and LCST Behavior of Short Elastin-Like Peptides. *Biomacromolecules* **2008**, *9* (10), 2755–2763.

[17] McDaniel, J. R.; Radford, D. C.; Chilkoti, A. A Unified Model for De Novo Design of Elastin-like Polypeptides with Tunable Inverse Transition Temperatures. *Biomacromolecules* **2013**, *14* (8), 2866–2872.

[18] Lin, C.-Y.; Liu, J. C. Incorporation of Short, Charged Peptide Tags Affects the Temperature Responsiveness of Positively-Charged Elastin-like Polypeptides. *J. Mater. Chem. B* **2019**, *7* (34), 5245–5256.

[19] Meyer, D. E.; Chilkoti, A. Quantification of the Effects of Chain Length and Concentration on the Thermal Behavior of Elastin-like Polypeptides. *Biomacromolecules* **2004**, *5* (3), 846–851.

[20] MacKay, J. A.; Callahan, D. J.; FitzGerald, K. N.; Chilkoti, A. Quantitative Model of the Phase Behavior of Recombinant pH-Responsive Elastin-Like Polypeptides. *Biomacromolecules* **2010**, *11* (11), 2873–2879.

[21] Cho, Y.; Zhang, Y.; Christensen, T.; Sagle, L. B.; Chilkoti, A.; Cremer, P. S. Effects of Hofmeister Anions on the Phase Transition Temperature of Elastin-like Polypeptides. *J. Phys. Chem. B* **2008**, *112* (44), 13765–13771.

[22] Mills, C. E.; Ding, E.; Olsen, B. D. Cononsolvency of Elastin-like Polypeptides in Water/Alcohol Solutions. *Biomacromolecules* **2019**, *20* (6), 2167–2173.

[23] Zhao, Y.; Singh, M. K.; Kremer, K.; Cortes-Huerto, R.; Mukherji, D. Why Do Elastin-Like Polypeptides Possibly Have Different Solvation Behaviors in Water–Ethanol and Water–Urea Mixtures? *Macromolecules* **2020**, *53* (6), 2101–2110.

[24] Tanaka, N.; Suyama, K.; Tomohara, K.; Maeda, I.; Nose, T. Branched Short Elastin-like Peptides with Temperature Responsiveness Obtained by EDTA-Mediated Multimerization. *J. Pept. Sci.* **2023**, *29* (2), e3449.

[25] Maeda, I.; Taniguchi, S.; Watanabe, N.; Inoue, A.; Yamasaki, Y.; Nose, T. Design of Phenylalanine-Containing Elastin-Derived Peptides Exhibiting Highly Potent Self-Assembling Capability. *Protein Pept. Lett.* **2015**, *22* (10), 934–939.

[26] Suyama, K.; Taniguchi, S.; Tatsubo, D.; Maeda, I.; Nose, T. Dimerization Effects on Coacervation Property of an Elastin-Derived Synthetic Peptide $(FPGVG)_5$. *J. Pept. Sci.* **2016**, *22* (4), 236–243.

[27] Suyama, K.; Mawatari, M.; Tatsubo, D.; Maeda, I.; Nose, T. Simple Regulation of the Self-Assembling Ability by Multimerization of Elastin-Derived Peptide $(FPGVG)_n$ Using Nitrilotriacetic Acid as a Building Block. *ACS Omega* **2021**, *6* (8), 5705–5716.

[28] Reiersen, H.; Clarke, A. R.; Rees, A. R. Short Elastin-like Peptides Exhibit the Same Temperature-Induced Structural Transitions as Elastin Polymers: Implications for Protein Engineering1. *J. Mol. Biol.* **1998**, *283* (1), 255–264.

[29] Bo, J.; Wang, L.; Li, W.; Zhang, X.; Zhang, A. Comb-like Polymers Pendanted with Elastin-like Peptides Showing Sharp and Tunable Thermoresponsiveness through Dynamic Covalent Chemistry. *J. Polym. Sci. Part Polym. Chem.* **2016**, *54* (20), 3379–3387.

[30] Kojima, C.; Sk, U. H.; Fukushima, D.; Irie, K.; Akazawa, N.; Umeda, M.; Niidome, T. Effect of Main Chain Conformation on Thermosensitivity in Elastin-like Peptide-Grafted Polylysine. *RSC Adv.* **2015**, *5* (127), 104900–104906.

[31] Conrad, R. M.; Grubbs, R. H. Tunable, Temperature-Responsive Polynorbornenes with Side Chains Based on an Elastin Peptide Sequence. *Angew. Chem. Int. Ed.* **2009**, *48* (44), 8328–8330.

[32] Fernández-Trillo, F.; Duréault, A.; Bayley, J. P. M.; Van Hest, J. C. M.; Thies, J. C.; Michon, T.; Weberskirch, R.; Cameron, N. R. Elastin-Based Side-Chain Polymers: Improved Synthesis via RAFT and Stimulus Responsive Behavior. *Macromolecules* **2007**, *40* (17), 6094–6099.

[33] Ayres, L.; Koch, K.; Adams P. H. H. M.; van Hest, J. C. M. Stimulus Responsive Behavior of Elastin-Based Side Chain Polymers. *Macromolecules* **2005**, *38* (5), 1699–1704.

[34] Hess, B.; Kutzner, C.; van der Spoel, D.; Lindahl, E. GROMACS 4: Algorithms for Highly Efficient, Load-Balanced, and Scalable Molecular Simulation. *J. Chem. Theory Comput.* **2008**, *4* (3), 435–447.

[35] Kim, K. H.; Nam, J.; Choi, J.; Seo, M.; Bang, J. From Macromonomers to Bottlebrush Copolymers with Sequence Control: Synthesis, Properties, and Applications. *Polym. Chem.* **2022**, *13* (16), 2224–2261.

[36] Arias, S.; Freire, F.; Calderón, M.; Bergueiro, J. Unexpected Chiro-Thermoresponsive Behavior of Helical Poly(Phenylacetylene)s Bearing Elastin-Based Side Chains. *Angew. Chem. Int. Ed.* **2017**, *56* (38), 11420–11425.

[37] Nan, Y.; Zhao, C.; Beaudoin, G.; Zhu, X. X. Synergistic Approaches in the Design and Applications of UCST Polymers. *Macromol. Rapid Commun.* **2023**, *44* (23), 2300261.

[38] Niskanen, J.; Tenhu, H. How to Manipulate the Upper Critical Solution Temperature (UCST)? *Polym. Chem.* **2017**, *8* (1), 220–232.

[39] Fu, X.; Xing, C.; Sun, J. Tunable LCST/UCST-Type Polypeptoids and Their Structure–Property Relationship. *Biomacromolecules* **2020**, *21* (12), 4980–4988.

[40] Tatsubo, D.; Suyama, K.; Miyazaki, M.; Maeda, I.; Nose, T. Stepwise Mechanism of Temperature-Dependent Coacervation of the Elastin-like Peptide Analogue Dimer, $(C(WPGVG)_3)_2$. *Biochemistry* **2018**, *57* (10), 1582–1590.

[41] Lopes, J. L. S.; Miles, A. J.; Whitmore, L.; Wallace, B. A. Distinct Circular Dichroism Spectroscopic Signatures of Polyproline II and Unordered Secondary Structures: Applications in Secondary Structure Analyses. *Protein Sci.* **2014**, *23* (12), 1765–1772.

[42] Tifany, M. L.; Krimm, S. Effwct of Temperature on the Circular Dichroism Spectra of Polypeptides in the Extended State. *Biopolymers* **1972**, *11* (11), 2309–2316.

[43] Arad, E.; Green, H.; Jelinek, R.; Rapaport, H. Revisiting Thioflavin T (ThT) Fluorescence as a Marker of Protein Fibrillation – The Prominent Role of Electrostatic Interactions. *J. Colloid Interface Sci.* **2020**, *573*, 87–95.

[44] Maeda, I.; Fukumoto, Y.; Nose, T.; Shimohigashi, Y.; Nezu, T.; Terada, Y.; Kodama, H.; Kaibara, K.; Okamoto, K. Structural Requirements Essential for Elastin Coacervation: Favorable Spatial Arrangements of Valine Ridges on the Three-Dimensional Structure of Elastin-Derived Polypeptide $(VPGVG)_n$. *J. Pept. Sci.* **2011**, *17* (11), 735–743.

[45] Sumiyoshi, S.; Suyama, K.; Tanaka, N.; Andoh, T.; Nagata, A.; Tomohara, K.; Taniguchi, S.; Maeda, I.; Nose, T. Development of Truncated Elastin-like Peptide Analogues with Improved Temperature-Response and Self-Assembling Properties. *Sci. Rep.* **2022**, *12* (1), 1–16.

[46] Suyama, K.; Murashima, M.; Maeda, I.; Nose, T. Enhancement of Aggregate Formation Through Aromatic Compound Adsorption in Elastin-like Peptide $(FPGVG)_5$ Analogs. *Biomacromolecules* **2023**, *24* (11), 5265–5276.

[47] Perskie, L. L.; Street, T. O.; Rose, G. D. Structures, Basins, and Energies: A Deconstruction of the Protein Coil Library. *Protein Sci.* **2008**, *17* (7), 1151–1161.

[48] Rousseau, R.; Schreiner, E.; Kohlmeyer, A.; Marx, D. Temperature-Dependent Conformational Transitions and Hydrogen-Bond Dynamics of the Elastin-Like Octapeptide GVG(VPGVG): A Molecular-Dynamics Study. *Biophys. J.* **2004**, *86* (3), 1393–1407.

Table 3-1. Retention time, yield, and *m/z* values of the branched ELPs.

Peptide	n	Retention time (min)[a]	Yield (%)	MS (ESI) *m/z*[b]	
				Calculated	Found
$[\alpha\text{-E(F1)}]_n\text{-F1}$	4	2.093	57	940.08 $[M + 3H]^{3+}$	940.12
	5	2.266	58	1135.30 $[M + 3H]^{3+}$	1135.26
	6	2.382	37	998.14 $[M + 4H]^{4+}$	998.11
$[\gamma\text{-E(F1)}]_n\text{-F1}$	4	1.860	15	940.08 $[M + 3H]^{3+}$	940.07
	5	2.008	13	1135.30 $[M + 3H]^{3+}$	1135.25
	6	2.127	8	998.14 $[M + 4H]^{4+}$	998.07

[a] Retention times in UPLC. The peptides were monitored in a linear gradient of solvent B in solvent A (24% to 56%) over 4.23 min.

[b] *m/z* in UPLC-MS. The calculated values are for the average mass.

Table 3-2. T_t values of the branched ELPs for LCST-like behavior.

Peptide	n	Concentration (mM)	T_t (°C)[a]
[α-E(F1)]$_n$-F1	4	4	21.12 ± 1.68
		2.5	29.98 ± 1.82
		1.5	47.04 ± 0.81
	5	2.5	13.86 ± 0.33
		1	30.11 ± 0.15
		0.5	56.92 ± 1.28
	6	2.5	7.68 ± 0.80
		1	19.76 ± 0.97
		0.5	33.80 ± 0.38
[γ-E(F1)]$_n$-F1	4	4	20.75 ± 0.47
		2.5	30.25 ± 0.23
		1.5	46.52 ± 0.67
	5	2.5	17.38 ± 0.10
		1	34.73 ± 0.52
		0.5	61.87 ± 0.60
	6	2.5	8.63 ± 0.31
		1	23.66 ± 0.06
		0.5	34.56 ± 0.48

[a] The T_t values are shown with standard errors.

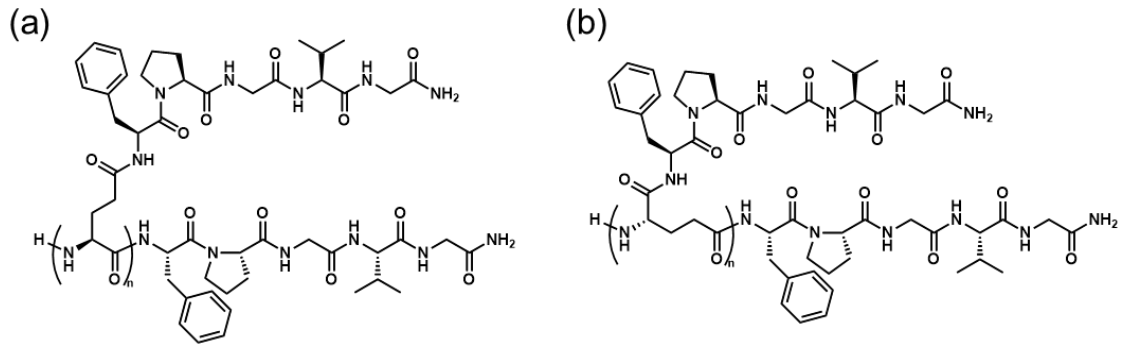

Figure 3-1. Structures of the branched ELPs used in this chapter.
(a) $[\alpha\text{-E(F1)}]_n$-F1 and (b) $[\gamma\text{-E(F1)}]_n$-F1, where n = 4, 5, or 6.

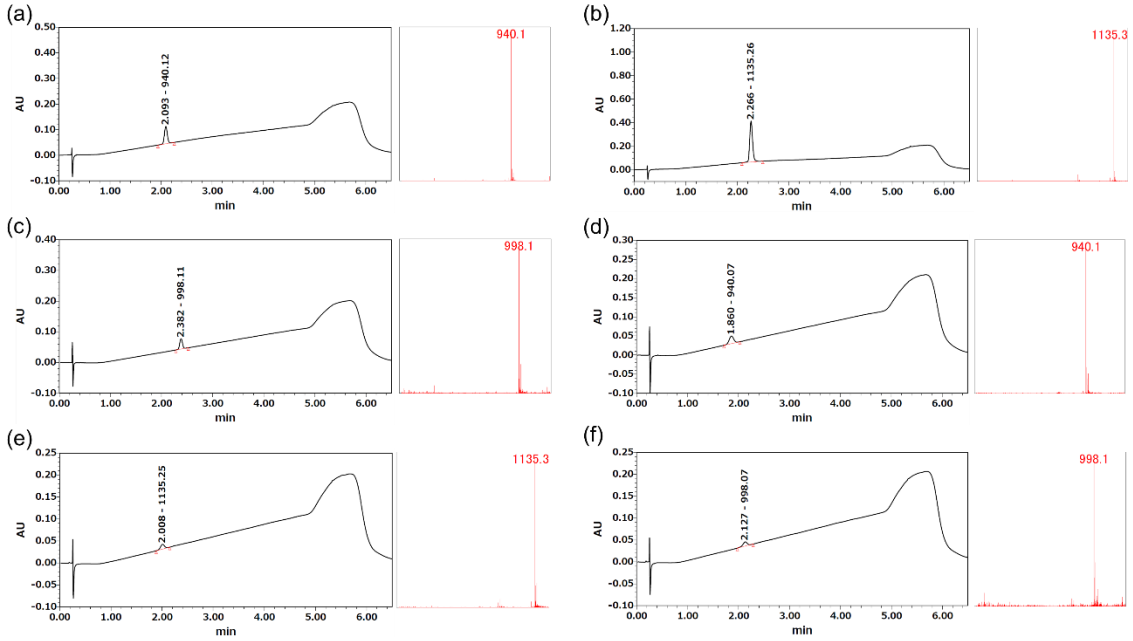

Figure 3-2. UPLC-MS characterization of the branched ELPs.
(a) $[\alpha\text{-E(F1)}]_4$-F1, (b) $[\alpha\text{-E(F1)}]_5$-F1, (c) $[\alpha\text{-E(F1)}]_6$-F1, (d) $[\gamma\text{-E(F1)}]_4$-F1, (e) $[\gamma\text{-E(F1)}]_5$-F1, and (f) $[\gamma\text{-E(F1)}]_6$-F1. In the left panels, the subscripts for each peak indicate the retention time and the *m/z* detected. The right panels show MS spectra of the corresponding peak determined by ACQUITY QDa mass spectrometer. The peptides were monitored in a linear gradient of solvent B in solvent A (24% to 56%) over 4.23 min.

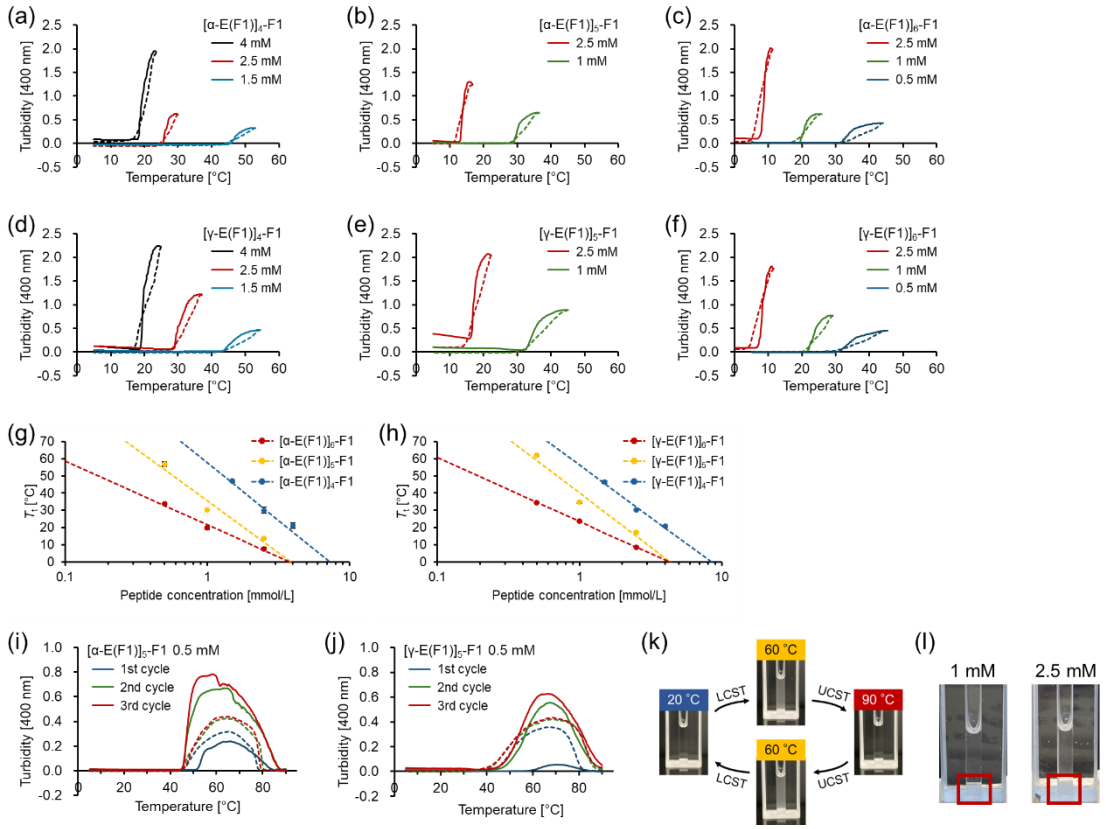

Figure 3-3. Turbidity profiles of branched ELPs showing LCST- and UCST-like behavior. Turbidity profiles (400 nm) of (a) [α-E(F1)]$_4$-F1, (b) [α-E(F1)]$_5$-F1, (c) [α-E(F1)]$_6$-F1, (d) [γ-E(F1)]$_4$-F1, (e) [γ-E(F1)]$_5$-F1, and (f) [γ-E(F1)]$_6$-F1 at various concentrations. T_t-concentration relationship of (g) [α-E(F1)]$_n$-F1 and (h) [γ-E(F1)]$_n$-F1. Turbidity profiles of (i) [α-E(F1)]$_5$-F1 at 0.5 mM and (j) [γ-E(F1)]$_5$-F1 at 0.5 mM. Images of (k) [α-E(F1)]$_5$-F1 at 0.5 mM, and (l) [α-E(F1)]$_5$-F1 at 1 mM and 2.5 mM at 90 °C. In panels (a–f), (i), and (j), solid and dashed lines represent the turbidity profiles upon heating and cooling, respectively. In panels (i) and (j), blue, green, and red lines represent the first, second, and third heating-cooling cycle, respectively. In (l), insoluble aggregates observed at the bottom of a measurement cell are highlighted in red frames.

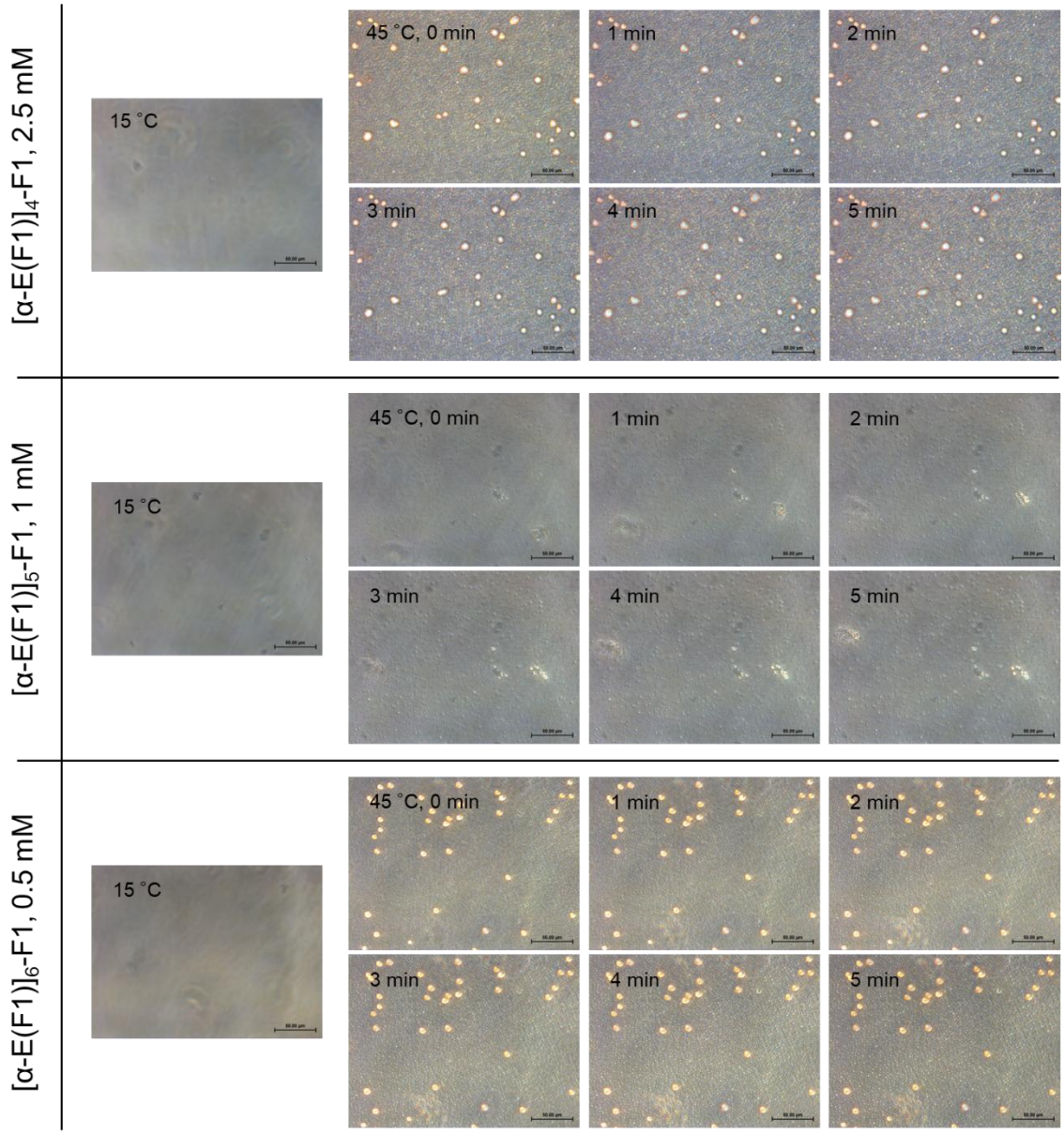

Figure 3-4. Bright-field microscopy images of $[\alpha\text{-E(F1)}]_n$-F1 below and above T_t.
Scale bars: 50 μm.

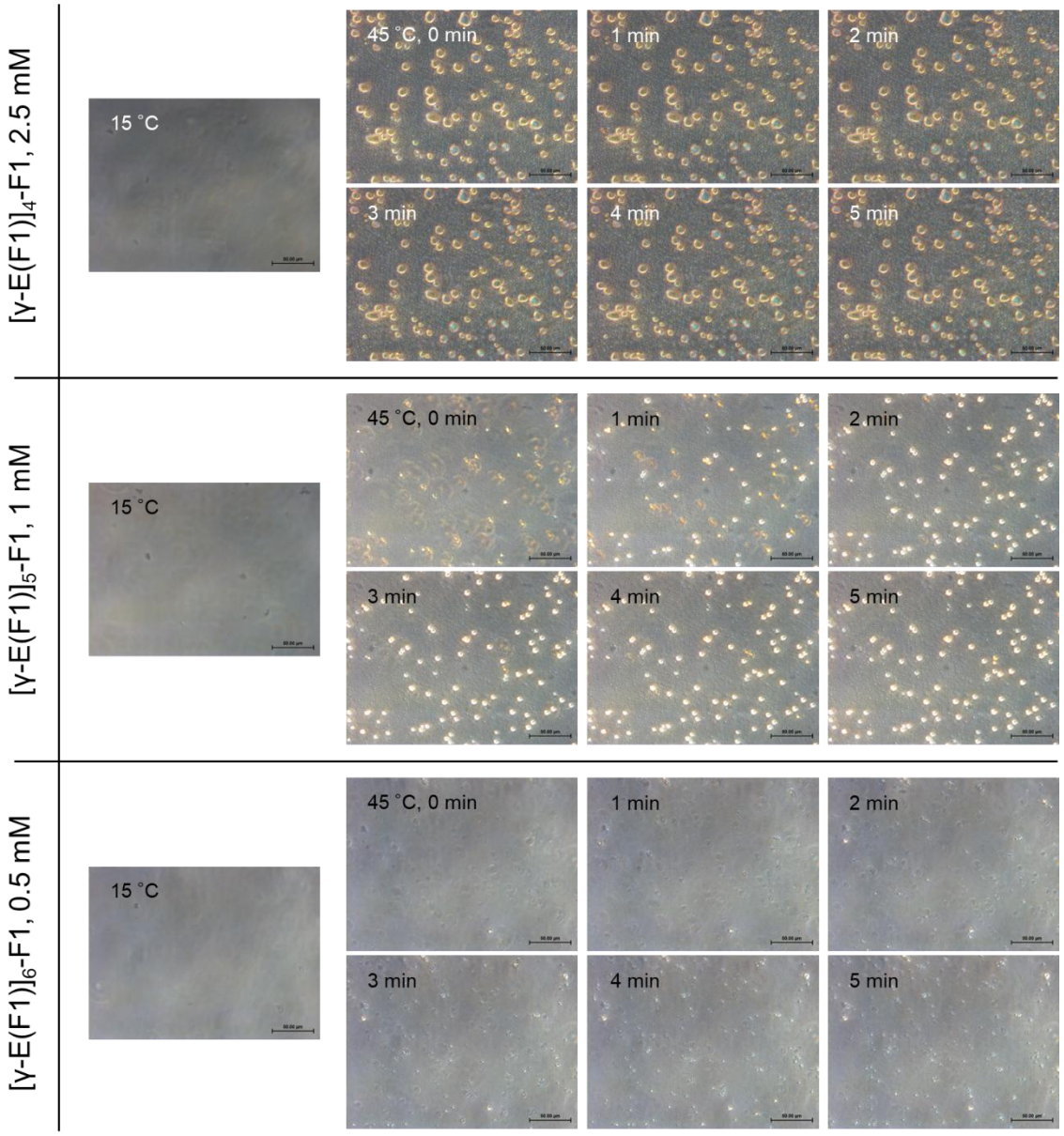

Figure 3-5. Bright-field microscopy images of [γ-E(F1)]$_n$-F1 below and above T_t.
Scale bars: 50 μm.

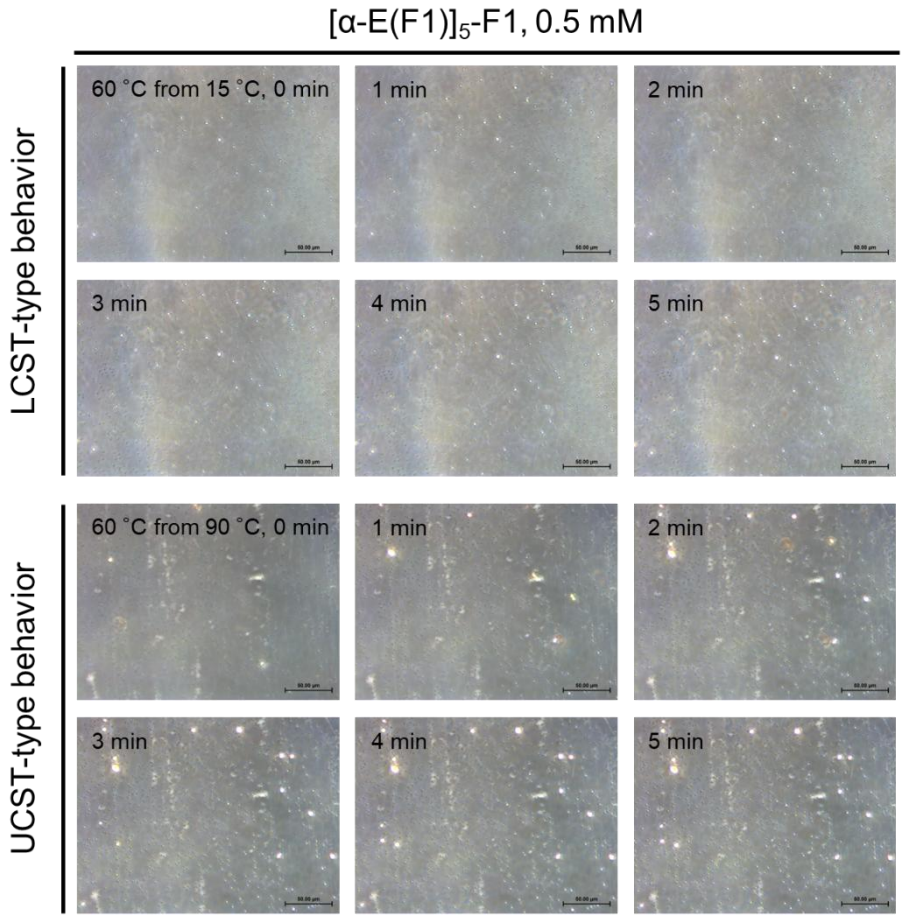

Figure 3-6. Microscopy images of $[\alpha\text{-E(F1)}]_5$-F1 (0.5 mM) under LCST- and UCST-like pathways. Scale bars: 50 μm.

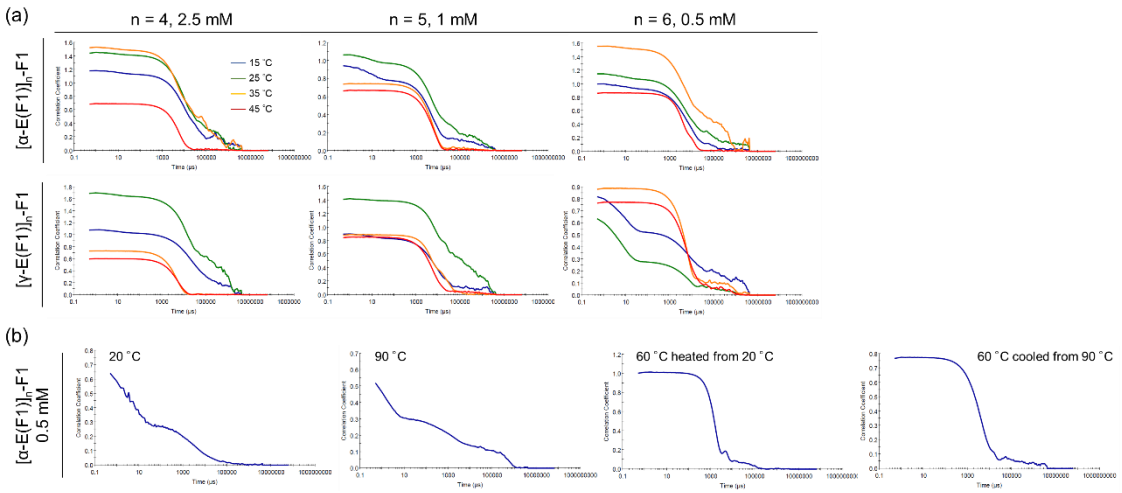

Figure 3-7. DLS autocorrelation curves for the branched ELP solutions.

(a) Curves for samples prepared under conditions where the ELPs have T_t around 30 °C for LCST-like behavior, and (b) curves for [α-E(F1)]$_5$-F1 at 0.5 mM measured at 20, 60, and 90 °C.

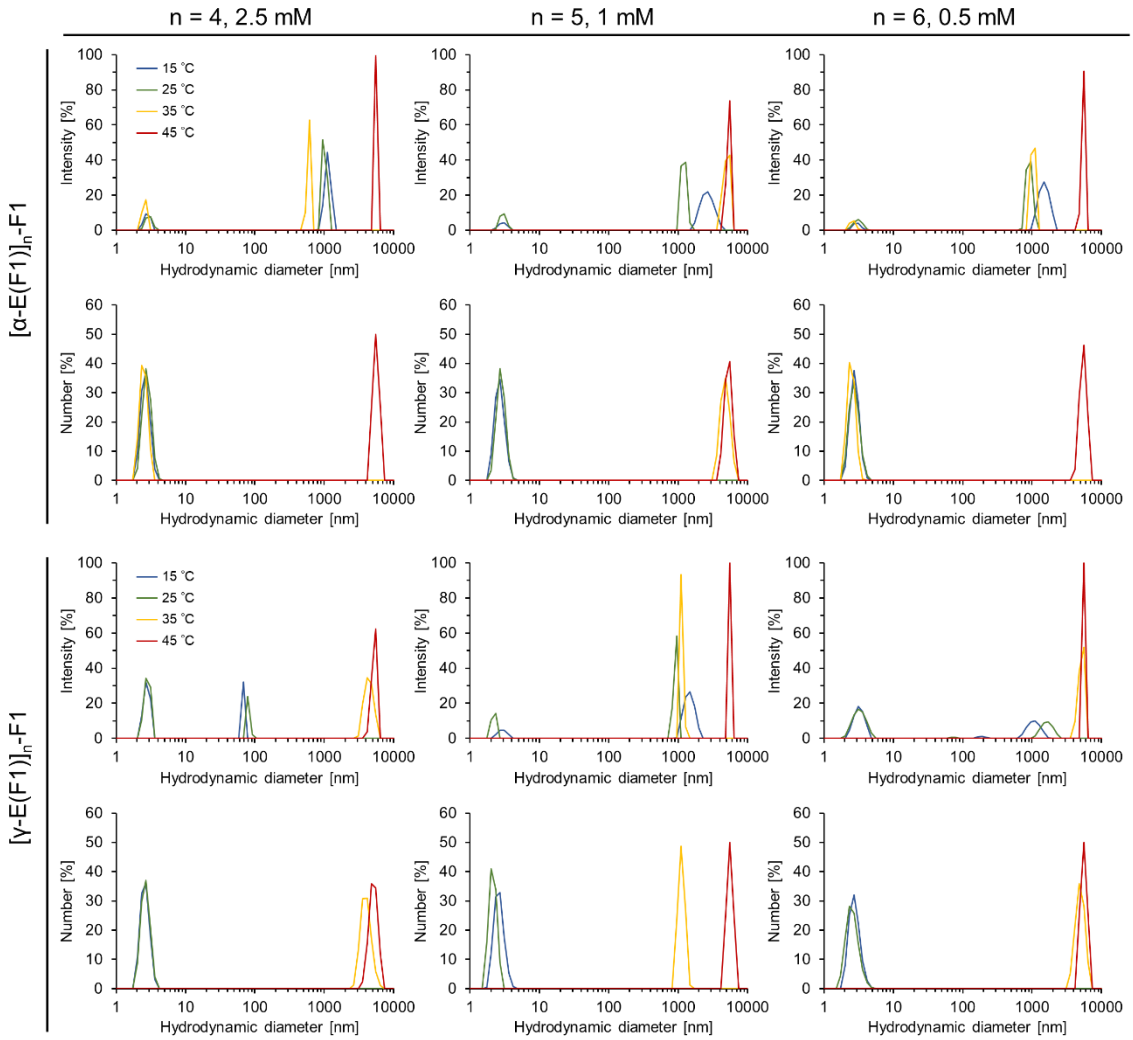

Figure 3-8. DLS measurements of the branched ELPs for LCST-like behavior.

Size distributions for $[\alpha\text{-E(F1)}]_n$-F1 and $[\gamma\text{-E(F1)}]_n$-F1 are shown as scattering intensity (upper panels) and number (lower panels). The samples were prepared at conditions where the branched ELPs have T_t around 30 °C.

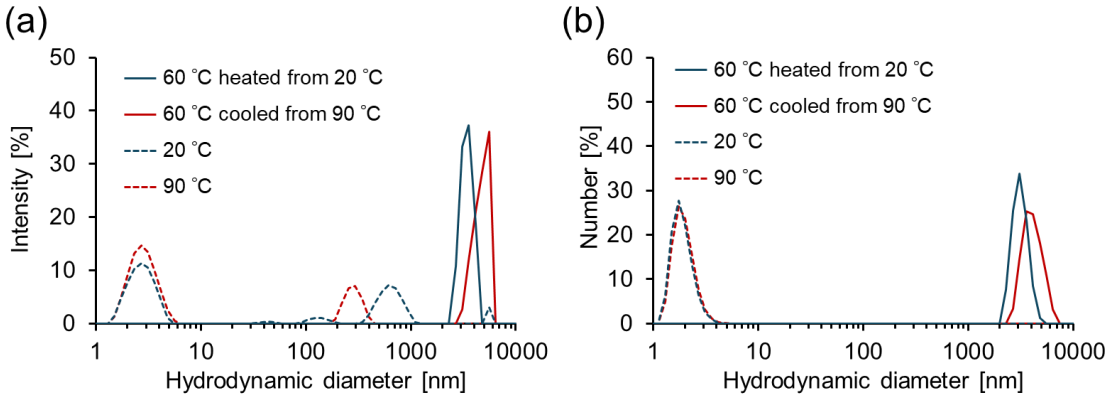

Figure 3-9. DLS analysis of aggregates size during LCST- and UCST-type transitions of [α-E(F1)]$_5$-F1 at 0.5 mM.

Size distributions are shown as (a) scattering intensity and (b) number.

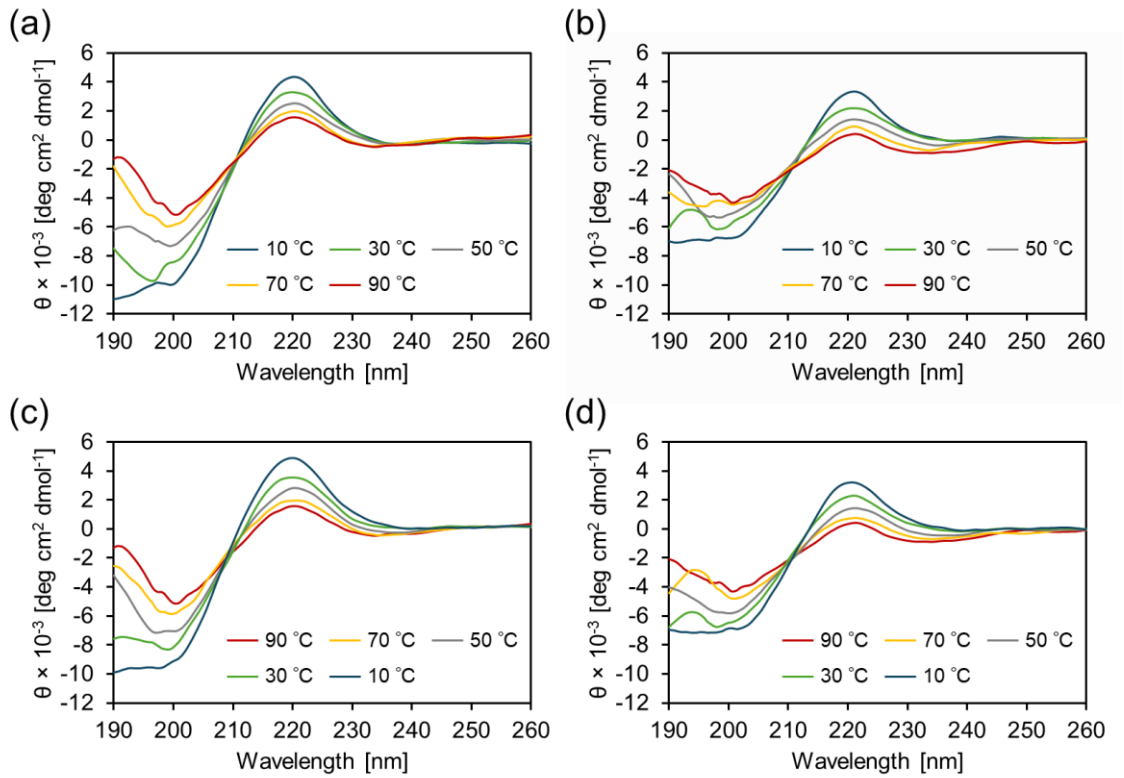

Figure 3-10. Temperature-dependent CD spectra of the branched ELPs.

Spectra recorded upon heating for (a) [α-E(F1)]$_5$-F1 and (b) [γ-E(F1)]$_5$-F1, and upon cooling for (c) [α-E(F1)]$_5$-F1 and (d) [γ-E(F1)]$_5$-F1.

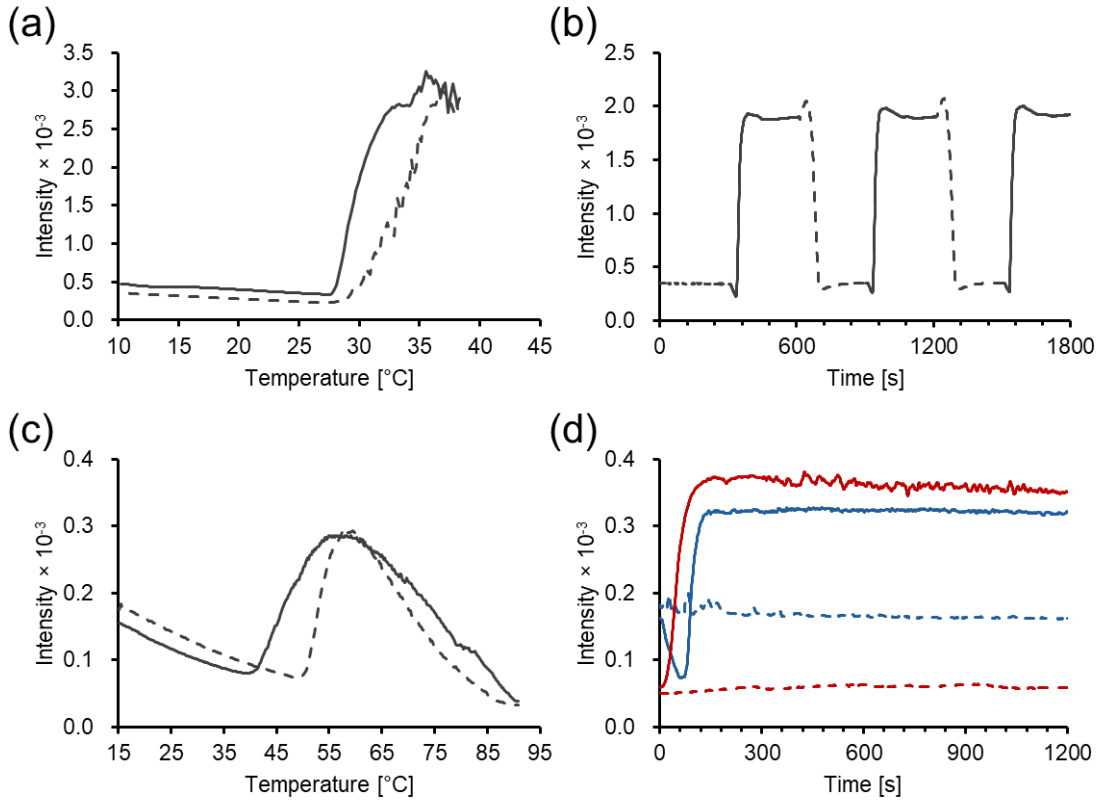

Figure 3-11. ThT fluorescence assays for [α-E(F1)]$_5$-F1.

(a) Temperature-dependent ThT fluorescence at 1 mM, (b) time-dependent ThT fluorescence at 1 mM with switching temperature, (c) temperature-dependent ThT fluorescence at 0.5 mM, and (d) time-dependent ThT fluorescence at 0.5 mM. In panels (a) and (c), the solid and dashed lines represent the fluorescence intensity changes upon heating and cooling, respectively. In panel (b), the solid and dashed lines represent fluorescence intensity profiles at 45 °C and 15 °C, respectively, with the beginning of each curve representing when the temperature was set at 45 °C or 15 °C. In panel (d), the solid blue line represents the fluorescence profile at 60 °C heated from 15 °C, the dashed blue line represents the profile at 15 °C, the solid red line shows the profile at 60 °C cooled from 90 °C, and the dashed red line corresponds to the profile at 90 °C.

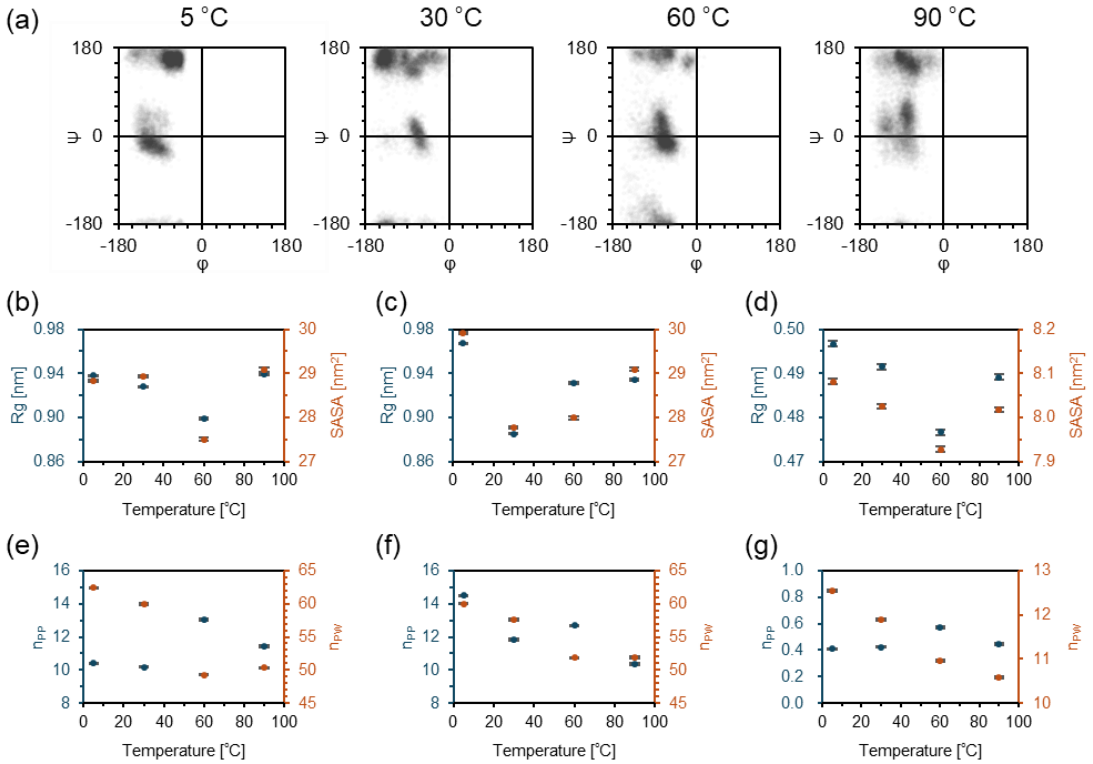

Figure 3-12. Single-molecule MD analyses of branched ELPs and AcF1.

(a) Ramachandran plots of backbone Glu residues of [α-E(F1)]$_5$-F1, (b) Rg and SASA of [α-E(F1)]$_5$-F1, (c) Rg and SASA of [γ-E(F1)]$_5$-F1, (d) Rg and SASA of AcF1, (e) n_{PP} and n_{PW} of [α-E(F1)]$_5$-F1, (f) n_{PP} and n_{PW} of [γ-E(F1)]$_5$-F1, (g) n_{PP} and n_{PW} of AcF1. In panels (b–g), the definitions of the parameters are follows: Rg, radius of gyration; SASA, solvent accessible surface areas; n_{PP}, number of intramolecular hydrogen bonds; n_{PW}, number of hydrogen bonds between water and peptide.

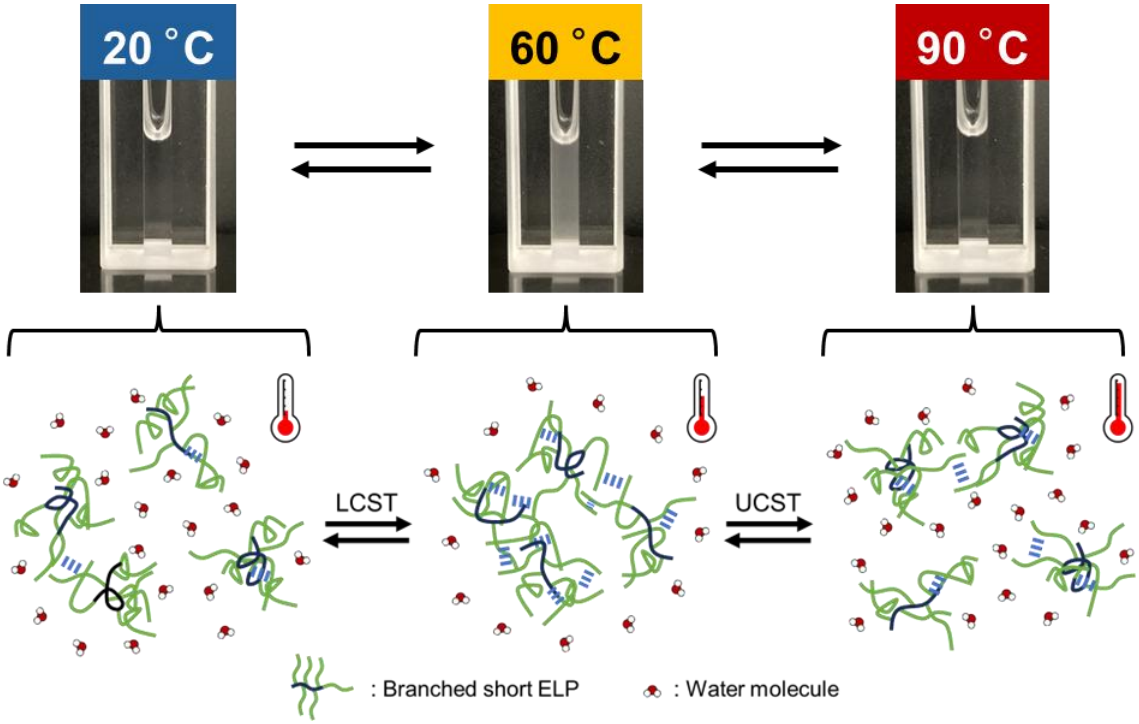

Figure 3-13. Schematic illustration of the LCST- and UCST-like behavior observed in the branched short-chain ELPs.

Formation of β-structures and dehydration account for aggregation at approximately 60 °C.

Chapter 4

Investigation of LCST-type phase behavior in mixtures of short-chain elastin-like peptides with minimal structural differences

This chapter is based on the manuscript published in *Biopolymers* **2026**, *117* (2), e70084.

Abstract

Elastin-like peptides (ELPs) exhibit lower critical solution temperature (LCST)-type behavior, being soluble at low temperatures and insoluble at high temperatures. Their temperature-responsive behavior has enabled their broad use in biomedical and chemical applications. Although the miscibility and interactions in long-chain ELP mixtures have been studied previously, it remains unclear whether mixtures of short-chain ELPs that differ only slightly in chain length or topology can exhibit distinct phase behavior. To address this question, in this chapter, the phase behavior of short-chain ELPs differing by only one or two repeat units in length or by molecular topology was investigated to clarify whether independent phase transitions can be observed in mixed systems. Linear ELPs with the sequence of H-(Phe-Pro-Gly-Val-Gly)$_n$-NH_2 (n = 2, 3, or 4) and a branched molecule bearing four FPGVG chains were examined in single-component and two-component ELP solutions under NaCl-supplemented solvent conditions in which each ELP exhibited LCST-type behavior. Turbidity measurements showed that while the single-component solutions displayed single-step turbidity increases upon heating, the binary mixtures exhibited two-step turbidity increases, indicating stepwise phase transitions. The stepwise behavior was further supported by UPLC-MS analysis, which verified differential depletion of each component from the dilute phase. Circular dichroism analysis suggested that the ELPs in the mixtures undergo a structural transition from polyproline type II helix to β-sheet or β-turn structures. Additionally, the sequential behavior of the mixtures appeared to be influenced by heterotypic interactions between the components. These results demonstrate that even minimal differences in ELP architecture can lead to distinct phase separation in mixed systems, providing insights into the design of multi-component, stimuli-responsive peptide-based materials.

1. Introduction

Elastin-like peptides (ELPs) undergo reversible liquid-liquid phase separation (LLPS) through lower critical solution temperature (LCST)-type phase behavior, resulting in an ELP-rich condensed phase and a dilute phase [1]. Their transition temperature (T_t) depends on multiple parameters, including amino acid composition [2–4], peptide chain length [5,6], concentration [5,6], ionic strength [7,8], and chemical modification [9–16]. Owing to this tunability, ELPs have been widely explored as versatile platforms for applications such as drug delivery, protein purification, tissue engineering, and metal recovery, and more recently, as building blocks of membraneless, phase-separated droplets for regulating (bio)chemical reactions [17–26]. These studies underscore that ELP-based applications can involve multicomponent systems, and highlight the importance of understanding phase behavior not only in single-component ELP systems but also in multicomponent systems, where interactions between the components may influence the LCST-type behavior of each component.

Previous studies on mixtures of ELPs have demonstrated that ELPs with large differences in molecular weights and/or sequences can undergo orthogonal phase behavior in mixtures. For example, a binary mixture of long-chain ELPs differing both in compositions and chain length (n = 150 and 160, $\Delta n = 10$) was shown to exhibit independent transitions [28], and mixtures of ELPs of $(VPGVG)_n$ with n = 20, 40, and 90 ($\Delta n \geq 20$) similarly underwent independent phase transitions upon heating [29]. In addition, the Holland group reported that mixtures of linear $(GVGVP)_{40}$ and trimeric $(GVGVP)_{40}$ showed two distinct behaviors at low concentration conditions [30]. In contrast, ELP pairs with highly similar compositions, or with dissimilar compositions but reduced molecular weight in one or both species have been reported to form mixed coacervates rather than showing independent phase separation [31] These findings suggest that the extent of differences in sequence or chain length is a critical determinant of whether the components in ELP mixtures phase-separate independently or form mixed coacervates.

Despite these insights into the mixtures of long-chain ELPs, the phase behavior of mixtures composed of short-chain ELPs remains largely unexplored. In particular, it is unclear whether independent phase behavior can be observed in mixtures of short-chain components with minimal differences in chain length, such as one or two repeat units. Clarifying the effects of these minimal structural differences in multicomponent systems is essential for advancing the rational design and application of short-chain, peptide-based stimuli-responsive materials.

From a practical standpoint, short-chain ELPs are attractive because of their ease of synthesis, purification, and modification [22]. While recombinant expression methods, such as recursive directional ligation, are suited for obtaining long-chain ELPs with precisely defined repeat numbers [32], chemical approaches including solid-phase peptide synthesis and liquid-

phase peptide synthesis are advantageous for synthesizing short-chain ELPs with tailored sequences [33–35], because they enable flexible variations of sequence or chain length through substitution, insertion, or deletion, as well as incorporation of nonnatural residues, which can strongly influence the material properties [36]. As for short-chain ELPs, previous studies have systematically analyzed the composition-dependent LCST behavior [37] and their switching behavior [38], demonstrating their potential as building blocks for smart biomaterials. In addition, the Renner group investigated the behavior of short-chain ELPs (one to three repetitions) under electrochemical conditions [39] and demonstrated the utility of single-repeat motifs for controlling ionomers [40,41]. Furthermore, Maeda *et al.* developed short-chain ELPs based on the $(FPGVG)_n$ sequence (abbreviated as Fn, where n represents the repeat number), and demonstrated that these peptides exhibited LCST-type behavior with approximately five repeats [42,43]. Nonetheless, while the phase behavior of individual short-chain ELPs has been characterized, their behavior in multicomponent mixtures remains less explored.

In this chapter, synthetic short-chain ELPs differing in chain lengths by only one or two repeats (i.e., 5- or 10-residue differences) or in molecular topology (linear or branched) were investigated for their phase behavior in single-component solutions and two-component mixtures. To this end, short-chain ELPs of Fn (n = 2, 3, or 4, corresponding to 10, 15, or 20 residues) and a branched ELP bearing four FPGVG chains were prepared. Although this chapter focused on the smallest differences in repeat number, such variations inevitably correspond to relatively large fractional changes in chain length in short-chain ELPs consisting of 10–20 residues. Turbidity measurements, combined with ultra-performance liquid chromatography (UPLC)-MS analysis, revealed that the two-component ELP mixtures exhibited stepwise phase transitions upon heating while their individual components showed single-step phase transitions. Mechanistic studies revealed structural changes from polyproline type II helix to β-structures upon aggregation, and suggested that the stepwise phase behavior was influenced by heterotypic interactions between the components in the mixtures.

2. Materials and Methods

Chemicals. 9-Fluorenylmethyloxycarbonyl (Fmoc)-amino acids, Fmoc-NH-SAL-MBHA resin (100–200 mesh), *N,N*-diisopropylethylamine (DIPEA), piperidine, trifluoroacetic acid (TFA), 1-[(1-(cyano-2-ethoxy-2-oxoethylideneaminooxy) dimethylamino-morpholino)] uronium hexafluorophosphate (COMU), 2-(1H-benzotriazole-1-yl)-1,1,3,3-tetramethyl uronium hexafluorophosphate (HBTU), and OxymaPure were purchased from Watanabe Chemical Industries (Hiroshima, Japan). Triisopropylsilane (TIS) was purchased from Tokyo Chemical Industry (Tokyo, Japan). *N,N*-dimethylformamide (DMF) was purchased from Kanto Chemical (Tokyo, Japan). Water used in the experiments was purified using a Milli-Q EQ 7000 (Merck

Millipore, Darmstadt, Germany). Other solvents and reagents were obtained from commercial suppliers and used without further purification.

Peptide synthesis. The linear peptides H-(FPGVG)$_n$-NH$_2$ (Fn, n = 1–4) and Fmoc-[α-E(OH)]$_3$-FPGVG-NH$_2$ (a backbone peptide for the synthesis of a branched ELP) were synthesized by Fmoc-based solid-phase synthesis either manually or using a CSBio II, an automated peptide synthesizer (Menlo Park, CA). HBTU and OxymaPure were used as coupling agents. After the peptide chain elongation, the peptide was cleaved from resin with a solution of 95% TFA, 2.5% TIS, and 2.5% H_2O. Then, for Fn, the crude TFA solution was purified using a Sep-Pak cartridge (C18, 10 g) and HPLC followed by lyophilization. For Fmoc-[α-E(OH)]$_3$-FPGVG-NH$_2$, the product was precipitated with cold diethyl ether, and dried under vacuum.

The branched ELP, [α-E(F1)]$_3$-F1 (H-[E(FPGVG-NH$_2$)]$_n$-FPGVG-NH$_2$), was synthesized by a method similar to that described in Chapter 3 [44]. Fmoc-[E(OH)]$_3$-FPGVG-NH$_2$ (0.03 mmol, 1 eq), F1 (0.108 mmol, 3.6 eq), COMU (0.18 mmol, 6 eq), and DIPEA (0.216 mmol, 7.2 eq) were dissolved in 400 μL of DMF and stirred at room temperature for 24 h. Then, 400 μL of water was added and stirred for 1 h. Piperidine was added to the solution to give 20% (v/v) piperidine solution and the mixture was stirred for 2 h. Then, the reaction mixture was filtered and applied to Sep-Pak (C18, 2 g) for pre-purification, and further purified with RP-HPLC (JASCO PU-4180 equipped with UV-4075, JASCO, Tokyo, Japan) using a C8 column (COSMOSIL 5C8-AR-300 Packed Column, 20 mmI.D. × 150 mm, Nacalai Tesque Inc., Kyoto, Japan). The RP-HPLC mobile phases were 0.1% TFA in water (v/v, solvent C) and a mixture of 80% acetonitrile/20% solvent C (v/v, solvent D). After evaporation and lyophilization, the target branched ELP [α-E(F1)]$_3$-F1 was obtained as a colorless solid. For brevity, this peptide is denoted as 4F1, meaning a molecule containing four F1 chains.

Peptide purity and molecular weight were confirmed using an ACQUITY UPLC H-Class (Waters Co., Milford, MA) equipped with an ACQUITY UPLC BEH C-18 column (50 mm, Waters Co.). The UPLC mobile phases were 0.1% formic acid in water (v/v, solvent A) and 0.1% formic acid in acetonitrile (v/v, solvent B).

Turbidity measurement. LCST-type phase behavior was investigated by monitoring turbidity at 400 nm using a JASCO V-660 spectral photometer (JASCO, Tokyo, Japan). Each ELP was dissolved either as single-component solutions or as two-component mixture solutions in phosphate buffer (pH 7.4, 27.4 mM Na_2HPO_4, 17.8 mM NaH_2PO_4) containing NaCl (1 M or 3 M NaCl). This NaCl concentration is used to induce LCST-type behavior for the inverse transition cycling, a method for purifying ELP-fused proteins through LCST behavior [18]. The turbidity profiles were recorded during increasing or decreasing the temperature at 0.5 °C/min. For single-

component ELP samples, the transition temperature (T_t) was defined as a temperature at which the turbidity reached half of its maximum value during heating. Measurements were performed at least three times.

UPLC-MS analysis. The amount of ELPs remaining in the dilute phase after LCST-type phase separation was quantified by UPLC-MS. Peak areas of ELPs were analyzed for the following samples to determine the percentages of ELPs remaining in the supernatant after incubation: (1) the mixture solution maintained at 5 °C, (2) the supernatant obtained after incubation at 25 °C, and (3) the supernatant obtained after incubation at 50 °C. To prepare samples (2) and (3), the mixture solution was incubated at either 25 °C or 50 °C for 30 minutes, followed by centrifugation at 14,000 rpm for 2 min at 25 °C. The resulting supernatants were analyzed using UPLC-MS. The percentages of remaining ELPs in the supernatant after incubation at 25 °C and 50 °C were calculated using the following equations:

Peptides remained at 25 °C (%) = 100 × peak area in sample (2)/ peak area in sample (1)

Peptides remained at 50 °C (%) = 100 × peak area in sample (3)/ peak area in sample (1)

Mixtures of F4 and F2 and mixtures of F3 and F2 were analyzed in a linear gradient of solvent B in solvent A (10% to 50%) over 4.51 min. Mixtures of F4 and F3 were analyzed in a linear gradient of solvent B in solvent A (24% to 56%) over 4.23 min. Mixtures of F4 and 4F1 were analyzed under an isocratic condition with solvent B in solvent A (27%) for 4.23 min. Measurements were performed at least three times.

Bright-field microscopy. Aggregate morphology was investigated using a Leica DM IL LED microscope (Leica Microsystems CMS GmbH, Wetzlar, Germany) equipped with a HI PLAN 40 × oil objective (Leica Microsystems CMS GmbH) and an HC PLAN 10 × eyepiece (Leica Microsystems CMS GmbH). Single-component and two-component solutions were prepared in the same manner as for turbidity measurements. Sample imaging was performed at 5 °C, 25 °C, and 50 °C after 2 min of equilibration using a temperature-controlled stage (Thermo Plate TP-CHSQM; Tokai Hit, Shizuoka, Japan).

Dynamic light scattering (DLS) measurement. Particle size distributions were analyzed using a Zetasizer Nano ZS (Malvern Instruments, Worcestershire, U.K.) in filtered phosphate buffer (pH 7.4, 27.4 mM Na_2HPO_4, 17.8 mM NaH_2PO_4) containing 3 M NaCl. DLS analysis was performed over a temperature range of 5–50 °C. Before measurements, the cell holder was purged with nitrogen gas. The measurement duration and attenuation were selected automatically. The "protein" parameter set (refractive index 1.450; absorption 0.001) and the "water" dispersant set (refractive index 1.330; viscosity 0.8872) were used. Measurements were performed at least three

times.

Circular dichroism (CD) measurement. CD spectra were obtained on a J-725 spectropolarimeter (JASCO) using a 1.0 mm path-length cuvette. The tested ELPs and their final concentrations were as follows: F4 + F3 (F4 0.0210 mg/mL and F3 0.0790 mg/mL, 0.1000 mg/mL in total), F4+ 4F1 (F4 0.0210 mg/mL and 4F1 0.0508 mg/mL, 0.0718 mg/mL in total), F4 (0.021 mg/mL), F3 (0.0790 mg/mL), and 4F1 (0.0508 mg/mL). The mixture concentrations were adjusted to maintain the same ratio used in turbidity measurements. These single-component or two-component ELPs were dissolved in filtered phosphate buffer (pH 7.4, 27.4 mM Na_2HPO_4, 17.8 mM NaH_2PO_4). Under these conditions, no obvious aggregation was observed. Spectra were obtained from 190 to 260 nm between 5 °C and 55 °C with 10 °C intervals after 2 min of equilibration at each temperature. After subtracting background spectra, Savitzky–Golay filters were used to smooth the spectra. Theoretical spectra of the binary mixtures were calculated in terms of mean residue ellipticity (θ, deg cm^3 $dmol^{-1}$) or CD signal (mdeg) using the following equations:

$$\theta_{calcd} = (C_A\theta_A+C_B\theta_B)/(C_A+C_B) \quad (1)$$

$$CD_{calcd} = CD_A+CD_B \quad (2)$$

where C_A and C_B represent the residue molar concentrations of peptide A and B, respectively; θ_A and θ_B denote the experimentally obtained θ of peptide A and B; and CD_A and CD_B are their corresponding CD signals in mdeg.

Molecular dynamics (MD) simulation. MD simulations were performed using GROMACS 2019 with AMBER99SB-ILDN force field on DELL PRECISION T3610 workstation (Dell Inc. Round Rock, TX, USA) [45]. Single-molecule trajectories were generated for F4, F3, F2, and 4F1 using TIP3P explicit solvent model. Initial structures were generated by Discovery studio 4.0 software (Dassault Systèmes BIOVIA, San Diego, CA, USA) and converted to .gro file by gmx pdb2gmx command in GROMACS. Each model was placed in a cubic box (F4 in 6 × 6 × 6 nm^3, F3 and 4F1 in 5 × 5 × 5 nm^3, and F2 in 4 × 4 × 4 nm^3), solvated by gmx solvate, and neutralized with appropriate number of Na^+ and CL^- ions. For simulations in the absence of NaCl, appropriate numbers of water molecules were replaced with a Cl^- via gmx genion. For simulations in the presence of 3 M NaCl, the minimum distance parameter (-rmin) was set to 0.51 nm (default 0.6 nm) to enable successful insertion of Na^+ and Cl^- without exhausting solvent replacement sites. The simulations were performed at 278, 298, and 323 K (5, 25, and 50 °C). These systems contained two minimizations, heating step, equilibrium step, and production step. The first minimization was performed by steepest descent algorithm, using a maximum of 10,000 steps, the maximum step size (emstep) of 0.01 nm, the tolerance (emtol) of 10.0 kJ mol^{-1} nm^{-1}, and no

constraints; The second minimization was performed by conjugate gradient algorithm, using a maximum of 20,000 steps, emstep of 0.01 nm, emtol of 10.0 kJ mol^{-1} nm^{-1}, and no constraints; heating step: parameters are 500,000 steps, time step 2 fs, initial temperature 0 K, target temperature (278/298/323 K), LINCS constraint to h-bond atoms, annealing type single, annealing npoints 2, and annealing time 200 ps; an equilibration step: parameters are 500,000 steps with a time step of 2 fs, target temperature (278/298/323 K), LINCS constraint to h-bond atoms, and reference pressure 1.0 bar; and finally, a production step consisting of 25,000,000 steps (50 ns) for F4, F3, and 4F1, and 50,000,000 steps (100 ns) for F2, time step 2 fs, target temperature (278/298/323 K), pressure coupling decay time (tau-p) = 1.0, LINCS constraint to h-bond atoms, nonbond list radius (rcoulomb, rvdw) = 1.0 nm, nonbond lower cutoff distance (rlist) = 1.0 nm, electrostatics = particle-mesh Ewald (PME) method, dynamics integrator = leapfrog, and random number seed = 1732. Trajectories (50,000 frames for F4, F3, and 4F1, and 100,000 frames for F2) were processed by gmx trjcomv command to correct the break in the molecular structure due to periodic boundary condition. During this process, the number of frames were reduced to 1/10 (5,000 or 10,000 frames). Then, the radius of gyration (Rg), solvent accessible surface areas (SASA), the number of intramolecular hydrogen bonds (n_{PP}), and the number of hydrogen bonds between water and peptide (n_{PW}) were analyzed using the processed trajectory files with omitting the first 10 ns.

3. Results and Discussion

Peptide synthesis. The linear Fn molecules were successfully obtained via solid-phase peptide synthesis (Figures 4-1a and 4-2a–c, and Table 4-1). The linear ELPs F4, F3, and F2 consist of 20, 15, and 10 amino acid residues, respectively. Thus, these ELPs share identical amino acid composition but differ in chain length by one or two repeats corresponding to 5- or 10-residue differences. The branched ELP, $[\alpha\text{-E(F1)}]_3$-F1 (referred to as 4F1, Figures 4-1b and 4-2d), was also successfully prepared through condensation of F1 units (H-FPGVG-NH_2) with the backbone peptide using a grafting-onto approach similar to that employed in Chapter 3. This branched peptide contains the same total number of FPGVG units as F4.

(Figures 4-1 and 4-2)
(Table 4-1)

Temperature-responsive behavior of single-component and two-component ELPs. LCST-type behavior of single-component ELPs and their mixture samples were investigated by turbidimetry. First, using phosphate buffer supplemented with 3 M NaCl as the solvent, single-component ELP samples were examined.

As a result, each ELP showed LCST-type behavior. For example, F4 exhibited LCST-type behavior with a T_t value of approximately 18 °C at 0.2 mM (Figure 4-3a, Table 4-2). F3 also exhibited LCST-type behavior with T_t values of approximately 40 °C at 1 mM and 21 °C at 2 mM (Figure 4-3b). Notably, in phosphate buffer containing 3 M NaCl, F2 also showed LCST-type behavior in the concentration range of 15–30 mM with T_t values of approximately 17–50 °C (Figure 4-3c). The branched ELP, 4F1, showed LCST-type behavior, with a T_t value of approximately 34 °C at 0.4 mM (Figure 4-3d). In addition, although only one concentration was tested for F4, the T_t values of the other ELPs showed peptide concentration dependence and followed the equation $T_t = a \log (C) + b$, where C is the ELP concentration, and a and b are constants (Figure 4-3e, and Table 4-2) [5]. Moreover, the individually prepared solutions of F4 and F3 exhibited a single increase in turbidity upon heating to 60 °C, followed by a decrease at high temperatures, which was attributed to precipitation of Fn coacervates (Figure 4-4).

(Figures 4-3 and 4-4)
(Table 4-2)

Next, the turbidity profiles of two-component mixtures of ELPs were investigated. On the basis of the turbidimetry results obtained for each single-component ELP, peptide concentration conditions for a mixture of two ELPs in phosphate buffer with 3 M NaCl were determined so that both ELPs could undergo self-assembly, and their T_t values were not too close to each other ($\Delta T_t \geq$ approximately 10 °C). The ELP pairs were selected so that the ELPs in a pair differ in chain length by one or two repeats (Δn = 1 or 2) or differ in topology but with the same numbers of the pentapeptide units. Accordingly, the following mixture conditions were used: (i) F4 (0.2 mM) + F2 (15 mM), Δn = 2; (ii) F4 (0.2 mM) + F3 (1 mM), Δn = 1, (iii) F3 (2 mM) + F2 (15 mM), Δn = 1; (iv) F4 (0.2 mM) + 4F1 (0.4 mM), Δn = 0. For each mixture, denoted as "A + B", the concentrations of each component were chosen such that the T_t value of peptide A was set to be lower than that of peptide B.

First, the mixture of F4 and F2, F4 + F2, was examined. This system was designed to have the same ratio of pentapeptide units as the previously reported mixture of $(VPGVG)_{40}$ and $(VPGVG)_{20}$ [29]. Upon heating, the mixture exhibited a two-step turbidity increase in contrast to the single-component F4, with the first transition occurring around 10 °C and the second around 35 °C (Figure 4-4a). This behavior indicated stepwise LCST-like behavior, in which F4 underwent phase separation at a lower temperature followed by F2 at a higher temperature. Notably, the onset of the first temperature increase occurred at a lower temperature than that observed in the single-component F4. This shift could be attributed to the higher total peptide concentration in the mixture, wherein heterotypic interactions between F4 and F2 might facilitate the initial transition.

In the present experiments, turbidity values were not normalized because the differences in turbidity might reflect changes in droplet characteristics such as size, number, and morphology. The turbidity values of the F4 + F2 mixture were higher than those of the single-component F4 solution. This result might suggest that heterotypic interactions between F4 and F2 in the mixture influenced droplet formation or properties during phase separation, even though they exhibited LCST-type behavior sequentially. The second turbidity increase, which is primarily attributed to the phase transition of F2, occurred at a lower temperature than that observed for single-component F2. This shift could be explained by the presence of F4 droplets formed before the phase separation of F2. These droplets likely reduced the effective volume available to F2 and increased its apparent concentration in the dilute phase, thereby promoting its phase separation. During cooling, the turbidity decreased in a single step rather than re-tracing the two-step turbidity increase observed upon heating. This difference could arise from several factors. One possibility is that the F4 droplets had already precipitated to the bottom of the measurement cell before initiating the cooling process after the second transition. Another possibility is that rehydration of F2 during cooling may have promoted the redissolution of F4.

To further validate the two-step phase separation, UPLC-MS analysis was performed for F4 + F2. After incubation at 25 °C or 50 °C, the samples were centrifugated and only the dilute phase was analyzed, as the volumes of the condensed phase were too small to collect and analyze (Figure 4-5). Based on the turbidity profiles, it was expected that incubation at 25 °C would result in the preferential depletion of peptide A while peptide B would remain in the supernatant (dilute phase), whereas incubation at 50 °C would lead to depletion of both ELP components. The UPLC-MS result for F4 + F2 showed that, with incubation at 25 °C, the amount of F4 in the supernatant decreased while that of F2 remained almost unchanged (Figure 4-4b). At 50 °C, F4 was further depleted from the dilute phase, and F2 was also partially decreased. These results demonstrate that F4 selectively exhibits phase separation at lower temperatures, followed by F2 at higher temperatures, supporting the stepwise phase transition inferred from turbidimetry.

Following the analysis of F4 + F2, the LCST-type behavior of additional two-component mixtures was examined by turbidimetry and UPLC-MS (Figure 4-4c–h). The F4 + F3 and F3 + F2 mixtures were designed such that the two ELPs differed by one pentapeptide repeat ($\Delta n = 1$). In contrast, the F4 + 4F1 mixture was designed so that both components contained the same number of FPGVG units and the same net charge (+1), while differing in topology (linear vs. branched). It should be noted that the chemical compositions of these ELPs were not strictly identical because 4F1 contains a triGlu backbone that serves as the branching core. In all mixtures examined, the onset of turbidity increases in the mixtures occurred at lower temperatures than those observed for the corresponding single-component peptide A. Upon further heating, the F4 + F3 and F4 + 4F1 systems exhibited clear two-step turbidity increases, indicative of stepwise

phase separation (Figure 4-4c, g). In the F3 + F2 mixture, although a distinct two-step turbidity increase was not observed upon heating to 60 °C, the decrease in turbidity was relatively gradual, and the turbidity values were higher than those of single-component F3 (Figure 4-4e). Notably, the onset temperatures of the second turbidity increase in the F4 + F3 and F4 + 4F1 mixtures were comparable to or higher than those of the corresponding single-component peptide B, in contrast to the profile obtained for the F4 + F2 system. These differences might be rationalized by the heterotypic interactions between the two components. Specifically, partial partitioning of peptide B into peptide A droplets, or co-assembly of the two components at lower temperature ranges (approximately 10–30 °C) would reduce the apparent concentration of peptide B in the dilute phase. As a result, a higher temperature would be required to induce the LCST-type behavior of peptide B, leading to a higher onset temperature for the second phase separation. In UPLC-MS analysis of these three pairs, at 25 °C, the amount of peptide A selectively decreased while peptide B partially decreased. After incubation at 50 °C, a greater reduction in the amount of both species was observed (Figure 4-4d, f, h). These results, showing a trend similar to that observed in F4 + F2, demonstrate that peptide A selectively phase-separates at lower temperatures, followed by the phase separation of peptide B at higher temperatures.

(Figures 4-4 and 4-5)

Additionally, the temperature-responsive behavior of single- and two-component samples was examined under a reduced ionic strength condition, specifically in phosphate buffer supplemented with 1 M NaCl. Under this condition, the single-component F4 showed LCST-type behavior with T_t values of 20 °C at 3 mM (Figure 4-6a, Table 4-3). Similarly, F3 at 10 mM and 4F1 at 5 mM also exhibited LCST-type behavior at around 36 °C and 33 °C, respectively (Figure 4-6b, c). Their T_t values also showed a concentration dependence in this buffer condition (Figure 4-6d). As observed in phosphate buffer with 3 M NaCl, the single-component F4 showed a single-step turbidity increase upon heating to 60 °C (Figure 4-7a, c). The decrease in turbidity at high temperatures was likely due to the precipitation of F4 coacervates. Based on these results, peptide concentration conditions in phosphate buffer with 1 M NaCl were selected as follows: (v) F4 (3 mM) + F3 (10 mM), $\Delta n = 1$; and (vi) F4 (3 mM) + 4F1 (5 mM), $\Delta n = 0$. Again, in the mixtures denoted as "A + B", the T_t value of peptide A was set to be lower than that of peptide B. The turbidity measurement of F4 + F3 mixture showed a turbidity increase at approximately 12 °C, which is lower than the T_t of single-component F4 under the same salt condition (Figure 4-7a). Although a distinct two-step turbidity increase was not observed upon heating to 60 °C, the turbidity decrease occurred relatively gradually, and the turbidity values remained higher than that of single-component F4. The F4 + 4F1 mixture exhibited a similar turbidity trend, showing

a turbidity increase at around 10 °C followed by a gradual turbidity decrease upon further heating (Figure 4-7c). The result that temperatures at the turbidity increased shifted to around 10 °C was again likely attributable to the higher total ELP concentration in the mixtures, which promoted the phase transition at a low temperature. Although no apparent stepwise turbidity increases were observed in these two-component systems, the relatively stable turbidity decreases observed in the temperature range of 25–60 °C suggested that peptide B in each pair exhibited LCST-type behavior at around 30–40 °C. The UPLC-MS results showed that at 25 °C, the amount of ELPs in the supernatant decreased, with a more pronounced reduction for peptide A (F4) in both F4 + F3 and F4 + 4F1 mixtures (Figure 4-7b, d). Upon incubation at 50 °C, F4 was further depleted, and the partner ELP also showed a decrease. These results indicated that at lower temperatures, one component underwent phase separation with the partner ELP partially co-assembled or partitioned into the condensed phase, whereas upon further heating, the partner ELP also gradually phase separated. This phase behavior could reflect distinct depletion kinetics of each component and suggest that heterotypic interactions between the ELPs influence the phase behavior.

(Figures 4-6 and 4-7)
(Table 4-3)

Morphological properties. Bright-field microscopy was used to examine the morphology of aggregates and differences between single-component and two-component samples. The higher turbidity observed in the mixtures suggested the presence of a larger number of aggregates that effectively scattered light at high temperatures compared with the corresponding single-component solutions. These results indicated that the coexistence of two ELPs might affect the aggregate structures and/or the number of light scatterers (at 400 nm) through homotypic and/or heterotypic intermolecular interactions. Based on these considerations, imaging was performed by optical microscopy.

Bright field microscopy revealed that the individually prepared F4 in phosphate buffer supplemented with 3 M NaCl formed spherical aggregates, which subsequently precipitated onto the bottom surface of the slide at 25 °C and 50 °C (Figure 4-8). In contrast, F2 formed spherical aggregates only at 50 °C. In the F4 + F2 mixture, the number of aggregates observed at 25 °C was clearly greater than that of the single-component F4 sample. At 50 °C, the precipitated aggregates coalesced to form larger aggregates on the slide surface. The increased number of aggregates in the mixture likely accounts for the enhanced turbidity observed in the turbidity measurements. Similar trends in aggregation behavior were observed for the F4 + F3, F3 + F2, and F4 + 4F1 mixtures (Figures 4-9–4-11). Under the reduced ionic strength condition (phosphate buffer

supplemented with 1 M NaCl), the single-component F4 also formed spherical aggregates and precipitated at 25 °C and 50 °C (Figure 4-12). For F4 + F3 and F4 + 4F1, aggregates rapidly precipitated at 25 °C, forming larger precipitates compared to those formed by the individually prepared F4 under the same condition. Upon heating to 50 °C, the precipitates became larger and denser due to the continued formation and precipitation of aggregates.

(Figures 4-8–4-12)

Comparison of size distributions and scattering intensities. DLS measurements were performed to investigate the temperature-dependent changes in particle size distributions and to compare them among the single-component and two-component samples. Autocorrelation curves are shown in Figure 4-13. Upon heating, increases in hydrodynamic diameters were observed for the single-component samples (F4, F3, F2, and 4F1) as well as for their mixtures (Figures 4-14 and 4-15). While DLS results shown in intensity indicated the presence of large aggregates in the samples (Figure 4-14), the number-weighted distributions suggested that these large aggregates constituted only a small fraction of the total particle population (Figure 4-15). Notably, the size distributions of each single-component ELP were not preserved in their two-component mixtures, particularly at low temperatures. This implied that the ELPs interact through both homotypic and heterotypic interactions in the mixtures, leading to aggregation states that differ from those formed by the individual components alone. In addition, the temperature-dependence of scattering intensity varied among the samples (Figure 4-16). For the single-component systems, scattering intensity increased when the temperature exceeded their T_t. Under the measurement conditions, the peptide A had a T_t below 25 °C, while the peptide B had a T_t above 25 °C. In contrast, the binary mixtures showed temperature-dependent scattering profiles that deviated from the trend observed in the single-component ELPs. Moreover, temperature-dependent changes in scattering intensity of the mixtures differed among the samples. In combination with the microscopy results, the DLS results suggested that the aggregation behavior in the mixed systems was affected by inter-peptide interactions, resulting in differences in aggregate sizes, size distributions, and number densities compared with the corresponding single-component samples.

(Figures 4-13–4-16)

Structural analysis by CD measurement. To investigate the structural changes involved in the LCST-type behavior and whether the structural characteristics of the short ELPs could be affected by the presence of other ELPs, CD spectra were obtained for the single-component and two-component samples. Among the mixtures tested above, F4 + F3 and F4 + 4F1 were selected for

the measurement, because the chain lengths of F4 and F3 differ only by one repeat, and F4 and 4F1 only differ in their topology while sharing the same number of the pentapeptide units. The mean residue ellipticity (θ, Figures 4-17 and 4-19) was calculated from the obtained CD data (mdeg, Figures 4-18 and 4-20).

As reported in the Chapters 2 and 3, and previous studies [46–48], H-$(FPGVG)_n$-NH_2 and $[\alpha\text{-E(F1)}]_n$-F1 exhibit a negative peak around 200 nm and a small positive peak at 225 nm at low temperatures, while at high temperatures, they showed decreases in these bands and a shoulder peak at 210 nm. These spectral changes have been attributed to a transition from a polyproline type II (PPII)-like helical structure at low temperatures [49] to β-turns or β-sheet-rich structures at high temperatures. Consistent with these reports, the single-component samples of F4, F3, and 4F1 in this study showed CD spectra similar to those previously obtained for H-$(FPGVG)_n$-NH_2 and $[\alpha\text{-E(F1)}]_n$-F1 (Figure 4-17a–c). Among these peptides, F4 showed somewhat less distinct CD spectra compared with the other ELPs, likely due to the lower peptide concentration used in the CD measurement (0.0210 mg/mL for F4, Figure 4-17a, d). Nonetheless, these individually prepared peptides showed a temperature-dependent decrease in the intensity of the negative peak near 200 nm and the small positive peak at 225 nm together with the emergence of the shoulder peak around 210 nm upon heating, indicating structural changes from PPII-like structures to β-structures upon heating. In addition, the CD spectra obtained during cooling confirmed the structural reversibility of these ELPs (Figures 4-17d–f and 4-18c, d).

The two-component mixtures of F4 + F3 and F4 + 4F1 also exhibited CD spectra characteristics of short-chain ELPs (Figure 4-19, left spectra in each panel). The CD spectra during cooling demonstrated structural reversibility upon temperature changes (Figures 4-19c, d and 4-20c, d). To assess whether mixing induced structural changes beyond a simple superposition of the individual components, theoretical CD spectra were calculated from the corresponding single-component spectra of F4 and its partner peptide (F3 or 4F1) using equation (1) and (2). As a result, these experimental CD spectra could be closely reproduced by the theoretical spectra in both θ (deg cm^2 $dmol^{-1}$) and CD (mdeg) (Figures 4-19 and 4-20, right spectra in each panel). For a quantitative comparison, the root mean square deviation (RMSD) values were calculated over the wavelength range of 195–260 nm. The RMSD values ranged from approximately 620–1500 deg cm^2 $dmol^{-1}$ (0.67–1.62 mdeg) for F4 + F3 and 220–1320 deg cm^2 $dmol^{-1}$ (0.24–2.75 mdeg) for F4 + 4F1 (Table 4-4), supporting the high degree of similarity between the experimental and calculated spectra [50]. The close agreement between the experimental and calculated CD spectra indicates that, under the dilute conditions used for CD measurements, heterotypic interactions in the mixtures were weak and did not induce substantial changes in the secondary structures of the two components [29]. However, turbidimetry, UPLC-MS, microscopy, and DLS revealed clear differences in phase behavior between single-component and two-component systems, and

demonstrated that the phase separation of the two components is not completely independent in the mixtures. Taken together, these results suggest that intermolecular interactions between the two components are sensitive to peptide concentration and ionic strength, and that such interactions can modulate the stepwise profiles of phase separation. A previous study by Ghoorchian and Holland demonstrated that mixtures of $(GVGVP)_{40}$ and its trimer prepared at low concentration conditions underwent two phase transitions, suggesting the importance of peptide concentration [30]. These observations highlight the importance of component composition, concentration, and solution conditions in controlling the phase behavior of multicomponent peptide-based systems.

(Figures 4-17–4-20)
(Table 4-4)

Conformational analysis by MD simulations. To obtain mechanistic insights into the stepwise phase separation, MD simulations were performed under NaCl-free conditions and in the presence of 3M NaCl (Figure 4-21). Under both ionic conditions, similar temperature-dependent trends were observed in the analyzed parameters, including Rg, SASA, n_{PP}, and n_{PW}. The MD simulations revealed distinct conformational changes in F4, F3, F2, and 4F1 upon temperature changes. For F4, F3, and 4F1, Rg and SASA showed decreasing trends upon heating, indicating that these ELPs become more compact in monomeric forms at elevated temperatures. In contrast, F2 showed increases in both Rg and SASA upon heating from 5 °C to 25 °C, which suggested that monomeric F2 adopts a more extended conformation in this temperature range. For F4 and F3, the n_{PP} increased and n_{PW} decreased upon heating, indicating heating-induced dehydration and formation of intramolecular hydrogen bonds. A similar decrease in n_{PW} was observed for 4F1 upon heating; however, its n_{PP} remained almost unchanged over the temperature range of 5–50 °C. In contrast, F2 showed only minor variations in both n_{PP} and n_{PW} in the same temperature range. These results suggest that monomeric F2 adopts inherently compact structures with only subtle conformational changes, limiting the dehydration and intramolecular hydrogen bonds in response to temperature changes.

These MD results indicate that subtle differences in chain length or molecular topology led to different temperature-dependent conformational characteristics. The subtle differences would modulate the balance between intra- and intermolecular interactions, thereby contributing to the partially independent, yet stepwise phase transitions observed experimentally. Moreover, these differences might play a role in the different trends in scattering intensity detected in the DLS measurements.

(Figure 4-21)

4. Conclusion

Elucidating how multicomponent systems composed of short-chain peptides capable of LCST-type LLPS behave represents a key step toward the development of functional peptide-based materials. In this study, the LCST-type behavior of two-component mixtures was investigated for the FPGVG-based synthetic short-chain ELPs that differed in chain length by only one or two pentapeptide repeat units, or in topology while sharing the same number of repeat units. While single-component solutions of these ELPs showed single-step turbidity increases, their mixtures showed two-step turbidity increases, which indicated stepwise phase separation, a behavior similar to that previously observed for mixtures of long-chain ELPs. Despite the stepwise phase behavior, however, microscopy and DLS suggested that heterotypic inter-peptide interactions play a role in modulating the phase separation properties of the mixed systems.

Under temperature gradients or thermal switching conditions, stepwise LCST-type phase behavior enables the sequential purification and spatiotemporal organization of ELP-fused components and coexisting molecules within complex mixtures. Overall, this study advances the understanding of phase behavior in multicomponent ELP systems and is expected to promote the use of artificial short-chain intrinsically disordered protein mimics as versatile building blocks for multicomponent peptide-based materials.

5. References

[1] Strader, R. L.; Shmidov, Y.; Chilkoti, A. Encoding Structure in Intrinsically Disordered Protein Biomaterials. *Acc. Chem. Res.* **2024**, *57* (3), 302–311.

[2] Urry, D. W.; Pattanaik, A. Elastic protein-based materials in tissue reconstruction. *Ann. N. Y. Acad. Sci.* **1997**, *831*, 32–46.

[3] Keeley, F. W.; Bellingham, C. M.; Woodhouse, K. A. Elastin as a self-organizing biomaterial: use of recombinantly expressed human elastin polypeptides as a model for investigations of structure and self–assembly of elastin. *Philos. Trans. R. Soc. Lond. B. Biol. Sci.* **2002**, *357* (1418), 185–189.

[4] Girotti, A.; Reguera, J.; Arias, F. J.; Alonso, M.; Testera, A. M.; Rodríguez-Cabello, J. C. Influence of the Molecular Weight on the Inverse Temperature Transition of a Model Genetically Engineered Elastin-like pH-Responsive Polymer. *Macromolecules* **2004**, *37* (9), 3396–3400.

[5] Meyer, D. E.; Chilkoti, A. Quantification of the Effects of Chain Length and Concentration on the Thermal Behavior of Elastin-like Polypeptides. *Biomacromolecules* **2004**, *5* (3), 846–851.

[6] McDaniel, J. R.; Radford, D. C.; Chilkoti, A. A Unified Model for De Novo Design of Elastin-like Polypeptides with Tunable Inverse Transition Temperatures. *Biomacromolecules* **2013**, 14 (8), 2866–2872.

[7] Luan, C. H.; Parker, T. M.; Prasad, K. U.; Urry, D. W. Differential scanning calorimetry studies of NaCl effect on the inverse temperature transition of some elastin-based polytetra-, polypenta-, and polynonapeptides. *Biopolymers* **1991**, *31* (5), 465–475.

[8] McPherson, D. T.; Xu, J.; Urry, D. W. Product Purification by Reversible Phase Transition Following Escherichia coli Expression of Genes Encoding up to 251 Repeats of the Elastomeric Pentapeptide GVGVP. *Protein Expr. Purif.* **1996**, *7* (1), 51–57.

[9] Zhang, Z.; Lynch, C. J.; Huo, Y.; Chakraborty, S.; Cremer, P. S.; Mozhdehi, D. Modulating Phase Behavior in Fatty Acid-Modified Elastin-like Polypeptides (FAMEs): Insights into the Impact of Lipid Length on Thermodynamics and Kinetics of Phase Separation. *J. Am. Chem. Soc.* **2024**, *146* (8), 5383–5392.

[10] Ji, J.; Hossain, M. S.; Krueger, E. N.; Zhang, Z.; Nangia, S.; Carpentier, B.; Martel, M.; Nangia, S.; Mozhdehi, D. Lipidation Alters the Structure and Hydration of Myristoylated Intrinsically Disordered Proteins. *Biomacromolecules* **2023**, *24* (3), 1244–1257.

[11] Zhang, T.; Peruch, F.; Weber, A.; Bathany, K.; Fauquignon, M.; Mutschler, A.; Schatz, C.; Garbay, B. Solution behavior and encapsulation properties of fatty acid–elastin-like polypeptide conjugates. *RSC Adv.* **2023**, *13*, 2190–2201.

[12] Kramer, J. R.; Petitdemange, R.; Bataille, L.; Bathany, K.; Wirotius, A.-L.; Garbay, B.; Deming, T. J.; Garanger, E.; Lecommandoux, S. Quantitative Side-Chain Modifications of Methionine-Containing Elastin-Like Polypeptides as a Versatile Tool to Tune Their Properties. *ACS Macro Lett.* **2015**, *4* (11), 1283–1286.

[13] Petitdemange, R.; Garanger, E.; Bataille, L.; Dieryck, W.; Bathany, K.; Garbay, B.; Deming, T. J.; Lecommandoux, S. Selective Tuning of Elastin-like Polypeptide Properties via Methionine Oxidation. *Biomacromolecules* **2017**, *18* (2), 544–550.

[14] Xiao, Y.; Chinoy, Z. S.; Pecastaings, G.; Bathany, K.; Garanger, E.; Lecommandoux, S. Design of Polysaccharide-b-Elastin-Like Polypeptide Bioconjugates and Their Thermoresponsive Self-Assembly. *Biomacromolecules* **2020**, *21* (1), 114–125.

[15] Weitzhandler, I.; Dzuricky, M.; Hoffmann, I.; Quiroz, F. G.; Gradzielski, M.; Chilkoti, A. Micellar Self-Assembly of Recombinant Resilin-/Elastin-Like Block Copolypeptides. *Biomacromolecules* **2017**, *18* (8), 2419–2426.

[16] Basheer, A.; Shahid, S.; Kang, M. J.; Lee, J. H.; Lee, J. S.; Lim, D. W. Switchable Self-Assembly of Elastin- and Resilin-Based Block Copolypeptides with Converse Phase Transition Behaviors. *ACS Appl. Mater. Interfaces* **2021**, *13* (21), 24385–24400.

[17] Varanko, A. K.; Su, J. C.; Chilkoti, A. Elastin-Like Polypeptides for Biomedical Applications.

Annu. Rev. Biomed. Eng. **2020**, 22, 343–369.

[18] Hassouneh, W.; Christensen, T.; Chilkoti, A. Elastin-like polypeptides as a purification tag for recombinant proteins. *Curr. Protoc. Protein Sci.* **2010**, *61*, Ch.6.

[19] Hassouneh, W.; MacEwan, S. R.; Chilkoti, A. Chapter nine - Fusions of Elastin-Like Polypeptides to Pharmaceutical Proteins. *Methods in Enzymology* **2012**, *502*, 215–237.

[20] Kostal, J.; Mulchandani, A.; Chen, W. Tunable Biopolymers for Heavy Metal Removal. *Macromolecules* **2001**, *34* (7), 2257–2261.

[21] Hussain, Z.; Kim, S.; Cho, J.; Sim, G.; Park, Y.; Kwon, I. Repeated Recovery of Rare Earth Elements Using a Highly Selective and Thermo-Responsive Genetically Encoded Polypeptide. *Adv. Funct. Mater.* **2022**, *32* (12), 2109158.

[22] Harris, R.; Veretnik, S.; Dewan, S.; Leshem, A. B.; Lampel, A. Regulation of enzymatic reactions by chemical composition of peptide biomolecular condensates. *Commun. Chem.* **2024**, *7*, 90.

[23] Lim, S.; Clark, D. S. Phase-separated biomolecular condensates for biocatalysis. *Trends Biotechnol.* **2024**, *42* (4), 496–509.

[24] Yuan, C.; Li, Q.; Xing, R.; Li, J.; Yan, X. Peptide self-assembly through liquid-liquid phase separation. *Chem* **2023**, *9* (9), 2425–2445.

[25] Dai, Y.; Chamberlayne, C. F.; Messina, M. S.; Chang, C. J.; Zare, R. N.; You, L.; Chilkoti, A. Interface of biomolecular condensates modulates redox reactions. *Chem* **2023**, *9* (6), 1594–1609.

[26] Shapiro, D. M.; Deshpande, S.; Eghtesadi, S. A.; Zhong, M.; Fontes, C. M.; Fiflis, D.; Rohm, D.; Min, J.; Kaur, T.; Peng, J.; Ney, M.; Su, J.; Dai, Y.; Asokan, A.; Gersbach, C. A.; Chilkoti, A. Synthetic biomolecular condensates enhance translation from a target mRNA in living cells. *Nat. Chem.* **2025**, *17*, 448–456.

[27] Leshem, A. B.; Sloan-Dennison, S.; Massarano, T.; Ben-David, S.; Graham, D.; Faulds, K.; Gottlieb, H. E.; Chill, J. H.; Lampel, A. Biomolecular condensates formed by designer minimalistic peptides. *Nat. Commun.* **2023**, *14* (1), 421.

[28] Meyer, D. E.; Kong, G. A.; Dewhirst, M. W.; Zalutsky, M. R.; Chilkoti, A. Targeting a Genetically Engineered Elastin-like Polypeptide to Solid Tumors by Local Hyperthermia. *Cancer Res.* **2001**, *61* (4), 1548–1554.

[29] Teeuwen, R. L. M.; de Wolf, F. A.; Zuilhof, H.; van Hest, J. C. M. Elastin-like polypeptides of different molecular weights show independent transition temperatures when mixed. *Soft Matter* **2009**, 5, 4305–4310.

[30] Ghoorchian, A.; Holland, N. B. Molecular Architecture Influences the Thermally Induced Aggregation Behavior of Elastin-like Polypeptides. *Biomacromolecules* **2011**, *12* (11), 4022–4029.

[31] Simon, J. R.; Carroll, N. J.; Rubinstein, M.; Chilkoti, A.; López, G. P. Programming molecular self-assembly of intrinsically disordered proteins containing sequences of low complexity. *Nat. Chem.* **2017**, 9, 509–515.

[32] McDaniel, J. R.; Mackay, J. A.; Quiroz, F. G.; Chilkoti, A. Recursive Directional Ligation by Plasmid Reconstruction Allows Rapid and Seamless Cloning of Oligomeric Genes. *Biomacromolecules* **2010**, *11* (4), 944–952.

[33] Aladini, F.; Araman, C.; Becker, C. F. W. Chemical synthesis and characterization of elastin-like polypeptides (ELPs) with variable guest residues. *J. Pept. Sci.* **2016**, *22* (5), 334–342.

[34] Suyama, K.; Shimizu, M.; Maeda, I.; Nose, T. Flexible customization of the self-assembling abilities of short elastin-like peptide Fn analogs by substituting N-terminal amino acids. *Biopolymers* **2022**, *113* (10), e23521.

[35] Yoshida, K.; Suyama, K.; Matsushita, S.; Maeda, I.; Nose, T. Development of the efficient preparation method for thermoresponsive elastin-like peptides using liquid-phase synthesis combined with fragment condensation strategy. *J. Pept. Sci.* **2023**, *29* (12), e3528.

[36] Tanaka, N.; Suyama, K.; Tomohara, K.; Maeda, I.; Nose, T. Branched short elastin-like peptides with temperature responsiveness obtained by EDTA-mediated multimerization. *J. Pept. Sci.* **2023**, 29 (2), e3449.

[37] Nuhn, N.; Klok, H.-A. Secondary Structure Formation and LCST Behavior of Short Elastin-Like Peptides. *Biomacromolecules* **2008**, 9 (10), 2755–2763.

[38] Hathorne, A. P.; Bermudez, H. Effects of short elastin-like peptides on filamentous particles and their transition behavior. *Biotechnol. Bioeng.* **2013**, *110* (7), 1822–1830.

[39] Su, Z.; Kim, C. O.; Renner, J. N. Quantification of the effects of hydrophobicity and mass loading on the effective coverage of surface-immobilized elastin-like peptides. *Biochem. Eng. J.* **2021**, 168, 107933.

[40] Su, Z.; Pramounmat, N.; Watson, S. T.; Renner, J. N. Engineered interaction between short elastin-like peptides and perfluorinated sulfonic-acid ionomer. *Soft Matter* **2018**, *14* (18), 3528–3535.

[41] Su, Z.; Kole, S.; Harden, L. C.; Palakkal, V. M.; Kim, C. O.; Nair, G.; Arges, C. G.; Renner, J. N. Peptide-Modified Electrode Surfaces for Promoting Anion Exchange Ionomer Microphase Separation and Ionic Conductivity. *ACS Mater. Lett.* **2019**, *1* (4), 467–475.

[42] Maeda, I.; Taniguchi, S.; Watanabe, N.; Inoue, A.; Yamasaki, Y.; Nose, T. Design of Phenylalanine-Containing Elastin-Derived Peptides Exhibiting Highly Potent Self-Assembling Capability. *Protein Pept. Lett.* **2015**, *22* (10), 934–939.

[43] Sumiyoshi, S.; Suyama, K.; Tanaka, N.; Andoh, T.; Nagata, A.; Tomohara, K.; Taniguchi, S.; Maeda, I.; Nose, T. Development of truncated elastin-like peptide analogues with improved temperature-response and self-assembling properties. *Sci. Rep.* **2022**, *12*, 19414.

[44] Tanaka, N.; Suyama, K.; Tomohara, K.; Nose, T. Exploring LCST- and UCST-like Behavior of Branched Molecules Bearing Repeat Units of Elastin-like Peptides as Side Components. *Biomacromolecules* **2024**, *25* (11), 7156–7166.

[45] Hess, B.; Kutzner, C.; van der Spoel, D.; Lindahl, E. GROMACS 4: Algorithms for Highly Efficient, Load-Balanced, and Scalable Molecular Simulation. *J. Chem. Theory Comput.* **2008**, *4* (3), 435–447.

[46] Taniguchi, S.; Watanabe, N.; Nose, T.; Maeda, I. Development of short and highly potent self-assembling elastin-derived pentapeptide repeats containing aromatic amino acid residues. *J. Pept. Sci.* **2016**, *22* (1), 36–42.

[47] Suyama, K.; Taniguchi, S.; Tatsubo, D.; Maeda, I.; Nose, T. Dimerization effects on coacervation property of an elastin-derived synthetic peptide $(FPGVG)_5$. *J. Pept. Sci.* **2016**, *22* (4), 236–243.

[48] Suyama, K.; Mawatari, M.; Tatsubo, D.; Maeda, I.; Nose, T. Simple Regulation of the Self-Assembling Ability by Multimerization of Elastin-Derived Peptide $(FPGVG)_n$ Using Nitrilotriacetic Acid as a Building Block. *ACS Omega* **2021**, *6* (8), 5705–5716.

[49] Lopes, J. L. S.; Miles, A. J.; Whitmore, L.; Wallace, B. A. Distinct circular dichroism spectroscopic signatures of polyproline II and unordered secondary structures: applications in secondary structure analyses. *Protein Sci.* **2014**, *23* (12), 1765–1772.

[50] Nagy, G.; Igaev, M.; Jones, N. C.; Hoffmann, S. V.; Grubmüller, H. SESCA: Predicting Circular Dichroism Spectra from Protein Molecular Structures. *J. Chem. Theory Compt.* **2019**, *15* (9), 5087–5102.

Table 4-1. Retention time, yield, and *m/z* values of the ELPs.

Peptide	Number of FPGVG units	Retention time (min)[a]	Yields (%)	MS (ESI) *m/z*[b] Calculated	Found
F4	4	1.982[c]	75	924.59 $[M + 2H]^{2+}$	924.48
F3	3	1.379[c]	71	695.82 $[M + 2H]^{2+}$	695.83
F2	2	2.376[d]	70	933.10 $[M + H]^{+}$	932.60
4F1	4	1.812[c]	61	1116.78 $[M + 2H]^{2+}$	1116.68

[a] Retention times in UPLC. The peptides were monitored in a linear gradient of solvent B in solvent A.

[b] *m/z* in UPLC-MS. The calculated values are for the average mass.

[c] The peptides were monitored in a linear gradient of solvent B in solvent A (24% to 56%) over 4.23 min.

[d] The peptide was monitored in a linear gradient of solvent B in solvent A (10% to 50%) over 4.51 min.

Table 4-2. T_t values of single-component ELPs in phosphate buffer with 3 M NaCl.

ELPs	ELP concentration [mM]	NaCl concentration [M]	T_t [°C]
F4	0.2	3	17.56 ± 0.49
F3	2	3	21.09 ± 1.32
	1.5	3	26.57 ± 1.44
	1	3	39.66 ± 1.09
F2	30	3	17.02 ± 1.18
	20	3	34.03 ± 1.09
	15	3	50.35 ± 2.00
4F1	1	3	11.61 ± 0.17
	0.5	3	26.28 ± 0.21
	0.4	3	33.67 ± 0.53

The T_t values are shown with standard errors.

Table 4-3. T_t values of single-component ELPs in phosphate buffer with 1 M NaCl.

ELPs	ELP concentration [mM]	NaCl concentration [M]	T_t [°C]
F4	3	1	20.02 ± 0.19
	2.5	1	22.88 ± 0.43
	1	1	44.66 ± 0.30
F3	15	1	24.78 ± 1.68
	10	1	36.15 ± 1.03
	7.5	1	44.98 ± 0.88
4F1	10	1	17.56 ± 0.60
	7.5	1	33.27 ± 0.64
	5	1	25.25 ± 0.89

The T_t values are shown with standard errors.

Table 4-4. RMSD of measured and calculated CD spectra.

		F4 + F3		F4 + 4F1	
		Heating	Cooling	Heating	Cooling
5 °C	deg cm^2 dmol^{-1}	1322.47	2060.27	1245.02	2132.73
	mdeg	1.43	2.23	1.29	2.62
15 °C	deg cm^2 dmol^{-1}	1499.54	2368.46	1318.13	2640.26
	mdeg	1.62	2.56	1.05	2.26
25 °C	deg cm^2 dmol^{-1}	1067.39	1921.41	976.06	2579.41
	mdeg	1.15	2.08	1.64	1.98
35 °C	deg cm^2 dmol^{-1}	836.39	1491.44	798.85	1530.74
	mdeg	0.90	1.61	1.34	1.17
45 °C	deg cm^2 dmol^{-1}	624.24	890.91	668.39	956.18
	mdeg	0.67	0.96	2.75	0.92
55 °C	deg cm^2 dmol^{-1}	697.74		222.83	
	mdeg	0.75		0.24	

RMSD were calculated in the range of 195–260 nm.

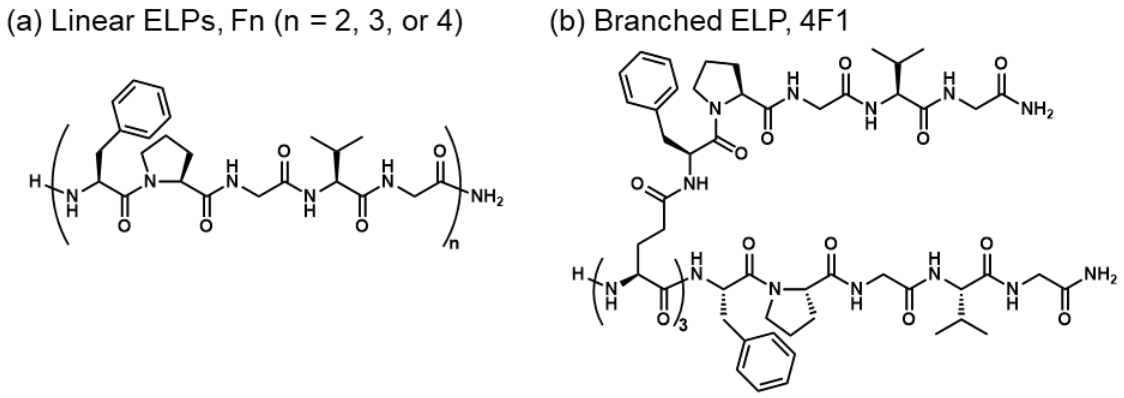

Figure 4-1. Structures of the short-chain ELPs used in this chapter.
(a) Linear ELPs (Fn, n = 2, 3, or 4), and (b) branched ELP [α-E(F1)]$_3$-F1 (4F1).

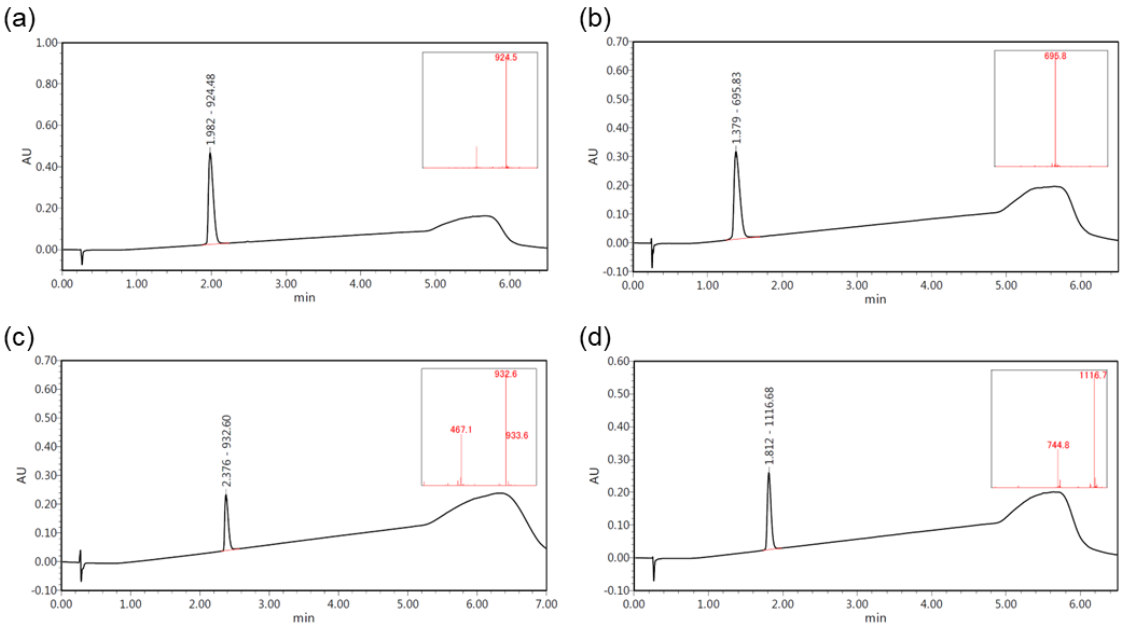

Figure 4-2. UPLC-MS analysis of the ELPs.
(a) F4, (b) F3, (c) F2, and (d) 4F1. The subscripts for each peak indicate the retention time and the *m/z* detected. The inset panels show MS spectra of the corresponding peak determined by ACQUITY QDa mass spectrometer. F4, F3, and 4F1 were monitored in a linear gradient of solvent B in solvent A (24% to 56%) over 4.23 min. F2 was monitored in a linear gradient of solvent B in solvent A (10% to 50%) over 4.51 min.

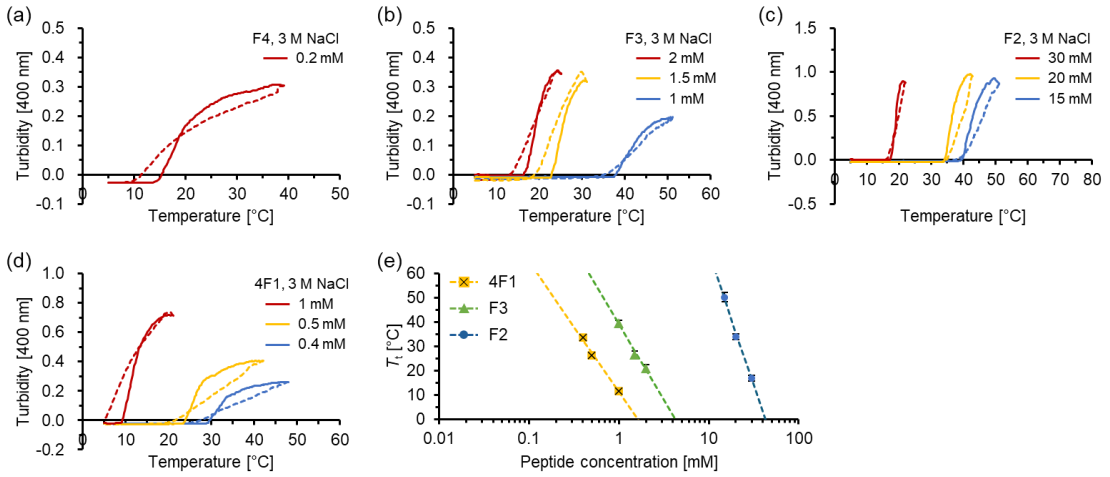

Figure 4-3. Turbidity profiles of single-component ELPs in phosphate buffer with 3 M NaCl. Turbidity profiles of (a) F4, (b) F3, (c) F2, and (d) 4F1, and (e) T_t-concentration relationship. In panels (a–d), solid and dashed lines represent the turbidity profiles upon heating and cooling, respectively. In panel (e), dotted lines represent the linear fit to the experimental T_t values, following the equation $T_t = a \log(C) + b$, where C is the ELP concentration, and the a and b are constant values.

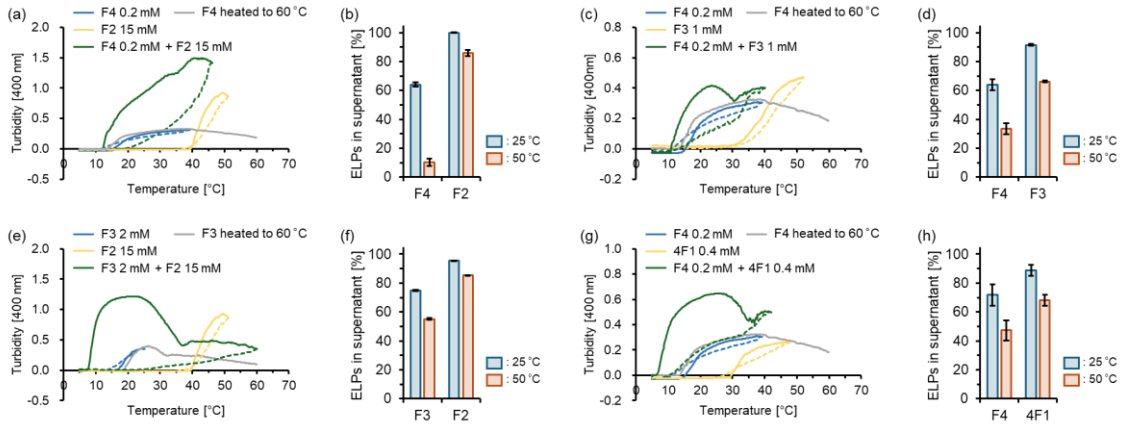

Figure 4-4. Turbidity profiles of the mixtures of ELPs in phosphate buffer with 3 M NaCl. Turbidity profiles of (a) F4, F2, and F4 + F2, (c) F4, F3, and F4 + F3, (e) F3, F2, and F3 + F2, and (g) F4, 4F1, and F4 + 4F1. UPLC-MS analysis for the quantification of ELPs remained in supernatant of the mixture after incubation at 25 °C or 50 °C for (b) F4 and F2, (d) F4 and F3, (f) F3 and F2, and (h) F4 and 4F1. Concentration conditions for the mixture samples were as follows: (a, b) 0.2 mM F4 and 15 mM F2, (c, d) 0.2 mM F4 and 1 mM F3, (e, f) 2 mM F3 and 15 mM F2, and (g, h) 0.2 mM F4 and 0.4 mM 4F1.

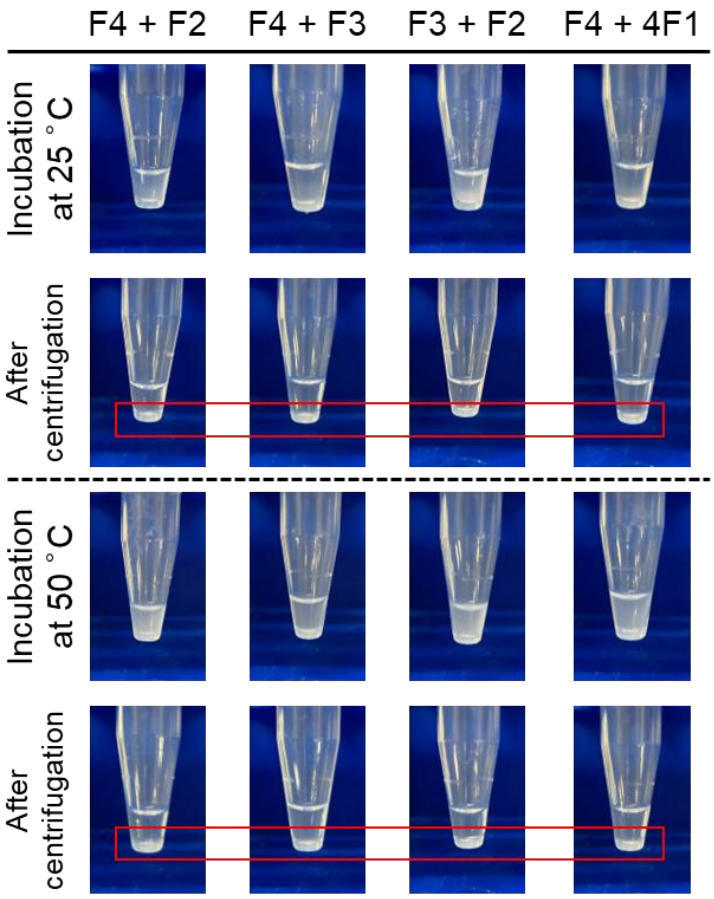

Figure 4-5. Pictures of ELP mixtures in phosphate buffer with 3 M NaCl after incubation and after centrifugation.

The peptides were dissolved in phosphate buffer with 3 M NaCl as follows: F4 + F2 (0.2 mM F4 and 15 mM F2 mM), F4 + F3 (0.2 mM F4 and 1 mM F3), F3 + F2 (2 mM F3 and 15 mM F2), and F4 + 4F1 (0.2 mM F4 and 0.4 mM 4F1. Pictures taken immediately after incubation at 25 °C or 50 °C, and after centrifugation, are shown. The red box highlights the small volumes of centrifuged ELPs, which were difficult to collect and challenging to analyze by UPLC-MS.

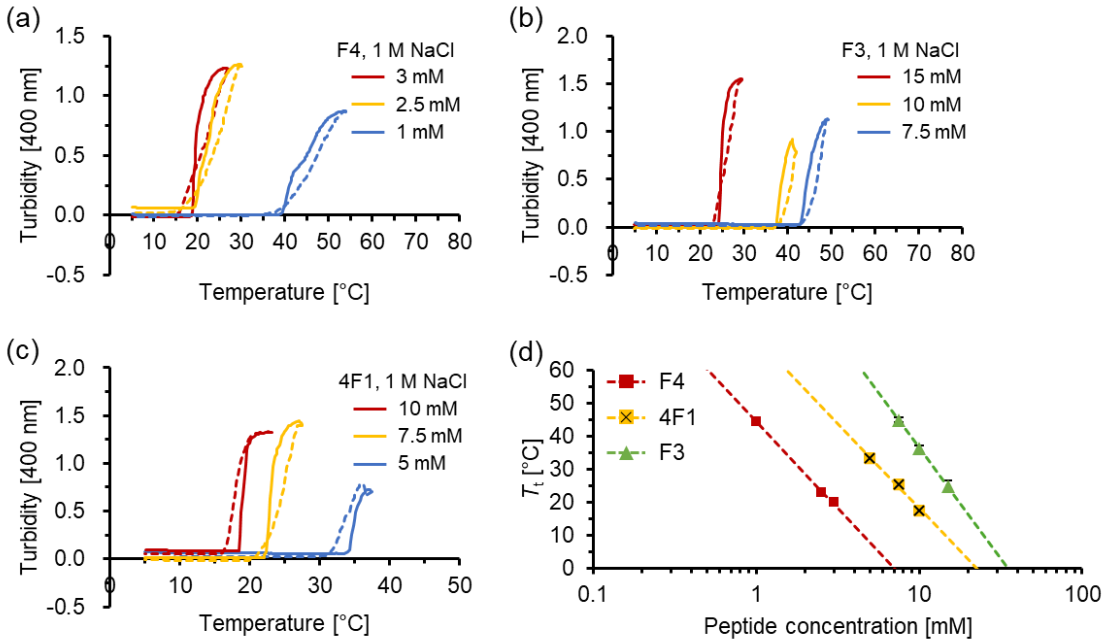

Figure 4-6. Turbidity profiles of single-component ELPs in phosphate buffer with 1 M NaCl. Turbidity profiles of (a) F4, (b) F3, and (c) 4F1, and (d) T_t-concentration relationship. In panels (a–c), solid and dashed lines represent the turbidity profiles upon heating and cooling, respectively. In panel (d), dotted lines represent the linear fit to the experimental T_t values, following the equation $T_t = a \log(C) + b$, where C is the ELP concentration, and the a and b are constant values.

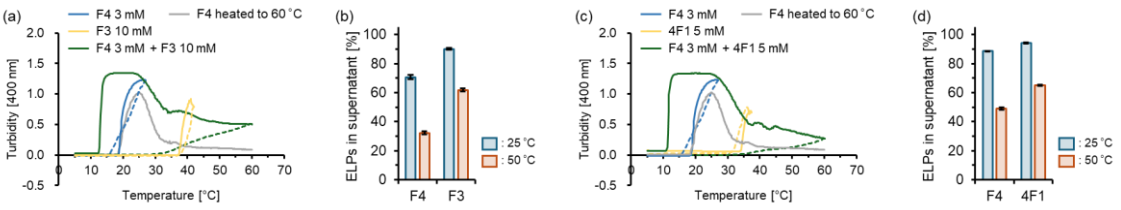

Figure 4-7. Turbidity profiles of the mixtures of ELPs in phosphate buffer with 1 M NaCl. Turbidity profiles of (a) F4, F3, and F4 +F3, and (c) F4, 4F1, and F4 + 4F1. UPLC-MS analysis for the quantification of ELPs remained in supernatant of the mixture after incubation at 25 °C or 50 °C for (b) F4 and F3, and (d) F4 and 4F1. Concentration conditions for the mixture samples were as follows: (a, b) 3 mM F4 and 10 mM F3, and (c, d) 3 mM F4 and 5 mM 4F1.

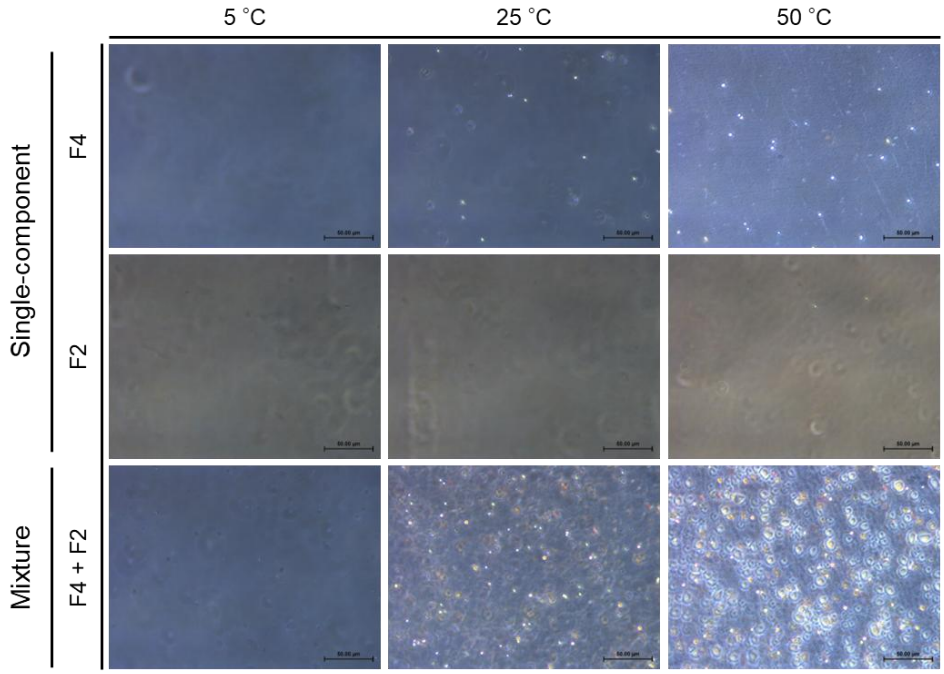

Figure 4-8. Microscopy images of F4, F2, and F4 + F2 in phosphate buffer with 3 M NaCl. For single-component samples, F4 and F2 were dissolved at 0.2 mM and 15 mM, respectively. In the mixture F4 + F2, F4 and F2 were dissolved at 0.2 mM and 15 mM, respectively. Scale bars: 50 μm.

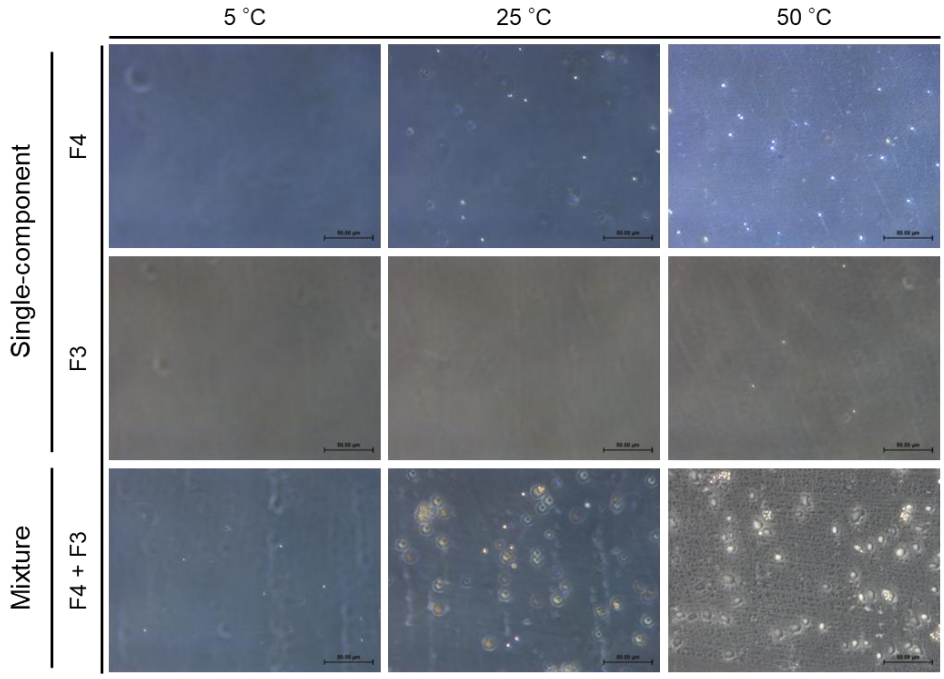

Figure 4-9. Microscopy images of F4, F3, and F4 + F3 in phosphate buffer with 3 M NaCl. For single-component samples, F4 and F3 were dissolved at 0.2 mM and 1 mM, respectively. In the mixture F4 + F3, F4 and F3 were dissolved at 0.2 mM and 1 mM, respectively. Scale bars: 50 μm.

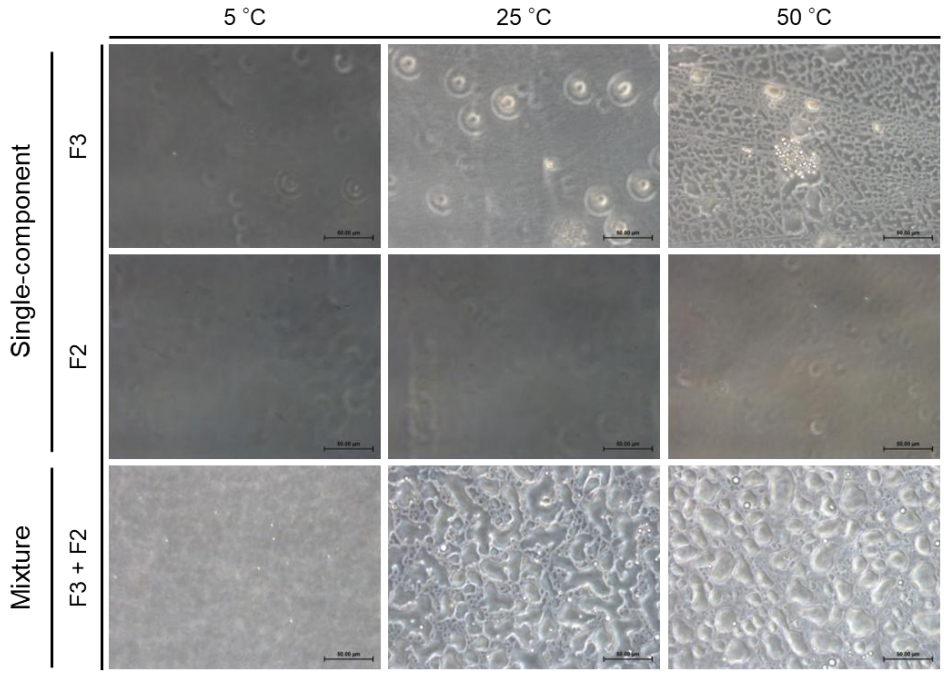

Figure 4-10. Microscopy images of F3, F2, and F3 + F2 in phosphate buffer with 3 M NaCl. For single-component samples, F3 and F2 were dissolved at 2 mM and 15 mM, respectively. In the mixture F3 + F2, F3 and F2 were dissolved at 2 mM and 15 mM, respectively. Scale bars: 50 μm.

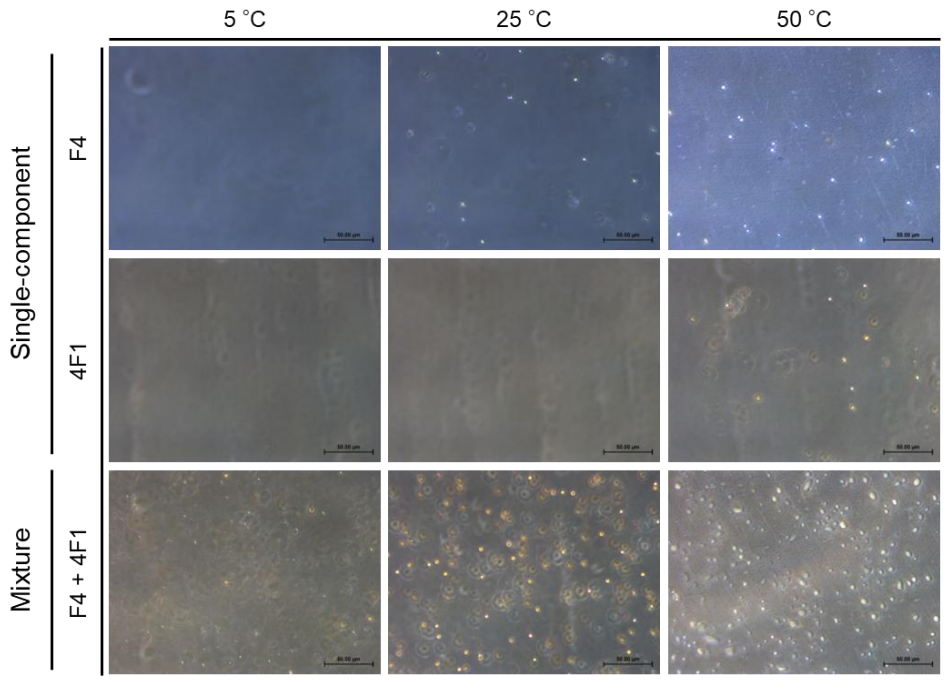

Figure 4-11. Microscopy images of F4, 4F1, and F4 + 4F1 in phosphate buffer with 3 M NaCl. For single-component samples, F4 and 4F1 were dissolved at 0.2 mM and 0.4 mM, respectively. In the mixture F4 + 4F1, F4 and 4F1 were dissolved at 0.2 mM and 0.4 mM, respectively. Scale bars: 50 μm.

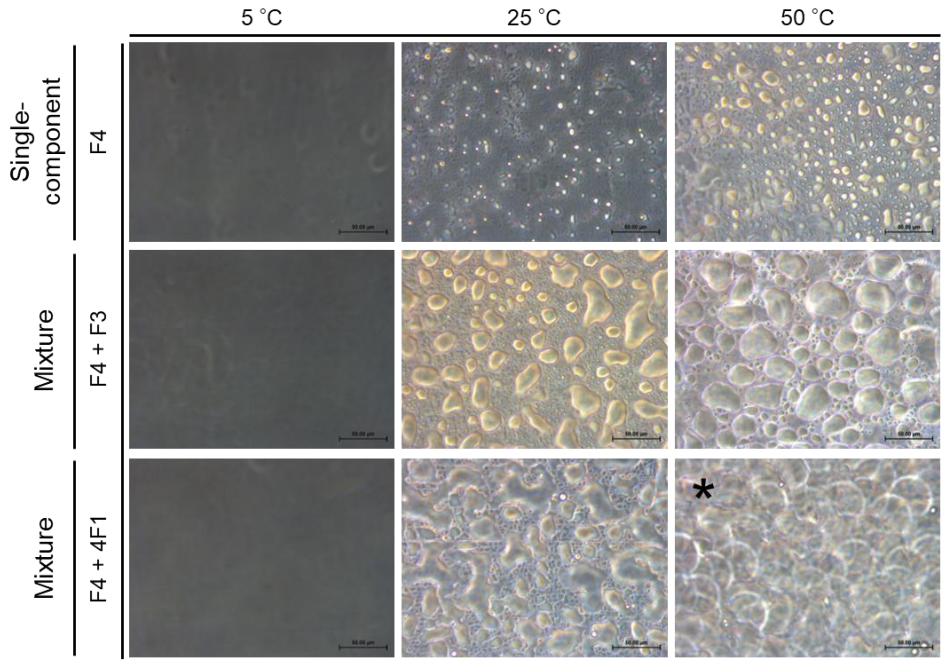

Figure 4-12. Microscopy images of F4, F4 + F3, and F4 + 4F1 in phosphate buffer with 1 M NaCl. The single-component F4 was dissolved at 3 mM. In F4 + F3, F4 and F3 were dissolved at 3 mM and 10 mM, respectively. In F4 + 4F1, F4 and 4F1 were dissolved at 3 mM and 5 mM, respectively. As for F4 + 4F1 at 50 °C (*), a clear, focused image could not be obtained because of the dense and large number of precipitates. Scale bars: 50 μm.

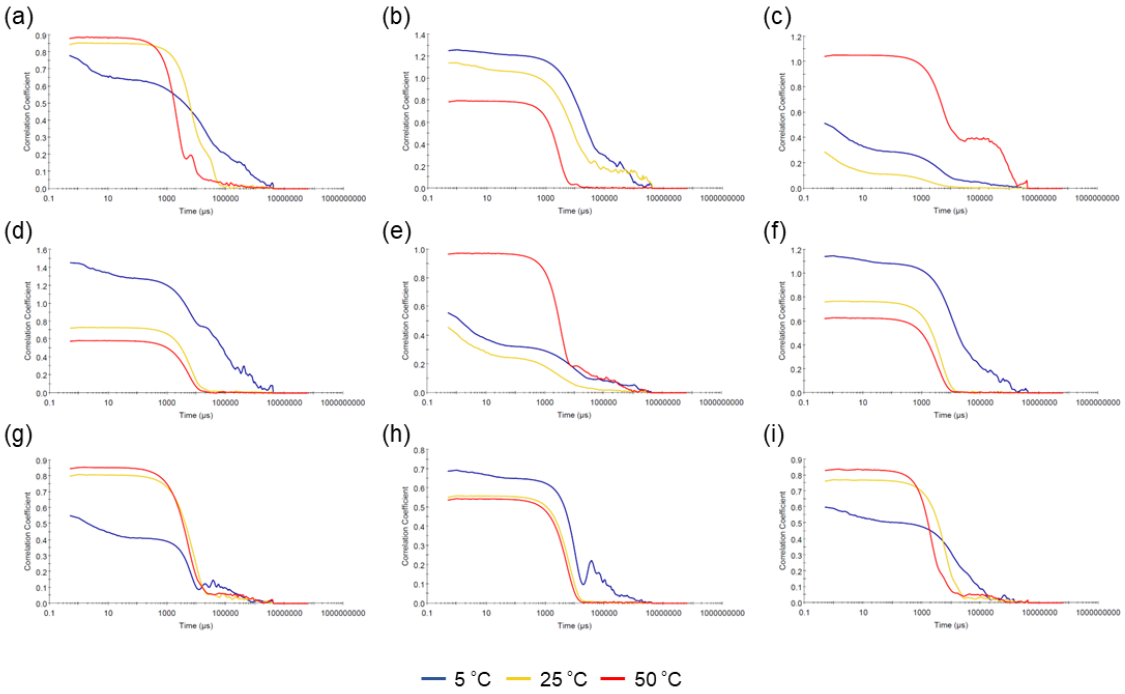

Figure 4-13. DLS Autocorrelation curves.

(a) F4 0.2 mM, (b) F2 15 mM, (c) F3 1 mM, (d) F3 2 mM, (e) 4F1 0.4 mM, (f) F4 + F2 (F4 0.2 mM and F2 15 mM), (g) F4 + F3 (F4 0.2 mM and F3 1 mM), (h) F3 + F2 (F3 2 mM and F2 15 mM), and (i) F4 +4F1 (F4 0.2 mM and 4F1 0.4 mM). The samples were prepared in filtered phosphate buffer supplemented with 3 M NaCl.

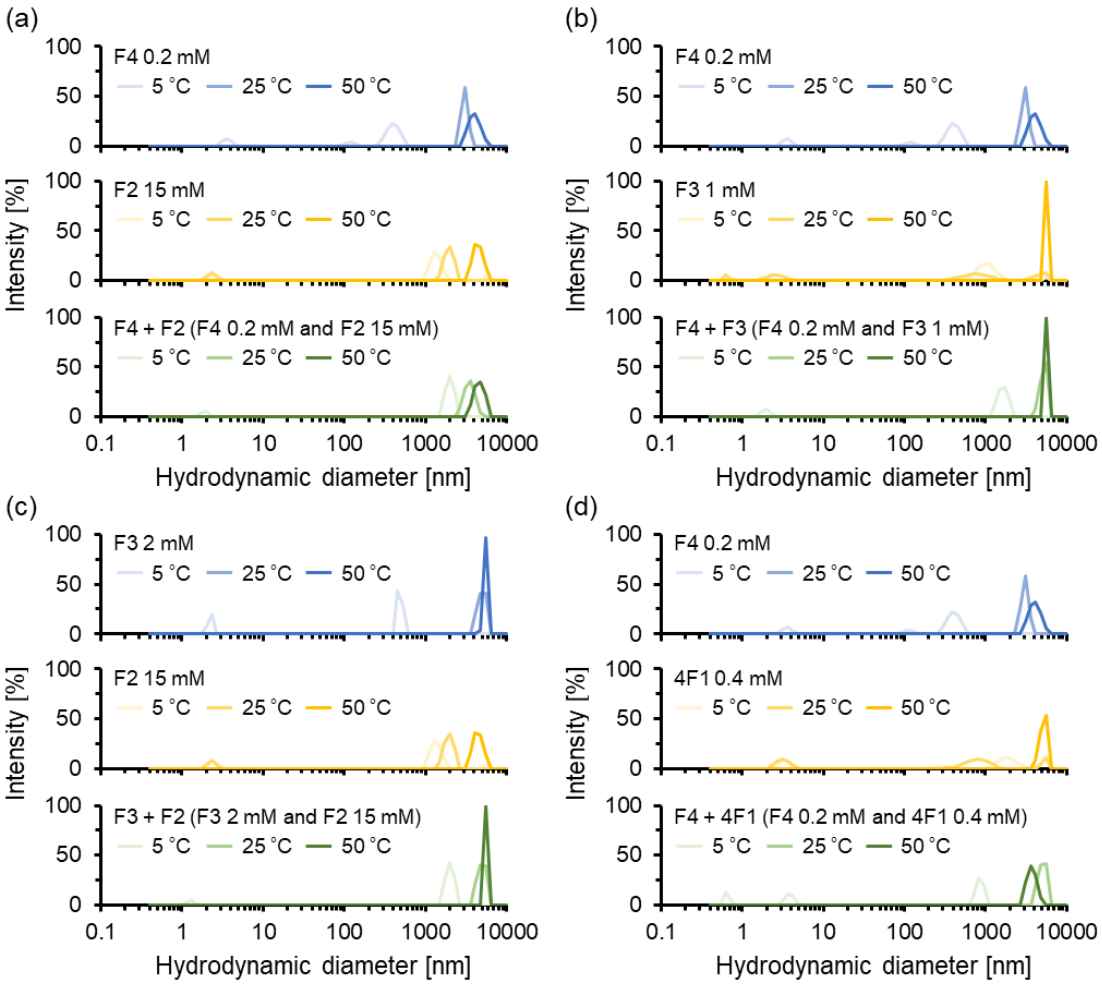

Figure 4-14. DLS results in intensity.

(a) F4, F2, and F4 + F2, (b) F4, F3, and F4 + F3, (c) F3, F2, and F3 + F2, and (d) F4, 4F1, and F4 + 4F1. Samples were prepared in phosphate buffer supplemented with 3 M NaCl. Results are shown in intensity (%).

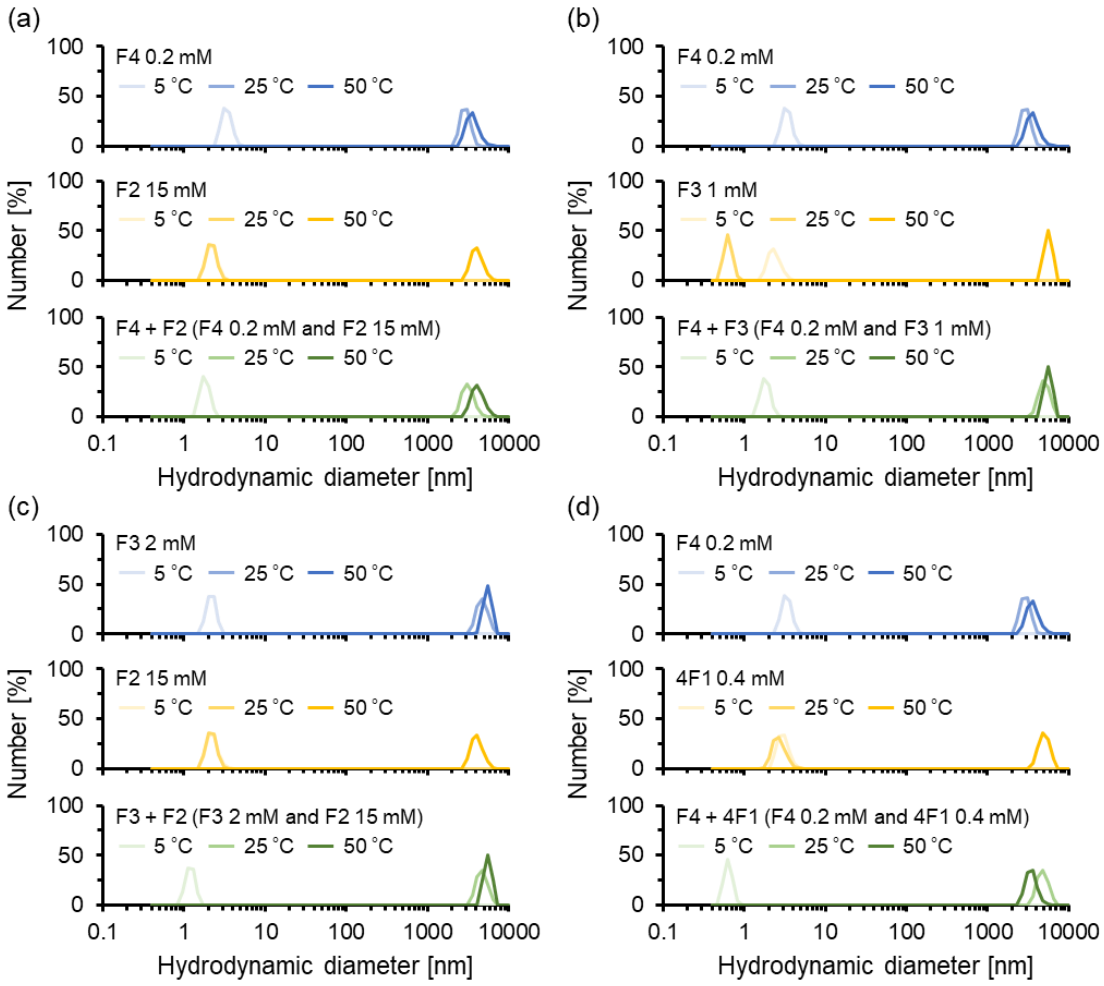

Figure 4-15. DLS results in number.

(a) F4, F2, and F4 + F2, (b) F4, F3, and F4 + F3, (c) F3, F2, and F3 + F2, and (d) F4, 4F1, and F4 + 4F1. Samples were prepared in phosphate buffer supplemented with 3 M NaCl. Results are shown in number (%).

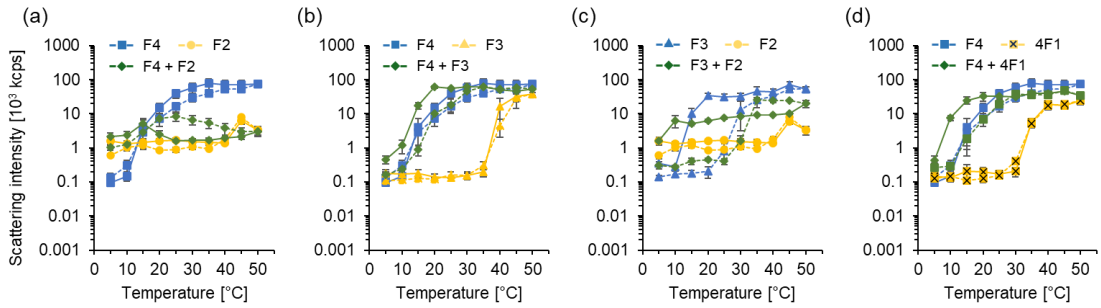

Figure 4-16. Temperature-dependent scattering intensity of the single-component and mixture samples.

(a) F4 0.2 mM, F2 15 mM, and F4 + F2 (F4 0.2 mM and F2 15 mM), (b) F4 0.2 mM, F3 1 mM, F4 + F3 (F4 0.2 mM and F3 1 mM), (c) F3 2 mM, F2 15 mM, and F3 + F2 (F3 2 mM and F2 15 mM), (d) F4 0.2 mM, 4F1 0.4 mM, F4 + 4F1 (F4 0.2 mM and 4F1 0.4 mM). Samples were prepared in phosphate buffer supplemented with 3 M NaCl. Solid lines and dashed lines represent heating and cooling, respectively.

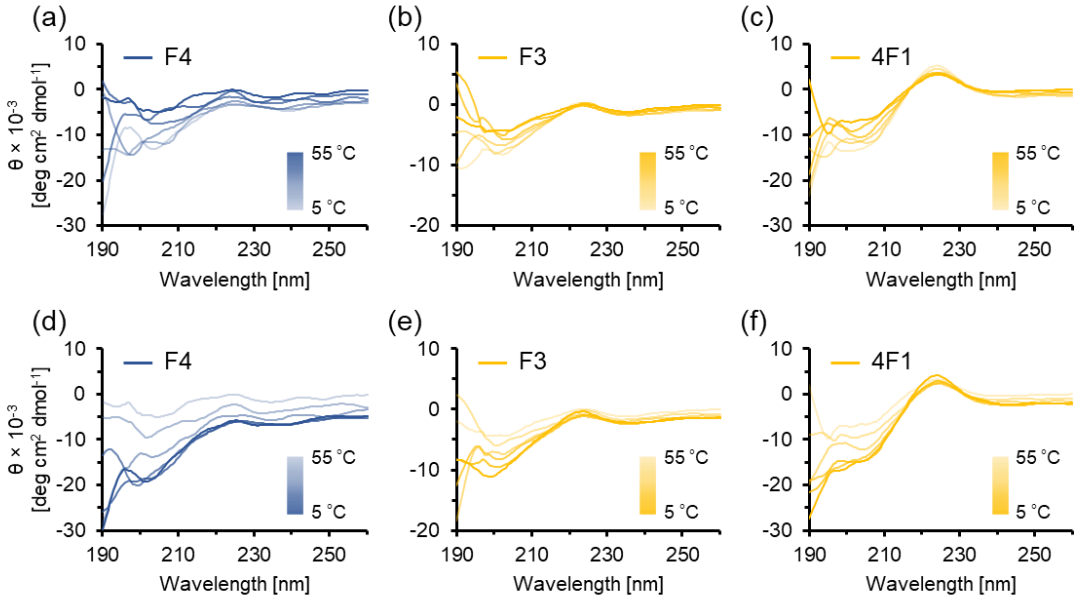

Figure 4-17. CD spectra of single-component ELPs.

Spectra in mean residue ellipticity obtained upon heating for (a) F4 (0.0210 mg/mL), (b) F3 (0.0790 mg/mL), and (c) 4F1 (0.0508 mg/mL), and spectra obtained upon cooling for (d) F4 (0.0210 mg/mL), (e) F3 (0.0790 mg/mL), and (f) 4F1 (0.0508 mg/mL).

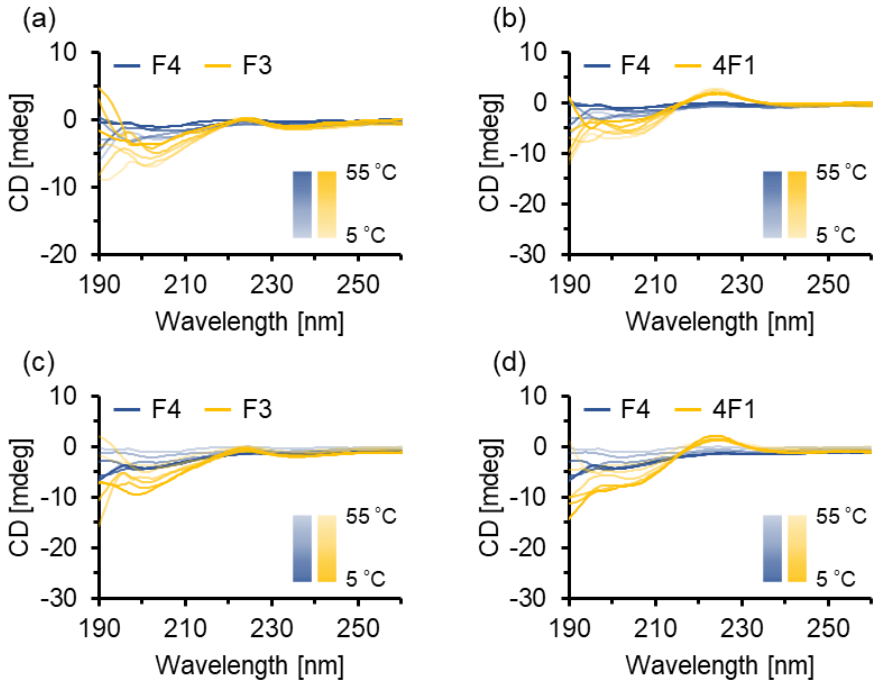

Figure 4-18. CD spectra in mdeg of single-component ELPs.

Spectra in mdeg obtained upon heating for (a) F4 (0.0210 mg/mL) and F3 (0.0790 mg/mL), and (b) F4 (0.0210 mg/mL) and 4F1 (0.0508 mg/mL), and spectra obtained upon cooling for (c) F4 (0.0210 mg/mL) and F3 (0.0790 mg/mL), and (d) F4 (0.0210 mg/mL) and 4F1 (0.0508 mg/mL).

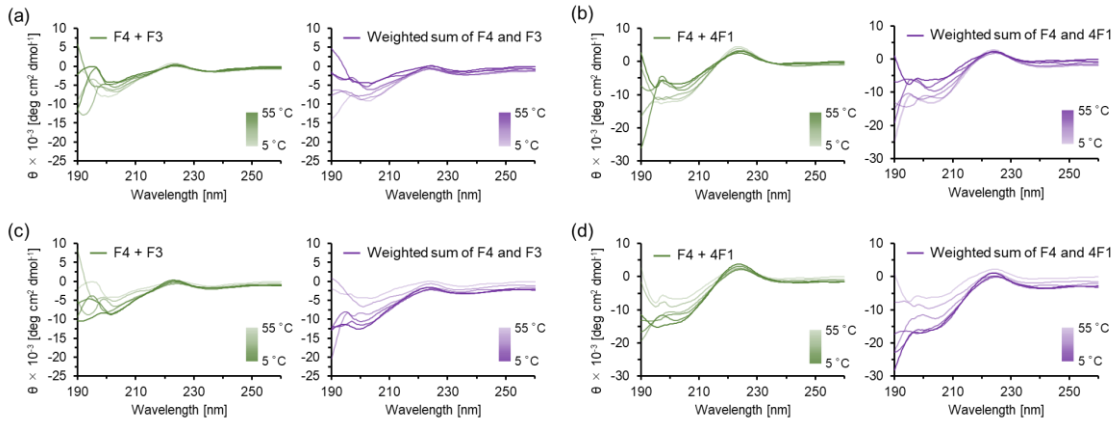

Figure 4-19. CD spectra of two-component ELPs.

Spectra in mean residue ellipticity obtained upon heating for (a) F4 + F3 (F4 0.0210 mg/mL and F3 0.0790 mg/mL, left) and calculated spectra based on the single-component F4 and F3 (right), and (b) F4 + 4F1 (F4 0.0210 mg/mL and 4F1 0.0508 mg/mL, left) and calculated spectra based on the single-component F4 and 4F1 (right), and spectra obtained upon cooling for (c) F4 + F3 (F4 0.0210 mg/mL and F3 0.0790 mg/mL, left) and calculated spectra based on the single-component F4 and F3 (right), and (d) F4 + 4F1 (F4 0.0210 mg/mL and 4F1 0.0508 mg/mL, left) and calculated spectra based on the single-component F4 and 4F1 (right).

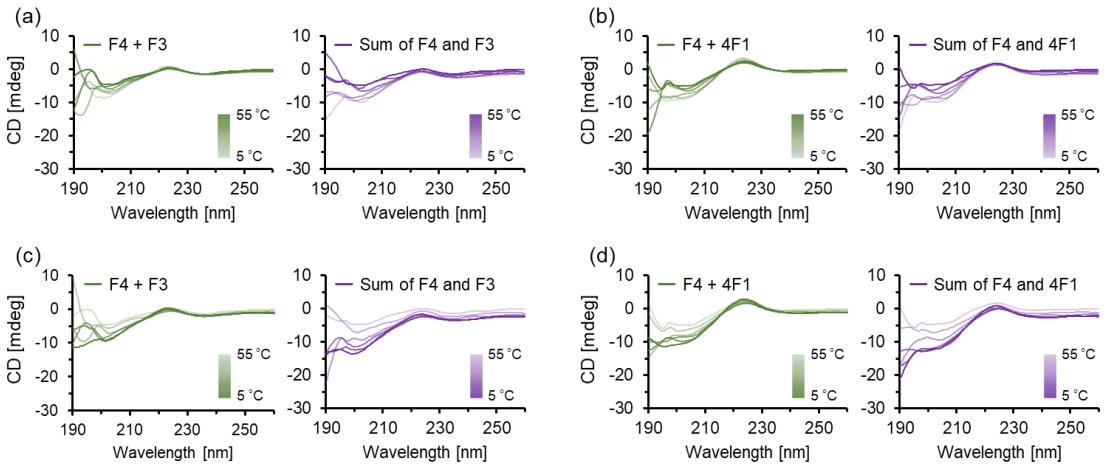

Figure 4-20. CD spectra in mdeg of two-component ELPs.

Spectra in mdeg obtained upon heating for (a) F4 + F3 (F4 0.0210 mg/mL and F3 0.0790 mg/mL, left) and calculated spectra based on the single-component F4 and F3 (right), and (b) F4 + 4F1 (F4 0.0210 mg/mL and 4F1 0.0508 mg/mL, left) and calculated spectra based on the single-component F4 and 4F1 (right), and spectra obtained upon cooling for (c) F4 + F3 (F4 0.0210 mg/mL and F3 0.0790 mg/mL, left) and calculated spectra based on the single-component F4 and F3 (right), and (d) F4 + 4F1 (F4 0.0210 mg/mL and 4F1 0.0508 mg/mL, left) and calculated spectra based on the single-component F4 and 4F1 (right).

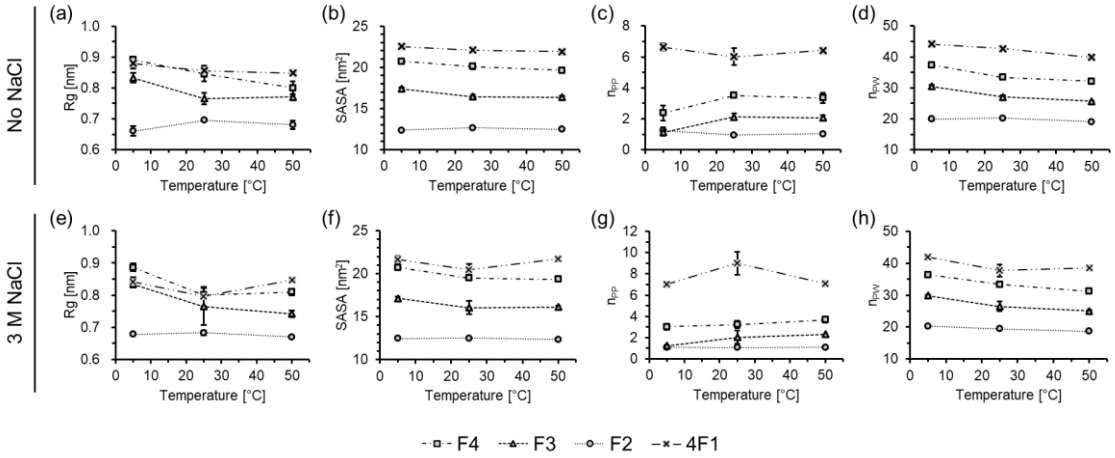

Figure 4-21. MD simulations in the absence of NaCl or in the presence of 3M NaCl.

The results obtained on the absence of NaCl for (a) Rg, (b) SASA, (c) n_{PP}, and (d) n_{PW}, and the results obtained under 3 M NaCl for (e) Rg, (f) SASA, (g) n_{PP}, and (h) n_{PW} for F4 (square), F3 (triangle), F2 (circle), and 4F1 (cross). Data represents the average values of three independent simulation runs, with standard errors (SE) shown as error bars. Values obtained at 5 °C, 25 °C, and 50 °C are connected by lines for clarity.

Chapter 5

General Conclusion and Future Perspectives

In this thesis, to deepen the understanding of the temperature-responsive behavior of short-chain ELPs, a series of chemically synthesized short-chain ELPs with FPGVG-based sequences were investigated for their phase behavior. This thesis focused on (i) whether molecules capable of coacervation could be obtained using short-chain ELPs as starting materials, (ii) how the synthesized branched ELPs behave, and (iii) how the short-chain ELPs with linear or branched structures behave when they are mixed.

In Chapter 2, it was demonstrated that short-chain ELPs such as F1 and F2, which did not exhibit LCST-type behavior in their monomeric forms, could exhibit clear and reversible LCST-type behavior upon covalent multimerization using EDTA as a central scaffold. These results indicated that temperature-responsive molecules can be developed using short-chain ELPs with weak to no coacervation abilities as starting materials, thereby expanding the design space of ELP-based thermoresponsive materials beyond conventional long-chain ELP-based materials.

In Chapter 3, motivated by the observation that the monomeric pentapeptide F1 exhibits temperature-dependent structural changes similar to those of long-chain $(FPGVG)_n$, branched molecules bearing multiple F1 chains were synthesized and investigated for their temperature-responsive behavior. Consequently, the branched molecules with five to seven F1 chains exhibited LCST-type behavior. Of note, the branched molecules with six F1 chains exhibited not only LCST-type behavior but also UCST-type behavior, showing solubility at both low and high temperature ranges. This study revealed a rare and previously unexplored mode of temperature-responsiveness in ELP-based molecules.

In Chapter 4, the phase behavior of multicomponent systems composed of linear or branched short-chain ELPs was investigated to clarify whether the short-chain ELPs with small structural differences could exhibit distinct phase separation when they are mixed. The ELPs comprised two to four pentapeptide units and differed only minimally in their structures, either by a difference of 5 or 10 residues in chain length or by molecular topology. Depending on the conditions such as peptide concentration or ionic strength, the binary mixtures of these short-chain ELPs exhibited stepwise phase separation upon heating. The results demonstrated that even subtle differences in molecular structure can lead to sequential phase transitions in multicomponent short-chain ELP systems, and provided insights into the design of multicomponent short-chain ELP systems.

Based on the findings of this thesis, further exploration of the applications of short-chain ELPs is expected. While long-chain ELPs have been predominantly employed in existing

applications, the use of short-chain ELPs has the potential to enable the development of materials with properties distinct from those of conventional long-chain ELP-based systems. For example, one promising direction is the development of conjugates of protein and short-chain ELPs. Although genetic fusion enables the linear attachment of long-chain ELPs to target proteins, the results of this thesis demonstrated that temperature-responsive behavior can also be achieved by tethering multiple short-chain ELPs to a single molecular scaffold. Extending this strategy to proteins, it is anticipated that conjugating multiple short-chain ELPs to a protein could impart ELP-derived temperature-responsiveness while preserving protein functionality. Such an approach may offer several advantages including greater structural flexibility of ELP chains, reduced overall molecular size, suppressed nonspecific interactions between proteins and ELP chains, and compatibility with further chemical modification strategies. Therefore, the multivalent conjugation of short-chain ELPs to proteins represents a promising strategy for creating novel thermoresponsive protein-based materials and is expected to broaden the scope of ELP-based biomaterials.

As a proof-of-concept application, this strategy was explored for the conjugation of short-chain ELPs to enzymes. One of the specific examples is conjugation with polyethylene terephthalate (PET)-degrading enzymes. Enzymatic plastic degradation has gained attention as an environmentally benign approach [1–3]. However, efficient PET degradation requires enzymes that remain active at temperatures near the glass transition temperature of PET (approximately 70 °C in aqueous environments), under acidic conditions generated by hydrolysis, and during long-term storage for practical use. Therefore, the properties of PET hydrolases have been tailored for realizing a circular plastic economy [1–8]. Previous studies have shown that ELPs can improve enzyme thermal stability, storage stability, and, in some cases, pH tolerance, in addition to enabling facile purification [9–11]. However, these approaches relied on conjugation with long-chain ELPs (approximately 200–250 residues). Given the low cost and synthetic accessibility of short-chain ELPs, multivalent post-translational conjugation of short-chain ELPs to enzymes is anticipated to provide a practical strategy for enhancing enzyme robustness, thereby contributing to the development of PET-degrading enzymes suitable for industrial recycling processes. During the course of this thesis, the author also attempted chemical conjugation of short-chain ELPs to PET-degrading enzymes (*Humicola insolens* cutinase, Novozym 51032) [12] (Table 5-1). However, conjugation of PET-degrading enzymes and short-chain ELPs was not successfully achieved under the conditions examined (Figures 5-1 and 5-2); either the target enzyme-ELP conjugates were not observed in MALDI-TOF MS or UPLC-MS, or insoluble aggregates were obtained. These results indicated that the efficient conjugation of short-chain ELPs to enzymes remains challenging and requires further optimization of reaction conditions. Possible factors contributing to the difficulty in obtaining the enzyme-ELP conjugates may include the limited

accessibility of reactive functional groups on the enzyme surface, which may be involved in stable intramolecular or intermolecular interactions. Furthermore, the solution behavior of short-chain ELPs, which may exist as microaggregates rather than monomeric species even below their T_t, may hinder efficient conjugation reactions. These aspects should be addressed in future studies. Nevertheless, given previous reports that long-chain ELP tags can enhance enzyme stability and enable facile purification, post-translational modification of enzymes with multiple short-chain ELPs remains a promising concept. Identification of suitable conjugation strategies may allow the extension of the multivalent short-chain ELP approach to enzyme-based systems, including those relevant to plastic recycling and other biotechnological applications.

(Table 5-1)
(Figures 5-1 and 5-2)

Collectively, this thesis demonstrated that the short-chain ELPs can exhibit diverse and tunable temperature-responsive behavior through molecular design and system composition. In particular, it demonstrated that short-chain ELPs, which individually exhibit weak or no LCST-type behavior, can be transformed into temperature-responsive molecules through multimerization, and mixtures of short-chain ELPs with small differences in chain length or topology can exhibit stepwise phase behavior. This thesis provides a foundation for the rational design and development of responsive materials based on short-chain ELPs for future advanced applications.

References

[1] Kawai, F. Emerging strategies in polyethylene terephthalate hydrolase research for biorecycling. *ChemSusChem* **2021**, *14* (19), 4115–4122.

[2] Wei, R.; Westh, P.; Weber, G.; Blank, L. M.; Bornscheuer, U. T. Standardization guidelines and future trends for PET hydrolase research. *Nat. Commun.* **2025**, *16*, 4684.

[3] Shi, L.; Zhu, L. Recent advances and challenges in enzymatic depolymerization and recycling of PET wastes. *ChemBioChem* **2024**, *25* (2), e202300578.

[4] Lu, H.; Diaz, D. J.; Czarnecki, N. J.; Zhu, C.; Kim, W.; Shroff, R.; Acosta, D. J.; Alexander, B. R.; Cole, H. O.; Zhang, Y.; Lynd, N. A.; Ellington, A. D.; Alper, H. S. Machine learning-aided engineering of hydrolases for PET depolymerization. *Nature* **2022**, *604*, 662–667.

[5] Tournier, V.; Topham, C. M.; Gilles, A.; David, B.; Folgoas, C.; Moya-Leclair, E.; Kamionka, E.; Desrousseaux, M. -L.; Texier, H.; Gavalda, S.; Cot, M.; Guémard, E.; Dalibey, M.; Nomme, J.; Cioci, G.; Barbe, S.; Chateau, M.; André, I.; Duquesne, S.; Marty, A. An engineered PET depolymerase to break down and recycle plastic bottles. *Nature* **2020**, *580*,

216–219.

[6] Shi, L.; Liu, P.; Tan, Z.; Zhao, W.; Gao, J.; Gu, Q.; Ma, H.; Liu, H.; Zhu, L. Complete depolymerization of PET wastes by an evolved PET hydrolase from directed evolution. *Angew. Chem. Int. Ed.* **2023**, *62* (14), e202218390.

[7] Zheng, Y.; Li, Q.; Liu, P.; Yuan, Y.; Dian, L.; Wang, Q.; Liang, Q.; Su, T.; Qi, Q. Dynamic docking-assisted engineering of hydrolases for efficient PET depolymerization. *ACS Catal.* **2024**, *14* (5), 3627–3639.

[8] Cui, Y.; Chen, Y.; Sun, J.; Zhu, T.; Pang, H.; Li, C.; Geng, W. -C.; Wu, B. Computational redesign of a hydrolase for nearly complete PET depolymerization at industrially relevant high-solids loading. *Nat. Commun.* **2024**, *15* (1), 1417.

[9] Addai, F. P.; Wang, T.; Kosiba, A. A.; Lin, F.; Zhen, R.; Chen, D.; Gu, J.; Shi, H.; Zhou, Y. Integration of elastin-like polypeptide fusion system into the expression and purification of *Lactobacillus* sp. B164 β-galactosidase for lactose hydrolysis. *Bioresour. Technol.* **2020**, *311*, 123513.

[10] Wang, S.; Lin, R.; Ren, Y.; Zhang, T.; Lu, H.; Wang, L.; Fan, D. Non-chromatographic purification of thermostable endoglucanase from *Thermotoga maritima* by fusion with a hydrophobic elastin-like polypeptide. *Protein Expr. Purif.* **2020**, *173*, 105634.

[11] Heidari-Japelaghi, R.; Haddad, R.; Valizadeh, M.; Dorani-Uliaie, E.; Jalali-Javaran, M. Elastin-like polypeptide fusions for high-level expression and purification of human IFN-γ in *Escherichia coli*. *Anal. Biochem.* **2019**, *585*, 113401.

[12] de Castro, A. M.; Carniel, A.; Nicomedes Junior, J.; da Conceição Gomes, A.; Valoni, É. Screening of commercial enzymes for poly(ethylene terephthalate) (PET) hydrolysis and synergy studies on different substrate sources. *J. Ind. Microbiol. Biotechnol.* **2017**, *44* (6), 835–844.

Table 5-1. Reaction conditions examined for conjugating short-chain ELPs and a PET degrading enzyme.

Entry	Enzyme (1 eq) [a]/ELP [b]/Condensing agent or linker	Solvent/pH/total volume [c]	Other conditions (temperature, duration time, and others) [d]
1	HiC/H-F2-NH_2 (8 eq)/DMT-MM (8 eq)	Water/pH ~8/929 μL	25 °C, 3 days
2	HiC/H-F2-NH_2 (15 eq)/DMT-MM (15 eq)	Water/pH ~8/929 μL	25 °C, 3 days
3	HiC/H-F2-NH_2 (45 eq)/DMT-MM (45 eq)	Water/pH ~8/929 μL	25 °C, 3 days
4	HiC/H-F2-NH_2 (150 eq)/DMT-MM (150 eq)	Water/pH ~8/949 μL	25 °C, 3 days
5	HiC/Ac-F2-OH (3 eq)/DMT-MM (3 eq)	Water/pH ~8/929 μL	25 °C, 3 days
6	HiC/Ac-F2-OH (6 eq)/DMT-MM (6 eq)	Water/pH ~8/929 μL	25 °C, 3 days
7	HiC/Ac-F2-OH (18 eq)/DMT-MM (18 eq)	Water/pH ~8/929 μL	25 °C, 3 days
8	HiC/Ac-F2-OH (60 eq)/DMT-MM (60 eq)	Water/pH ~8/949 μL	25 °C, 3 days
9	HiC/H-F5-NH_2 (15 eq)/DMT-MM (15 eq)	Water/pH ~8/929 μL	25 °C, 3 days
10	HiC/H-F5-NH_2 (15 eq)/DMT-MM (15 eq)	Water/pH ~8/929 μL	60 °C (microwave), 4.5 hours
11	HiC/Ac-F5-OH (6 eq)/DMT-MM (6 eq)	Water/pH ~8/929 μL	25 °C, 3 days
12	HiC/Ac-F5-OH (18 eq)/DMT-MM (18 eq)	Water/pH ~8/929 μL	25 °C, 3 days
13	HiC/H-[α-E(F1)]$_5$-F1-NH_2 (15 eq)/DMT-MM (15 eq)	Water/pH ~8/929 μL	25 °C, 3 days
14	HiC/H-GGGGG-F1-K(NBD)-NH_2 (15 eq)/DMT-MM (15 eq)	Water/pH ~8/364 μL	25 °C, 2 days
15	HiC/H-GGGGG-F1-K(NBD)-NH_2 (45 eq)/DMT-MM (45 eq)	Water/pH ~8/364 μL	25 °C, 2 days
16	HiC/H-GGGGG-F1-K(NBD)-NH_2 (45 eq)/DMT-MM (15 eq)	Water/pH ~8/364 μL	40 °C, 2 days

Table 5-1. Reaction conditions examined for conjugating short-chain ELPs and a PET degrading enzyme (continued).

Entry	Enzyme (1 eq) [a]/ELP [b]/Condensing agent or linker	Solvent/pH/total volume [c]	Other conditions (temperature, duration time, and others) [d]
17	HiC/H-GGGGG-F1-K(NBD)-NH_2 (15 eq)/DMT-MM (15 eq)	Water/pH ~8/364 μL	40 °C, 2 days
18	HiC/H-GGGGG-F1-K(NBD)-NH_2 (45 eq)/DMT-MM (45 eq)	Water/pH ~8/997 μL	40 °C, 1 day
19	HiC/H-GGGGG-F1-K(NBD)-NH_2 (45 eq)/DMT-MM (45 eq)	Phosphate buffer (μ = 0.100)/pH 7.4/987 μL	25 °C, 2.5 hours
20	HiC/H-GGGGG-F1-K(NBD)-NH_2 (45 eq)/DMT-MM (45 eq)	Phosphate buffer (50 mM)/pH 7.0/987 μL	50 °C, 1 hour
21	HiC/H-GGGGG-F1-NH_2 (45 eq)/DMT-MM (45 eq)	Phosphate buffer (50 mM)/pH 7.0/987 μL	50 °C, 1 day
22	HiC/H-GGGGG-F1-NH_2 (45 eq)/DMT-MM (45 eq)	MES buffer (50 mM)/pH 7.0/987 μL	50 °C, 1day
23	HiC 4 mg/H-GGGGG-F1-NH_2 (45 eq)/DMT-MM (45 eq)	MES buffer (50 mM)/pH 7.0/1974 μL	50 °C (microwave), 3 hours
24	Diafiltrated HiC/H-GGGGG-F1-NH_2 (45 eq)/DMT-MM (45 eq)	MES buffer (50 mM)/pH 7.0/984 μL	50 °C, 1 day
25	Diafiltrated HiC/H-GGGGG-F1-NH_2 (45 eq)/DMT-MM and DIPEA (45 eq each)	MES buffer (50 mM)/pH 7.0/984 μL	50 °C, 1 day
26	Diafiltrated HiC/H-GGGGG-F1-NH_2 (45 eq)/DMT-MM (45 eq)	Phosphate buffer (50 mM)/pH 8.0/984 μL	50 °C, 1 day

Table 5-1. Reaction conditions examined for conjugating short-chain ELPs and a PET degrading enzyme (continued).

Entry	Enzyme (1 eq) [a]/ELP [b]/Condensing agent or linker	Solvent/pH/total volume [c]	Other conditions (temperature, duration time, and others) [d]
27	Diafiltrated HiC/H-GGGGG-F1-NH_2 (45 eq)/DMT-MM (45 eq)	MES buffer (50 mM)/pH 7.0/984 μL	50 °C; Mixing HiC and DMT-MM for 10 min, followed by ELP addition; 6 hours
28	Diafiltrated HiC/H-GGGGG-F1-NH_2 (45 eq)/DMT-MM (45 eq)	MES buffer (50 mM)/pH 7.0/984 μL	50 °C; Mixing HiC and ELP for 10 min, followed by DMT-MM addition; 6 hours
29	Diafiltrated HiC/H-GGGGG-F3-NH_2 (45 eq)/DMT-MM (45 eq)	MES buffer (50 mM)/pH 7.0/984 μL	50 °C; Mixing HiC and DMT-MM for 10 min, followed by ELP addition; 1 day
30	Diafiltrated HiC/H-GGGGG-F3-NH_2 (45 eq)/DMT-MM (45 eq)	MES buffer (50 mM)/pH 7.0/984 μL	50 °C; Mixing HiC and ELP for 10 min, followed by DMT-MM addition; 1 day
31	HiC/Ac-CGGGG-F1-NH_2 (12 eq)/EMCS (0.5 M in DMSO, 12 eq)	Phosphate buffer (50 mM)/pH 7.5/800 μL	Reaction of HiC and linker for 2 hours; diafiltration; ELP conjugation for 2 hours
32	HiC/Ac-CGGGG-F1-NH_2 (12 eq)/EMCS (5 M in DMSO, 12 eq)	Phosphate buffer (50 mM)/pH 7.5/800 μL for reaction of linker; 400 μL for ELP conjugation	Reaction of HiC and linker for 2 hours; diafiltration; ELP conjugation for 1 day
33	HiC/Ac-CGGGG-F1-NH_2 (12 eq)/EMCS (2.5 M in DMSO, 12 eq)	Phosphate buffer (50 mM)/pH 7.5/800 μL for reaction of linker; 400 μL for ELP conjugation	Reaction of HiC and linker for 2 hours; diafiltration; ELP conjugation for 1 day
34	Diafiltrated HiC/Ac-CGGGG-F1-NH_2 (12 eq)/EMCS (0.5 mM in DMSO, 60 eq)	Phosphate buffer (50 mM)/pH 7.5/800 μL for reaction of linker; 400 μL for ELP conjugation	Reaction of HiC and linker for 2 hours; diafiltration; ELP conjugation for 2 hours

Table 5-1. Reaction conditions examined for conjugating short-chain ELPs and a PET degrading enzyme (continued).

Entry	Enzyme (1 eq) [a]/ELP [b]/Condensing agent or linker	Solvent/pH/total volume [c]	Other conditions (temperature, duration time, and others) [d]
35	Diafiltrated HiC/Ac-F1-GGGGC-NH_2 (12 eq)/Maleimide-PEG2-NHS ester (60 eq)	Phosphate buffer (50 mM)/pH 7.5/800 µL for reaction of linker; 400 µL for ELP conjugation	Reaction of HiC and linker for 2 hours; diafiltration; ELP conjugation for 2 hours
36	Diafiltrated HiC/Ac-F3-GGGGC-NH_2 (12 eq)/Maleimide-PEG2-NHS ester (60 eq)	Phosphate buffer (50 mM)/pH 7.5/800 µL for reaction of linker; 400 µL for ELP conjugation	Reaction of HiC and linker for 2 hours; diafiltration; ELP conjugation for 2 hours
37	Diafiltrated HiC/Ac-F1-GGGGC-NH_2 (12 eq)/EMCS (0.5 mM in DMSO, 60 eq)	Phosphate buffer (50 mM)/pH 7.5/800 µL for reaction of linker; 400 µL for ELP conjugation	Reaction of HiC and linker for overnight; diafiltration; ELP conjugation for 4 days
38	Diafiltrated HiC/Ac-F1-GGGGC-NH_2 (12 eq)/Maleimide-PEG2-NHS ester (60 eq)	Phosphate buffer (50 mM)/pH 7.5/800 µL for reaction of linker; 400 µL for ELP conjugation	Reaction of HiC and linker for overnight; diafiltration; ELP conjugation for 4 days
39	Diafiltrated HiC/Ac-F1-GGGGC-NH_2 (12 eq)/Maleimide-PEG2-NHS ester (60 eq)	Phosphate buffer (50 mM)/pH 7.5/800 µL for reaction of linker; 400 µL for ELP conjugation	Reaction of HiC and linker for overnight; diafiltration; ELP conjugation for 4 hours
40	Diafiltrated HiC/Ac-F1-GGGGC-NH_2 (30 eq)/Maleimide-PEG2-NHS ester (60 eq)	Phosphate buffer (50 mM)/pH 7.5/400 µL for reaction of linker; 400 µL for ELP conjugation	Reaction of HiC and linker for 1 hour; diafiltration; ELP conjugation for overnight

Table 5-1. Reaction conditions examined for conjugating short-chain ELPs and a PET degrading enzyme (continued).

Entry	Enzyme (1 eq) [a]/ELP [b]/Condensing agent or linker	Solvent/pH/total volume [c]	Other conditions (temperature, duration time, and others) [d]
41	Diafiltrated HiC/Ac-F1-GGGGC-NH_2 (30 eq)/Maleimide-PEG2-NHS ester (90 eq)	Phosphate buffer (50 mM)/pH 7.5/400 µL for reaction of linker; 400 µL for ELP conjugation	Reaction of HiC and linker for 1 hour; diafiltration; ELP conjugation for overnight
42	Diafiltrated HiC/Ac-F1-GGGGC-NH_2 (30 eq)/Maleimide-PEG2-NHS ester (120 eq)	Phosphate buffer (50 mM)/pH 7.5/400 µL for reaction of linker; 400 µL for ELP conjugation	Reaction of HiC and linker for 1 hour; diafiltration; ELP conjugation for overnight
43	Diafiltrated HiC/Ac-F1-GGGGC-NH_2 (30 eq)/Maleimide-PEG2-NHS ester (180 eq)	Phosphate buffer (50 mM)/pH 7.5/400 µL for reaction of linker; 400 µL for ELP conjugation	Reaction of HiC and linker for 1 hour; diafiltration; ELP conjugation for overnight
44	Diafiltrated HiC/Ac-F1-GGGGC-NH_2 (30 eq)/Maleimide-PEG2-NHS ester (180 eq)	Phosphate buffer (50 mM)/pH 7.5/800 µL for reaction of linker; 400 µL for ELP conjugation	Reaction of HiC and linker for 1 hour; diafiltration; ELP conjugation for overnight
45	Diafiltrated HiC/Ac-CGGGG-F3-NH_2 (30 eq)/Maleimide-PEG2-NHS ester (120 eq)	Phosphate buffer (50 mM)/pH 7.5/400 µL for reaction of linker; 400 µL for ELP conjugation	Reaction of HiC and linker for overnight; diafiltration; ELP conjugation for overnight
46	Diafiltrated HiC/Ac-CGGGG-F3-NH_2 (30 eq)/Maleimide-PEG2-NHS ester (180 eq)	Phosphate buffer (50 mM)/pH 7.5/400 µL for reaction of linker; 400 µL for ELP conjugation	Reaction of HiC and linker for overnight; diafiltration; ELP conjugation for overnight

Table 5-1. Reaction conditions examined for conjugating short-chain ELPs and a PET degrading enzyme (continued).

Entry	Enzyme (1 eq) [a]/ELP [b]/Condensing agent or linker	Solvent/pH/total volume [c]	Other conditions (temperature, duration time, and others) [d]
47	Diafiltrated HiC/Ac-CGGGG-F1-NH_2 (60 eq)/Maleimide-PEG2-NHS ester (60 eq)	Phosphate buffer (50 mM)/pH 7.5/400 μL for reaction of linker; 400 μL for ELP conjugation	Reaction of HiC and linker for overnight; diafiltration; ELP conjugation for 1 week
48	Diafiltrated HiC/Ac-CGGGG-F1-NH_2 (60 eq)/Maleimide-PEG2-NHS ester (90 eq)	Phosphate buffer (50 mM)/pH 7.5/400 μL for reaction of linker; 400 μL for ELP conjugation	Reaction of HiC and linker for overnight; diafiltration; ELP conjugation for 1 week
49	Diafiltrated HiC/Ac-CGGGG-F1-NH_2 (60 eq)/Maleimide-PEG2-NHS ester (120 eq)	Phosphate buffer (50 mM, pH 7.5) 400 μL for reaction of linker; 400 μL for ELP conjugation	Reaction of HiC and linker for overnight; diafiltration; ELP conjugation for 1 week
50	Diafiltrated HiC/Ac-CGGGG-F1-NH_2 (60 eq)/Maleimide-PEG2-NHS ester (180 eq)	Phosphate buffer (50 mM)/pH 7.5/400 μL for reaction of linker; 400 μL for ELP conjugation	Reaction of HiC and linker for overnight; diafiltration; ELP conjugation for 1 week

[a] For HiC, solutions containing 2 mg of the protein were used unless otherwise stated. Bradford assay was used to estimate protein concentration. The definition of abbreviations used in the table are follows: HiC, *Humicola insolens* cutinase (Novozym 51032; this protein contains 15 carboxyl groups and 6 amino groups.); Diafiltrated HiC, HiC diafiltrated with buffer using Microcon, Ultracel-10 Membrane, 10 kDa (Millipore); Fn, $(FPGVG)_n$; H-GGGGG-F1-K(NBD)-NH_2, H-GGGGG-F1-K-NH_2 labeled with 4-fluoro-7-nitro-2,1,3-benzoxadiazole (NBD-F); DMT-MM, 4-(4,6-dimethoxy-1,3,5-triazin-2-yl)-4-methylmorpholinium chloride; EMCS, *N*-(6-Maleimidocaproyloxy)succinimide; Maleimide-PEG2-NHSester, *N*-Succinimidyl 13-Maleimido-11-oxo-4,7-dioxa-10-azatridecanoate.

[b] FPGVG-based ELPs were used. Gly-rich spacers were introduced into some ELPs.

[c] For reactions conducted in unbuffered water, the pH of the reaction solution was adjusted with a 1 M NaOH solution and confirmed with a universal

indicator. MES stands for 2-(*N*-morpholino)ethanesulfonic acid.

[d] Experimental conditions, including temperature, duration time, order of reagent addition, and the use of diafiltration to remove linkers, were specified. Unless otherwise stated, mixing of the protein, ELP, and condensing reagent or linker was initiated simultaneously.

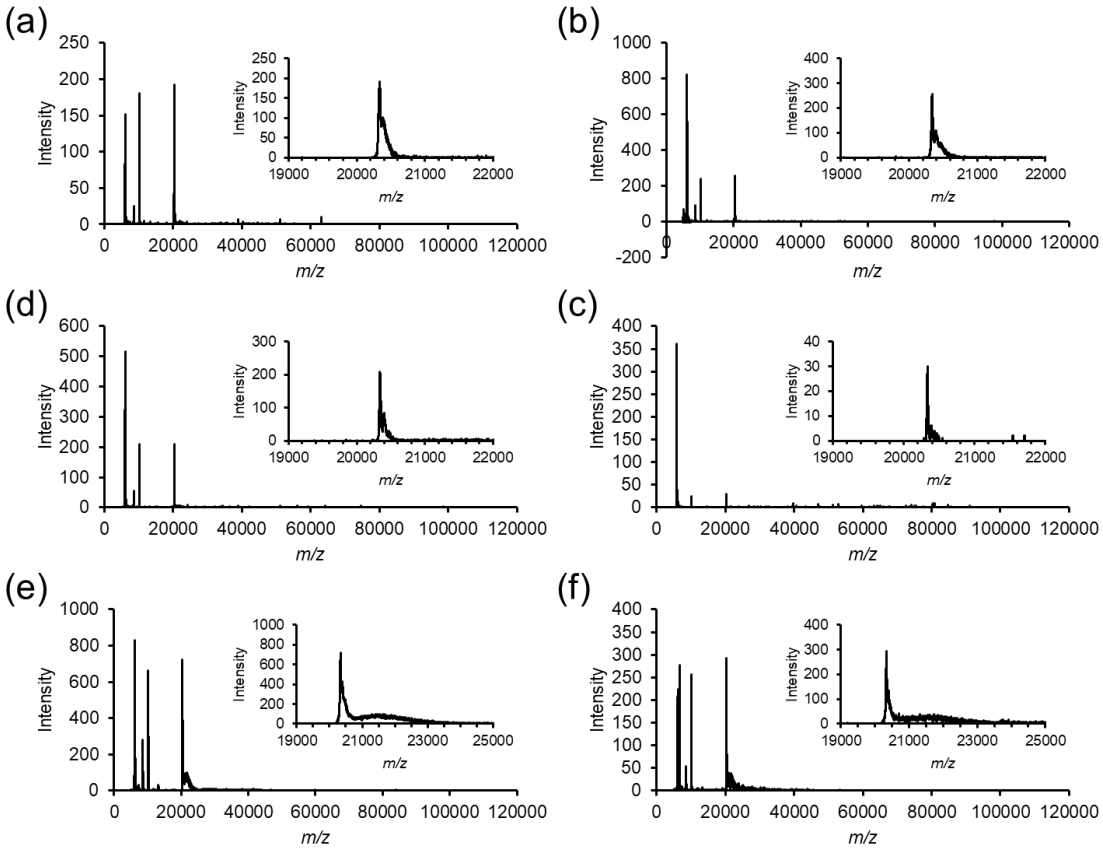

Figure 5-1. Representative MALDI-TOF MS spectra showing the reaction progress.
Spectra of (a) diafiltrated HiC and diafiltrated products corresponding to (b) entry 2, (c) entry 6, (d) entry 10, (e) entry 11, (f) entry 13 in Table 5-1. Measurements were performed using a MALDI-TOF mass spectrometer (Bruker Autoflex II) using 2',6'-dihydroxyacetophenone as the matrix. Inset panels show the enlarged views of the region around *m/z* of 20,000.

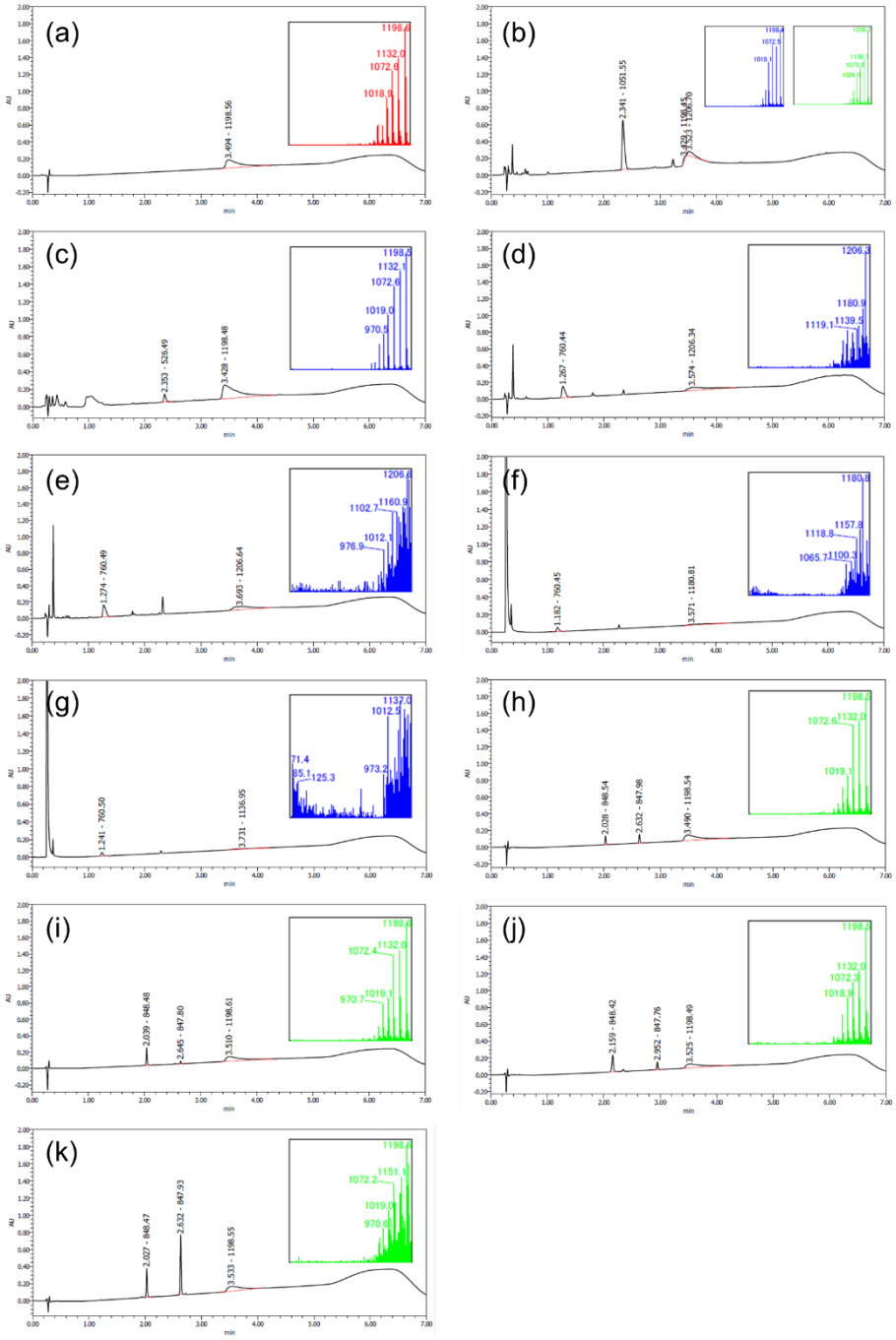

Figure 5-2. Representative UPLC-MS analysis showing the reaction progress. Chromatograms of (a) diafiltrated HiC, entries (b) 14, (c) 17, (d) 21, (e) 22, (f) 27, (g) 28, (h) 33, (i) 34, (j) 42, and (k) 50. The samples were monitored by UPLC (ACQUITY UPLC H-Class, Waters) equipped with an ACQUITY UPLC BEH C-18 column (100 mm; flow rate, 0.6 mL/min) in a linear gradient of solvent B in solvent A (10% to 50%) over 4.51 min, where solvent A was 0.1% formic acid in water (v/v) and solvent B was 0.1% formic acid in MeCN (v/v). The subscripts for each peak indicate the retention time and the *m/z* values detected for the peptide

tags (1.2–3.0 min) or HiC (3.5 min). Inset panels show MS spectra of the peak around 3.5 min determined by ACQUITY QDa mass spectrometer.

Acknowledgements

This work would not have been possible without the guidance and support of many individuals, to whom the author, Naoki Tanaka, would like to express his sincere gratitude.

First and foremost, the author expresses his deepest appreciation to Professor Takeru Nose, Kyushu University, for his supervision, insightful discussions, and unwavering support throughout this work. His thoughtful advice and encouragement were invaluable to the completion of this work.

The author is also deeply grateful to Assistant Professor Keitaro Suyama, Kyushu University, for his generous support in experimental design and data analysis, as well as his constructive discussions and practical advice throughout the study. The author would also like to thank Lecturer Keisuke Tomohara, Kyoto Pharmaceutical University, for his insightful discussions and helpful suggestions. In addition, the author is grateful to Professor Iori Maeda, Kyushu Institute of Technology, for valuable discussions and contributions to the research on short-chain ELPs. The author also sincerely acknowledges Professor Ayami Matsushima, Kyushu University, for her valuable support in the CD measurements, and Assistant Professor Kenta Goto, Kyushu University, for his assistance with MALDI-TOF MS analysis. Finally, the author would like to extend his appreciation to his laboratory colleagues for their helpful discussions, collaboration, and encouragement throughout his research activities.

This work was supported by JSPS KAKENHI Grant Number JP23KJ1744.